Department of Earth and Planetary Sciences

Macquarie University, Australia

DIFFERENT MODES OF ALTERATION IN CARBONACEOUS CHONDRITES: TIMELINES AND PROCESSES

Stephanie Kovach, BSc

A thesis submitted for the partial fulfilment of the degree:

MASTER OF RESEARCH

9th October 2017

"Observe always that everything is the result of change, and get used to thinking that there is nothing Nature loves so well as to change existing forms and to make new ones like them"

Meditations- *Marcus Aurelius*

Statement of Originality

All the work submitted within this thesis is the original work of the author except where otherwise acknowledged. No part of this thesis has been previously submitted to any other university or institution.

Signed: Stephanie Kovach	9-10-17 Date

Acknowledgments

It is often said that a Masters of Research is a learning experience and this could not be more accurate. In these last 10 months, many problems have arisen, from sample dramas to project changes; however, in this short amount of time, I have learnt so much about meteorites and discovered just how many unknowns there are in planetary sciences, which makes it a very exciting discipline to undertake research in! Plus, meteorites are cool!

My first thanks and appreciations go to my supervisors; Tracy Rushmer, Sandra Piazolo and Simon Turner. I thank them for their suggestions, feedback, meetings, time and effort they have given me, without them this thesis would not have been possible. Throughout my years at Macquarie, Tracy has always been ready for a chat and provide guidance and this did not change when I began the Masters program. Her encouragement also led me present at the SSERVI Australia Shock Metamorphism Conference 2017 and have a poster at the Accretion, Differentiation and Early Evolution of the Terrestrial Planets 2017, with further enriched my maters experience. Another special thanks go to Sandra. Her timely and extensive feedback was always appreciated and encouraged me to think about ideas with added depth and detail. With Sandra's move to the UK, I was given the opportunity to undertake some of my research in the University of Leeds, which was another great and enriching experience. Each of my supervisors have given me their time and effort, in their busy lives, which I really appreciate and cannot thank enough.

Many thanks go to the support of Macquarie University's Department of Earth and Planetary Sciences and the Macquarie Planetary Research Group for their project support and providing funding to attend the Shock Metamorphism conference in Perth.

My thanks are also extended to the research staff at Macquarie University GeoAnalytical. A big thank you goes to Timothy Murphy for being so patient with my altered (and hard to analyse) samples and helping me along the way. Another big thanks go to Stefan Loehr for always finding time to set up the NanoMin analysis, allowing me to use the processing computers and offering his expertise on the NanoMin. Thanks also to Steve Craven and Manal Bebbington for sample preparation.

Thank you also to School of Earth and Environment, Institute of Geophysics and Tectonics in the University of Leeds for allowing me to undertake some research there. With thanks to Harri Wyn

Williams for his careful sample preparation and Duncan Hedges at the Leeds Electron Microscopy and Spectroscopy Centre for further sample preparation.

My final thanks go to my family, friends and work! Thank you, Bridgeport Energy, for being so very understanding and flexible with my working arrangements. Throughout my time at university, I have developed many friendships and much of this masters cohort has been with me through the whole university experience. Carla Raymond and Anthony Finn, Tasman Gillfeather-Clark and Michael Farmer - thank you for all the chats and catch ups! Tasman, thanks for taking over as co-chair for GESSS-NSW 2017 and Michael, for putting up with me while we were in Leeds. A huge thank you goes to my wonderful boyfriend Sam, thanks for being supportive, offering wisdom and advice you gained through your PhD experience, proof-reading my work and being a wonderful individual. My biggest thanks go to my loving and so very supportive family – the Kovach clan. In *Surely You're Joking Mr. Feynman* (1992) he describes himself as a volcano, quietly working away during dormancy and then erupting every now again. Usually my eruptions were looking for snacks or complaining that I didn't know what the meteorites were doing, much to my family's dismay saying, "because I said so" doesn't quite cut it. Thank you to my awesome brother, William and my caring, patient and wonderful parents, Mato and Marijana. Thank you all so very much!

Contents

Acronyms and Abbreviations

AOA	Amoeboid olivine rain
AU	Astronomical unit
BSE	Back-scattered electron
CAI	Calcium-aluminium inclusion
CGR	Coarse grained rim
CPO	Crystallographic-preferred orientation
CM	Mighei-like group carbonaceous chondrite
CV	Vigarano-like group carbonaceous chondrite
EBSD	Electron backscatter diffraction
FEG	Field emission gun
FGR	Fine grained rim
EDS	Energy dispersive x-ray spectroscopy
Ga	Billion years ago
IPF	Inverse pole figure
Ma	Million years ago
MMSN	Minimum mass solar nebula
My	Million years
NanoMin	FEI Teneo Lovac FEG-SEM with dual Bruker Series 6 detectors
NWA	Northwest Africa
ROI	Region of interest
SEM	Scanning electron microscope
XRF	X-Ray fluorescence

Abstract

There are many unknowns when it comes to understanding our Solar System, one of them being the alteration processes that meteorites undergo. Meteorites represent a point in time from which they were extracted from the prevailing Solar System processes, therefore their microstructures, microtextures and composition provide invaluable evidence to the role of volatiles and early Solar System processes. This study examines three carbonaceous chondrites; NWA 3118, a CV and two CMs – Murchison and Sutter's Mill. These samples were analysed using SEM-EBSD and FEI Teneo Lovac FEG-SEM with dual Bruker Series 6 detectors (also referred to as NanoMin), each method presented various advantages and disadvantages. The observed microstructures enable the development of a timeline, where it is inferred whether the chondrites preserve primary formation or secondary alteration processes. From discussing and interpreting these microtextures, it was inferred that NWA 3118 provides an insight into predominantly primary formation features. In comparison, the microstructures seen in this Murchison sample indicate alteration on its parent body and multiple additions to the chondrite. Sutter's Mill underwent the same early processes as Murchison; however, its highly unusual lithology is attributed to potential asteroidal mixing. These findings are then linked to the role of volatiles, therefore gaining an insight into early Solar System processes.

Chapter 1 - Introduction and Aims

Meteorites are extra-terrestrial, early solar objects that have survived passage through the Earth's atmosphere; therefore, they provide invaluable physical evidence for processes occurring in our Solar System while it was still forming. The relationships between microstructures, microtextures and compositions found in carbonaceous chondrites reflect processes that were occurring during the early Solar System. This study focuses on a small set of carbonaceous chondrites and their microstructures to determine the nature and timing of alteration, whether it is single or multiple alteration events, in an asteroidal setting or on the parent body. The carbonaceous chondrites examined are, include NWA 3118, a CV and two CMs - Murchison and Sutter's Mill. A variety of qualitative and quantitative techniques have been previously applied to study meteorites; however, with technological advances, two unique and non-destructive methods have been used in this study - SEM-EBSD and the FEI Teneo Lovac FEG-SEM with dual Bruker Series 6 detectors (hereafter referred to as NanoMin). SEM-EBSD has existed for many years; however, it has had minimal application in the study of meteorites, despite its potential to provide quantitative and structural data on the behaviour of minerals. The newly acquired NanoMin, uses pioneering methods to provide high quality and high-resolution data to develop compositional phase maps. The NanoMin was chosen over other methods in hopes to discover its capabilities in analysing extra-terrestrial samples. The efficacies of each method with respect to the sample will be discussed; however, it becomes clear that when SEM-EBSD and NanoMin results are combined, they help to provide a bigger picture.

From this cryptocrystalline analysis on the three carbonaceous chondrites, the results have identified numerous microstructures and characteristics. The interpretation of these suggest the features are related to initial chondrite agglomeration, then followed by either primary and/or secondary alteration. Many chondritic groups have undergone aqueous alteration, which documents early Solar System volatile processes. Whether these processes occur on the meteorite parent body or in the solar nebula, the role of volatiles and the timescales regarding alteration remain vague and contentious.

This study aims to help shed light on the specifics of alteration - whether alteration occurred before or after chondrule formation, in the solar nebula or during planetesimal growth. These carbonaceous chondrites also allow the investigation of what effects shock-induced compaction and heating have on chondrite formation and whether there was aqueous alteration in the pre-solar nebula. In attempting to answer these questions, this thesis will also address whether CVs and CMs are linked, whether they have a very different history or are each part of the same larger picture.

Each of the samples demonstrates different features and processes. From the study of this set of samples, a sequence of alteration can be developed. It is hypothesised that NWA 3118 is the least altered sample and provides information on chondrule and chondrite formation processes along with minor alteration occurring on its parent body. Murchison is hypothesised as having undergone further and more extensive (multiple) alteration events at different times during chondrite formation, both in the nebula and on its parent body. The third sample, Sutter's Mill, shows unique features that are attributed to heavy alteration and thermal processing. The results suggest that these processes potentially occurred on two different parent bodies and interestingly shares some of the same alteration events that Murchison experienced. From this, the overall hypothesis developed from this study is that the CV (NWA 3118) underwent different and less alteration events compared to the CMs (Murchison and Sutter's Mill), where the chondrule formation and alteration processes occurred in a different region of the solar nebula.

From these considerations and through developing a sequence of alteration events seen in the cryptocrystalline features in NWA 3118, Murchison and Sutter's Mill a time-line of chondrule and chondrite formation and alteration is established. This allows important questions to be addressed, such as the types of volatile processes that could occur in the early Solar System.

Chapter 2 – Background

2.1 Introduction

In order to provide a context for the different modes of alteration in carbonaceous chondrites in the Solar System, it is important to first understand the background processes that led to the presently observed microstructures. In this regard, this chapter first contains a section outlining the formation of the Solar System. The next section outlines meteorite and chondrite formation models, with a focus on volatiles. This leads onto a discussion of chondrite origins, which allows the chondrite classification scheme and parent bodies to then be examined. The final section will briefly outline the different modes of alteration reported to occur in carbonaceous chondrites.

2.2 Formation of the Solar System

Our Solar System began its formation 4.5 to 4.6 Ga, with creation of a new star, which was surrounded by disk-shaped region of dust and gas: hydrogen, helium and volatile materials such as water and carbon monoxide (Chambers, 2004). This material was mostly composed of dust and it would eventually form the first fragments that led to terrestrial planetary formation, as explained by the planetesimal theory (Canup & Agnor, 2000). The planetesimal theory explains the size of the planets, the orbits and formation timescales; however, does not account for the size and location discrepancy of Mars and Mercury. This is where the Grand Tack model offers a solution. Walsh et al., (2011) found that the gas giant planets, Jupiter and Saturn, were major forces in the protoplanetary disk and underwent inward and then outward migration. In this case, Mars' small size is attributed to it forming in the outer edge of the planetesimal disk. Jupiter's movement would have reduced the ability of smaller planetesimal accretion and therefore permitted terrestrial planet accretion and formation, this is seen in Figure 2.1 (Walsh et al., 2012).

Despite being a basic building block of our Solar System and ultimately resulting in water on Earth, volatile formation and their role in Solar System processes remain controversial. Volatiles and heat processes in the Solar System are inherently linked. A volatile element has a low vapourisation temperature, such as the alkalis (K, Na) or Pb (Canup & Righter, 2000) and highly volatile elements include hydrogen, carbon, nitrogen, oxygen and the noble gases (Davis, 2006).

^{26}Al is a short-lived radioisotope that has led to the development of core-accretion planet formation models (Lichtenberg et al., 2016). The radioactive decay of ^{26}Al is believed to be the main heat source for the first 2 My after Solar System formation, during which time planetesimals and planetary embryos were forming (Grimm & McSween, 1993). This heat source enabled melting and

differentiation in the early Solar System. In response to these processes, (melting and differentiation) the previously accreted volatile elements were largely lost (Shearer et al., 1998). The volatiles observed today were probably accreted after this initial peak of internal heating (Sarafin et al., 2014). After ~ 2 My, the amount of ^{26}Al decreased, and there was not enough to melt and differentiate most planetesimals. This period after 2 My is preserved in chondritic meteorites (Alexander, 2017a).

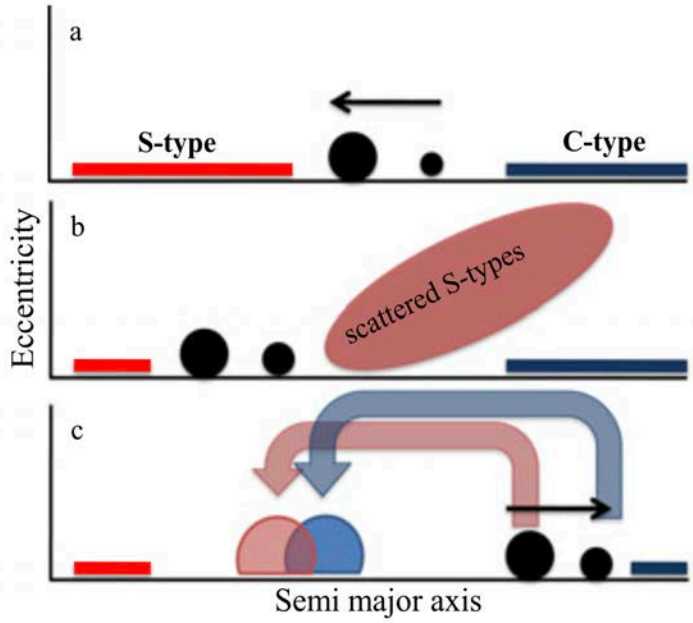

Figure 2.1 *- Grand Tack model schematic. The large black circle is Jupiter and Saturn is the small circle. The S-type planetesimal disk is red and represents the diverse population of volatile- poor or dry, asteroids. The C-type disk is blue and is located both between and beyond the giant planets, it represents the more primitive populations of asteroids. Inset A) inward migration of Jupiter and Saturn (arrow pointing to the left) B) outward migration C) scattering of the two distinct populations of planetesimals. C) Shows how the final configuration is a truncated inner disk of planetesimals that would be needed to reproduce the Earth/ Mars mass ratio and if the asteroid belt is repopulated with bodies from both the S- and C-type parent populations (Walsh et al., 2012)*

2.3 Meteorite and chondrite formation models

Meteorites were formed in the early Solar System when there was a presence of volatile activity (McSween, 1999). They originate from heated portions of the solar nebula, when protoplanets were accumulating from condensed material with some volatile elements. Meteorites can therefore be described as aggregates that can contain chemically and thermally processed Solar System material and pre-solar grains (Wasserburg et al., 2006). Within the meteorite groups, there are differing volatile contents and these differences are interpreted to be due to different degrees of volatile depletion processes acting upon the meteorite (Bland et al., 2009). Various models of volatile depletion have been presented in previous studies, with the major hypotheses being the 1) two component model and 2) incomplete condensation models. The two-component model was suggested by Anders (1964) and Larimer & Anders (1967) and states that evaporation during chondrule formation led to element fractionation. Then variations in the mixing ratio of volatile-depleted chondrule and associated undepleted matrix resulted in different volatile element abundances in bulk meteorite parent bodies. This caused discussion within the scientific

community, because the two-component model was based on poorly known condensation temperatures and weakly determined elemental abundances (Davis, 2006).

Subsequently, Wasson & Chou (1974) and Wai & Wasson (1977) developed the incomplete condensation model where equilibrium condensation from the continuous loss of nebular gas and resulted in chondrites containing moderately volatile elements. These earlier studies suggest that complete volatile loss during chondrule formation was unlikely due to the determined high cooling rates of chondrules and the volatile abundance pattern would be smooth function between condensation and temperature. More recently, Alexander et al., (2001) demonstrated an enhanced model with a two-component system arguing that during chondrule formation, kinetically controlled volatile fractionation would explain the difference in volatile components. This model explains how the volatile rich component (the matrix) accreted together with volatile-depleted chondrules. The debate regarding volatile depletion models continues with new research and it is becoming clear is that the role of volatiles is increasingly important in our understanding of early Solar System processes.

2.4 Chondrule formation models

All chondrites provide information on Solar System processes and therefore, the progression of volatiles (Alexander et al., 2001). It is thought that chondrules are representative of coalesced dust aggregates that underwent rapid melting and cooling in lower temperature regions (< 1000 K) in the Solar System, which ultimately resulted in porphyritic textures (Scott, 2007). Connelly et al., (2012) state that despite chondrites originating from different parent bodies and having undergone various alteration processes, one commonality is present; they were exposed to brief, high-temperature events at least once during their development.

Many models attempting to explain chondrule formation are presented in Boss, (1996); however, in recent times models which incorporate multiple components are favoured. This section will examine chondrule formation through colliding molten planetesimals, recycling of fragmented differentiated planetesimals, the nebular shock wave model and impact jetting model.

2.4.1 Colliding of molten planetesimals model

Asphaug et al., (2011) present the idea that when molten or partially molten planetesimals, approximately 30 – 100 km in diameter collide, there is not enough velocity to produce shocks. Modelling displays that the inner portions of the colliding material slows down when it reaches its planetesimal, while the rest of the material in the nebula achieves equilibrium with the surface

energy of chondrule-sized droplets. Some of these droplets go back to the planetesimal, while the rest is dispersed. This agrees with ^{26}Al data and deduced collisional accretion times (Bizzarro et al., 2005).

2.4.2 Recycling of fragmented differentiated planetesimals model

Libourel & Krot (2007) examined the mineralogy of magnesian chondrules and proposed that Type 1 porphyritic chondrules are composed of nebular and asteroidal materials and must have post-dated accretion, thermal metamorphism and differentiation of some early generation planetesimals. This indicates that some chondrules were formed from the remnants of already differentiated planetesimals. This model corresponds with the Pb-Pb and Al-Mg relative model ages of CV bulk chondrules (Bizzarro et al., 2004 and Amelin et al., 2004).

2.4.3 Nebular shock wave model

The chondrule formation models described in Sections 2.4.1 and 2.4.2 are based on the assumption that there was 1 -2 My between CAI formation and chondrule formation. This does not agree with models stating that CAI and chondrule formation occurred simultaneously (Connelly et al., 2012), which is when nebular shock wave models are preferred. This was first proposed by Hood & Horányi (1991) and Hood & Horányi (1993) and states that when a shock wave propagates through the interior of the nebula, precursor aggregates are overtaken, resulting in melting. The melting processes may arise from; gas drag, gas thermal energy that is lost by gas-grain collisions and thermal radiation generated from the other dust grains. The plausibility of this model is explained through the heterogeneity currently observed in chondrules, where when considering the scale of the nebula, the shock waves would be quite localised and not homogenise their products (Boss, 1996).

2.4.4 Impact jetting model

Johnson et al., (2015) expanded findings by Connelly et al., (2012) and postulated that during the first 5 My of planetary accretion, impacts between protoplanetary bodies resulted in melting (Johnson et al., 2014). Some material was ejected at high speeds (Johnson et al., 2014) and Monte Carlo simulations show the ejecta forms millimetre-scale droplets. It predicts that the earliest chondrule-forming impacts occur closest to the Sun, then over time move away (Figure 2.2). This model also states that only a small amount of terrestrial planet mass has been processed into chondrules, therefore chondrules are the by-product of planetary accretion, rather than being the direct building blocks (Johnson et al., 2015).

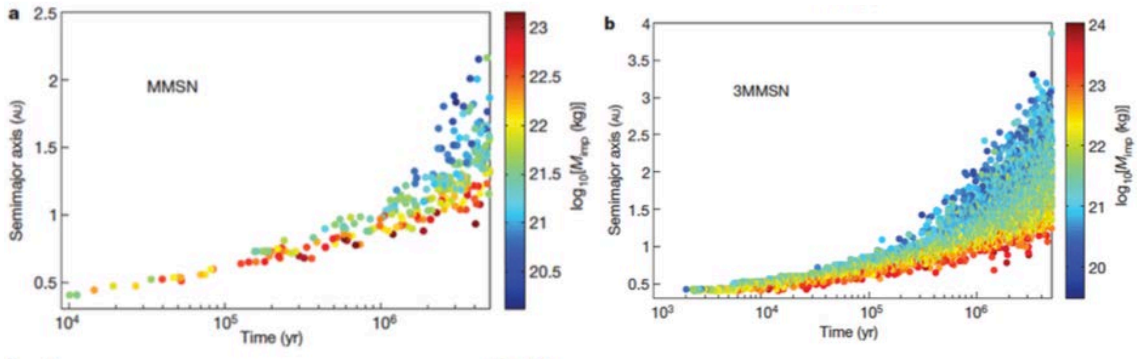

Figure 2.2- *Timing and location of chondrule-forming impact. A) Chondrule-forming impacts with velocities above 2.5kms^{-1} for MMSN model. B) 3MMSN model. Johnson et al. (2015)*

2.5 Chondrite classification and parent bodies

In order to examine the prevalent chondrite classification scheme, it is first important to understand the systematics of meteorite classification, seen in Figure 2.3. This classification divides the meteorites into their respective class, clan, group and subgroup based on various features (Weisberg et al., 2006). The first division examines whether the meteorite is differentiated and contains chondrules. The next division is termed a class and is determined on refractory lithophile-element abundances. The clan subdivision is also based on refractory lithophile-element abundances; however, also encompasses the O-isotopic mixing line, isotopic anomalies and petrological characteristics. Finally, the group subdivision infers the meteorite parent body (Weisberg et al., 2006). In this way, different chondritic groups represent single parent bodies in the asteroid belt (Jones et al., 2000).

Bottke & Morbidelli (2017) state the asteroid belt is in the inner Solar System, located between 2.1 – 3.2 AU and contain a large population of remnant planetesimals. There are many asteroid families within the asteroid belt and these families are the remains of cratering and catastrophic disruption events of planetesimals in the main belt. There are a large variety of meteorite types, however, this thesis will examine the parent bodies of CV3, CM2 and enstatite/aubrite chondrites.

2.5.1 CV parent bodies

The CV used in this study NWA 3118, is thought to originate from the Eos asteroid family (Hardersen et al., 2011 and Mothe-Dinz et al., 2008). There are spectral similarities in visible and near-infrared between CV chondrites and Eos family asteroids (Figure 2.4). The Eos family has over 9000 members, composed of K-type asteroid and is an outer main-belt family (Nesvorný et al., 2015). Mothe-Dinz et al., (2008) found through mineralogical analysis that the Eos asteroids are composed of forsterite-rich olivine with minor low calcium pyroxene.

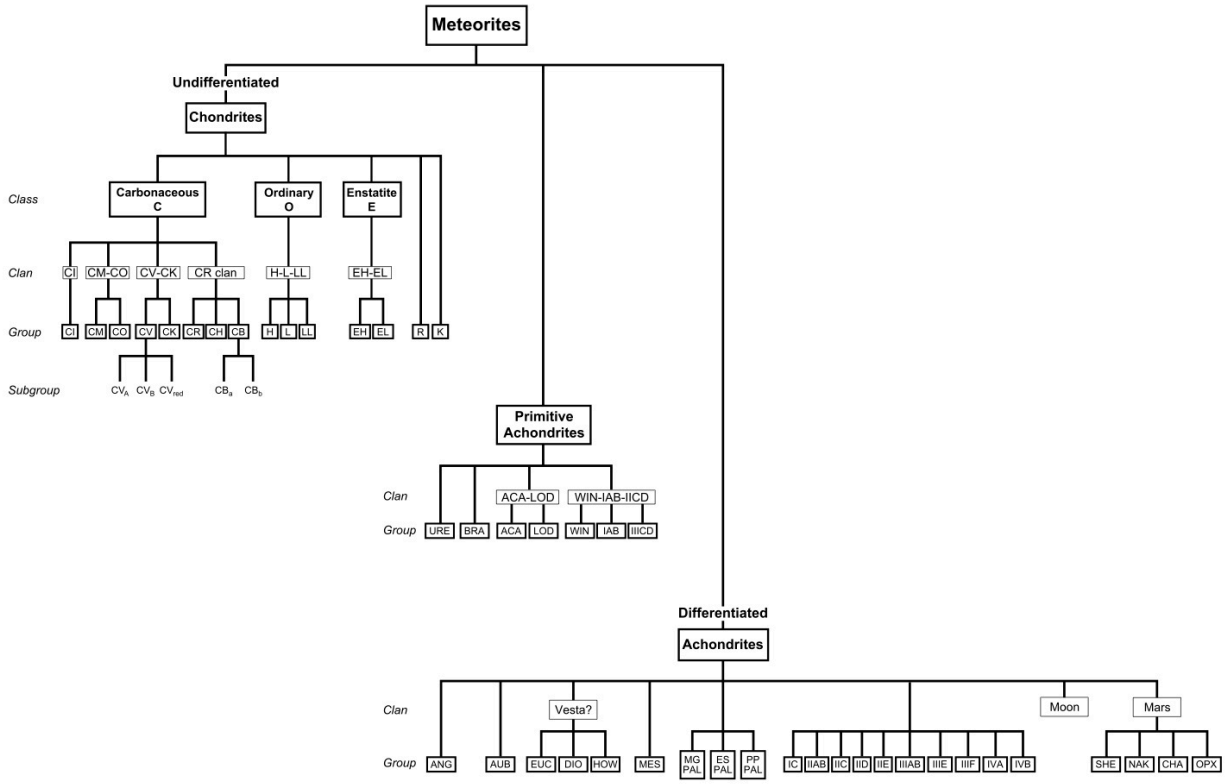

Figure 2.3- *Meteorite classification diagram, demonstrating the divisions, classes, clans and groups. URE - ureilite, ACA – acapulcoite, LOD – lodranite, ANG – angrite, AUB – aubrite, BRA – brachinite, WIN – winonaite, HED – howardite-eucrite-diogenite, MES – mesosiderite, MG PAL – main-group pallasite, ES PAL – Eagle Station pallasite, PP PAL – pyroxene pallasite, SHE – shergottite, NAK – nakhlite, CHA – chassignite, OPX – orthopyroxenite (Weisberg et al., 2006).*

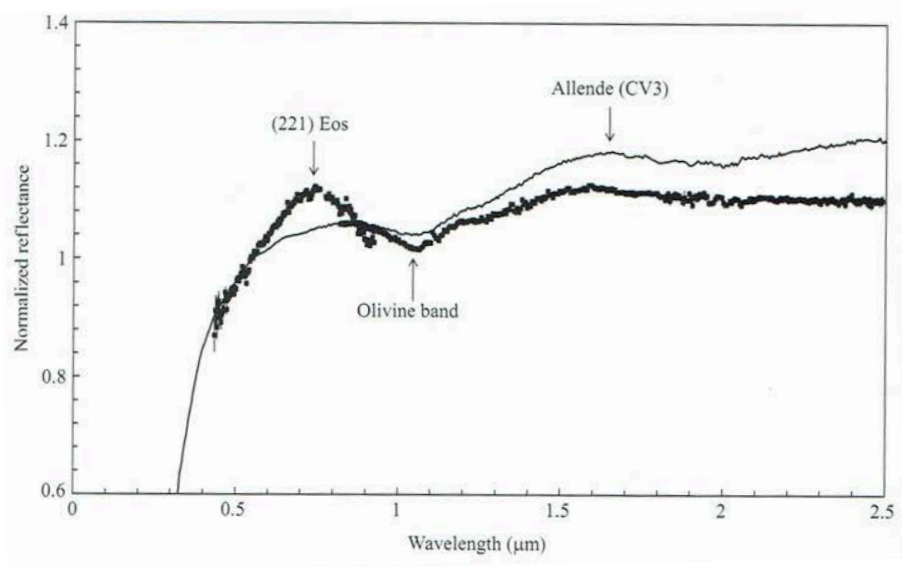

Figure 2.4 - *Reflectance spectrum of K-type Eos and a CV3 (Allende). There is a weak overlap of spectrum in the near-infrared. Shown in Burbine et al., (2017) and adapted from Clark et al., (2009); Bus (2011) and Sunshine et al., (2008).*

2.5.2 CM parent bodies

Murchison is a CM chondrite, while Sutter's Mill contains CM-like properties. The CM chondrites are believed to have originated from C-type asteroids (Beck et al., 2010). C-type asteroids are thought to be the most common asteroids in the main belt and are potentially from the outer part of the main belt (Jones et al., 1990). The observation that both the CM chondrites and C-type asteroids having corresponding absorption bands (Figure 2.5) for hydrated minerals suggest a genetic link. Phyllosilicates produce a weak absorption band in both CM chondrite and C-type asteroid from the Fe content in phyllosilicates and organic matter content (Figure 2.4) (McSween, 1999).

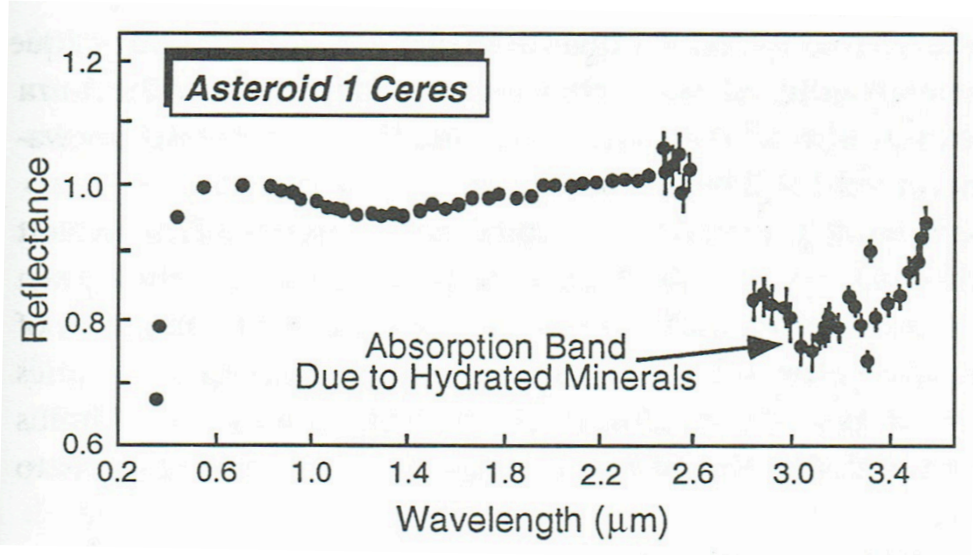

Figure 2.5 *- Ceres is a C-type asteroid and this graph shows the 1 Ceres spectrum. There is a deep absorption band in the infrared region (3 μm wavelength), which is thought to be due to hydrated minerals (McSween, 1999).*

2.5.3 Enstatite/Aubrite parent bodies

Although Sutter's Mill has been found to contain mostly CM clasts (Zolenksy et al., 2014), there are some indications that Sutter's Mill also has lithologies corresponding to enstatite/aubrite chondrites (Zolensky et al., 2012). Aubrite and enstatite chondrites are inferred to be from E-type parent bodies due to both having a high visible albedo and a relatively featureless reflectance spectrum in the visible and near infra-red (Figure 2.6) (Zellner et al., 1977). The E-type asteroids are from the Hungaria family, which are also from the Hungaria region (1.78 – 2.0 AU) and there are approximately 3000 members (Nesvorný et al., 2015). The spectrum is relatively featureless and this is thought to be due to the FeO-poor enstatite composition (Gaffey, 1976). McCoy et al., (1999) also infer that melting is common on E-type asteroids.

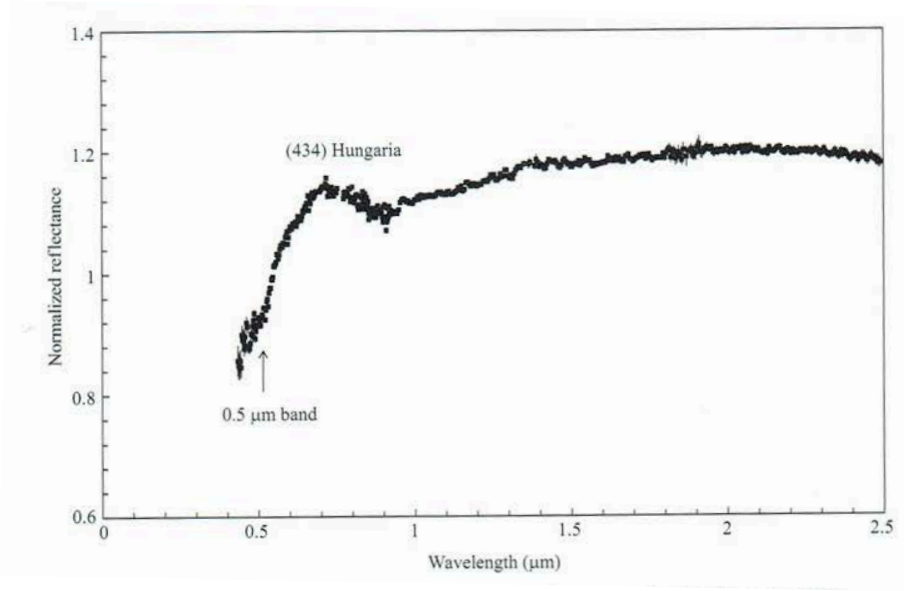

Figure 2.6 *- Reflectance spectrum of E-type Hungaria. There is a weak overlap of visible spectrum and the near-infrared spectrum in the visible wavelengths. Shown in Burbine et al., (2017) and adapted from Clark et al., (2004) and Bus, (2011).*

2.6 Modes of alteration in carbonaceous chondrites

Chondrules can either undergo primary or secondary processes (Brearley & Jones, 1998). Primary processes are when individual components of the chondrule are affected during its formation. While secondary processes affect the whole rock after accretion and include; aqueous alteration and both thermal and shock metamorphism. The degree of alteration seen in carbonaceous chondrites varies amongst the carbonaceous chondrite groups and this is seen in Figure 2.7. Jones et al., (2005) discuss how secondary processes potentially occurred on the chondritic parent bodies, either in the nebula or parent body, where there was a series of reactions between gas and solids.

2.6.1 Aqueous alteration

Aqueous alteration is amongst the most prevalent processes that has affected chondritic meteorites and primitive Solar System materials (Brearley, 2006). In chondrites, the initial, anhydrous, primary precursor assemblage underwent aqueous alteration, growth of hydrous phases and secondary hydrous minerals are produced (such as phyllosilicates) (Brearley & Jones, 1998, and Doyle et al. 2015). Aqueous alteration would have ceased with the exhaustion of the fluid supply, leading to the preservation of anhydrous silicates presently seen in many meteorite samples (Doyle et al., 2015). Zolensky et al., (2008) undertook studies using isotopes, thermodynamics and observed mineralogies and presented the idea that aqueous alteration occurred in an asteroidal setting, due to the interaction between rock and aqueous fluid.

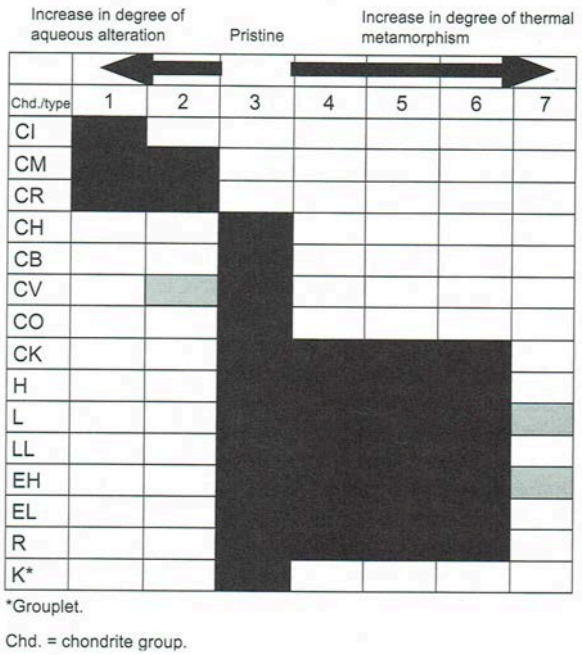

Figure 2.7- *Diagram displaying the chondrite groups and their petrological types (Weisberg et al., 2006).*

2.6.2 Metasomatism

Naumann, (1826) first defined metasomatism as a metamorphic process by which a rock's chemical component undergoes pervasive alteration due to its interaction with aqueous fluids. These fluids either add or remove chemical components in the rock and the rock remains in a solid state. These fluids involved during aqueous alteration and metasomatism substantially change the existent primary phase structures and compositions to secondary alteration products (Brearley & Krot, 2013).

2.6.3 Thermal metamorphism

Thermal metamorphism is another secondary process that alters chondrites and it is generally thought it occur on parent bodies, within a few million years after accretion (Brearley & Jones, 1998 and Huss et al., 2006). During thermal metamorphism, some phyllosilicates were dehydrated and amorphous silicate phases are subsequently produced (McAdam et al., 2015). The source of thermal metamorphism is thought to be due to accretional or collisional heating, electromagnetic induction (Wood & Pellas, 1991) or the decay of short-lived radionuclides (Sapah, 2016).

2.6.4 Shock metamorphism

Many chondrites have been subjected to varying degrees of impact processing (Bunch & Rajan, 1998). Sharp & DeCarli (2006) state that shock metamorphism in chondrites either results in deformation or transformation and is often a combination of both. Where deformational effects

include; fracturing, plastic deformation and twinning. While, transformational effects consist of; shock melting – which results in localised melt veins and pockets, transformation of precursor minerals to high pressure polymorphs and crystallisation of highly deformed material (Sharp & DeCarli, 2006).

2.7 Concluding Remarks

It is currently not possible to observe processes in the early Solar System, which is why the study of meteorites is crucial in our attempts to answer the unknowns. It is through this research, that we gain a more holistic picture with regards to; the formation of the Solar System, chondrite and chondrule formation processes and modes of alteration on carbonaceous chondrites.

Chapter 3 - Methodology

3.1 Introduction

This chapter is divided into three sections. The first section provides an outline on the NWA 3118, Murchison and Sutter's Mill backgrounds with references to the main studies for each sample. The next section provides a brief description on instrument information for the SEM-EBSD and a more detailed description for the NanoMin. And finally, the last section describes the sample preparation and the operating conditions used during the micro-XRF, SEM-EBSD and NanoMin analysis.

3.2 Sample Background

3.2.1 NWA 3118

The 89th Meteoritic Bulletin by Russell et al., (2005) states how 5895 g of NWA 3118 fragments were purchased in Erfoud, Morocco in December 2003. As it was a desert find, it has undergone some degree of weathering and alteration. NWA 3118 is a carbonaceous, CV3 chondrite, with a low weathering grade and is described as olive-grey to tan in colour, depending on the degree of weathering. Ivanova et al., (2010a, 2010b, 2011a, 2011b & 2013) found various CAI grains present in the chondrite, where heterogeneity in bulk composition resulted in enrichment in Zr, Sc and Y. And Akos et al., (2014) examined the implications of 'ripple-like' features found in the matrix.

3.2.2 Murchison

Murchison is classified as a type II carbonaceous chondrite that has undergone aqueous alteration. It was an observed fall near the town, Murchison in Victoria, Australia on the 28th September 1969. Fuchs et al., (1973) was amongst the first studies conducted on Murchison and outlined how the meteorite fall consisted of samples varying from a few grams to several kilograms. More than 100 kg was recovered, for the most part after the fall and most of the pieces are surrounded by a fusion crust. However, in some cases the fusion crust was either broken off or cracked. Several samples also have evidence of extreme desiccation cracking and this is likely due to the loss of volatiles. The mineralogy of Murchison was also first examined by Fuchs et al., (1973) and described as mostly pyroxene, enstatite, serpentine, olivine and iron oxides. This CM2 has been subject of many subsequent studies; including, Fujumura et al., (1983); Bunch & Chang, (1980); Scott et al., (1992); Metlzer et al., (1992); Palmer & Lauretta, (1992); Hanna et al., (2015); Lindgren et al., (2015); King et al., (2017) and Ireland et al., (1988).

3.2.3 Sutter's Mill

A detailed study by Jenniskens et al., (2012) states how Doppler weather radar imaging detected the Sutter's Mills meteorite fall on the 22nd April 2012, therefore enabling fast recovery of the meteorite on the impact site on the foothills of the Sierra Nevada in northern California. Three pieces were collected on the 24th April; however, afterwards there was heavy rainfall in the area. Over 100 pieces were collected, amounting to 943 g, with the largest pieces weighing 205 g. Zhao et al., (2014) describes Sutter's Mill as a regolith breccia that is comprised of CM2 clasts with varying degrees of aqueous alteration and thermal metamorphism. Within the meteorite suite there is substantial mineralogical, petrographic, isotopic and organic chemistry diversity and this is attributed to the complex formation history of the parent body surface (Jenniskens et al., 2012). Zolensky et al., (2012) attributes this complexity to different asteroid mixing. The Sutter's Mill meteorite fall was the topic of a special Meteoritical Society bulletin, some of the studies include; Jilly et al., (2014); Zhao et al., (2014), Yesiltas et al., (2014); Nishiizumi et al., (2014) and Zolensky et al., (2014).

3.3 Background Instrument Information

3.3.1 Micro-XRF

The Micro-XRF operates based on a focused X-ray beam penetrating the material, from this a small volume of the material is excited and produces characteristic X-rays- unique to each of the elements in the material. These X-rays result in the sample having fluorescence, and can then be detected by the energy dispersive detector (Bruker, 2017).

3.3.2 SEM-EBSD

The conventional SEM is described by Seiler (1983) and is based on the production of electrons from a source, the electrons are focused into a monochromatic beam and accelerated towards a sample. When the electrons hit the sample surface, the electrons scan the sample and the difference between the sample and the electron response is measured.

While the EBSD is an application of the SEM, where the sample is tilted to 70° under a high vacuum. When the sample is highly tilted to 70°, the electrons are reflected relative to the incident electron beam, this results in Bragg diffraction from the crystal structure. The produced EBSD patterns are unique for different crystal orientations at the point of beam incidence. Watt et al., (2006) provides more detail pertaining to how EBSD works and its application when analysing meteorites.

3.3.3 NanoMin

The NanoMin is considered an extension of the SEM, it generally has the same mechanical components; however, the NanoMin has additional detectors which means the results differ from those obtained by the SEM. In the NanoMin there are three separate in-lens detectors that operate simultaneously and this allows simultaneous detection from all angles. In this way, the NanoMin does not constrain the number of minerals per pixel and assign the material as a pure phase. Rather, it classifies the material as a mix of minerals where multiple mineral variety end members are linked to that end-member solution. FEI (2016) states how the NanoMin delivers ultra-high-resolution imaging and high output analytical performance. It can analyse a wide variety of samples, relatively quickly and it is easily interpreted. This ultimately saves time and maximises the information acquired. This also prevents sample contamination and damage.

One of the main benefits of using the NanoMin include, its ability to analyse fine-grained materials. In the past, the matrix would have been unclassified, miss-indexed or assigned one phase, while on the Nanomin multiple minerals and elements are assigned to these fine-grained areas. The NanoMin reduces the amount of time needed on processing and once the analysis is completed, it is straightforward to add or remove meteorite specific minerals and produce new maps. However, there also some corresponding limitations when using NanoMin. It is spectra specific and defined by chemical variations. Additionally, it is also user specific, the user determines the minerals that will be used for further analysis.

3.4 Sample preparation

The three samples NWA 3118, Murchison and Sutter's Mill were mounted in epoxy mounts and polished in preparation for analysis. For SEM-EBSD analysis, further polishing was undertaken using a Kent- 3 polisher, Kemet Col-K polishing slurry that was diluted with water and acted as an abrasive. Before analysis, the mounts were also carbon coated, for SEM-EBSD the carbon coats were thin, while for the NanoMin, the carbon coat was thicker. No sample preparation was needed for the XRF.

3.5 Operating Conditions

3.5.1 Micro-XRF

Initially, micro-XRF analysis was conducted through the Bruker M4 Tornado on the whole sample in Macquarie University GeoAnalytical, Sydney, Australia. The spot size was 20 μm, at 50 kV accelerating voltage and with a 30 ms dwell time.

3.5.2 EBSD

SEM-EBSD analysis of NWA 3118 was undertaken in the Leeds Electron Microscopy and Spectroscopy Centre in the University of Leeds, United Kingdom. The instrument operating conditions were as follows; working distance 27.40 mm, beam diameter 5µm and accelerating voltage 20 kV.

The other analysis was completed in Macquarie University GeoAnalytical, Sydney. A Zeiss EVO MA15 SEM (with OXFORD Instruments Aztec Synergy EDS/ EBSD) was used to obtain data on Murchison, with the following instrument operating conditions; working distance 20.0 mm, beam diameter 2.10 µm and accelerating voltage 15 kV. On the Aztec software, the results were exported for post processing on HKL Channel 5 Software, were the results seen in Chapter 4 were developed.

3.5.3 NanoMin

The three samples were also analysed using the NanoMin - FEI Teneo Lovac FEG-SEM with dual Bruker Series 6 detectors, in Macquarie University GeoAnalytical, Sydney. For the three samples, some operating parameters remained the same, these include; working distance 13 mm, accelerating voltage 15 kV, x-ray spacing 2.5 µm and a resolution of 2048 by 2048. In NWA 3118, the horizontal field width was 1.66 µm and for Murchison it was 82.8 µm. For Sutter's Mill, the overall sample analysis had a horizontal field width of 500 µm, ROI 1 horizontal field width 41.1 µm and ROI 2 horizontal field width 2 µm.

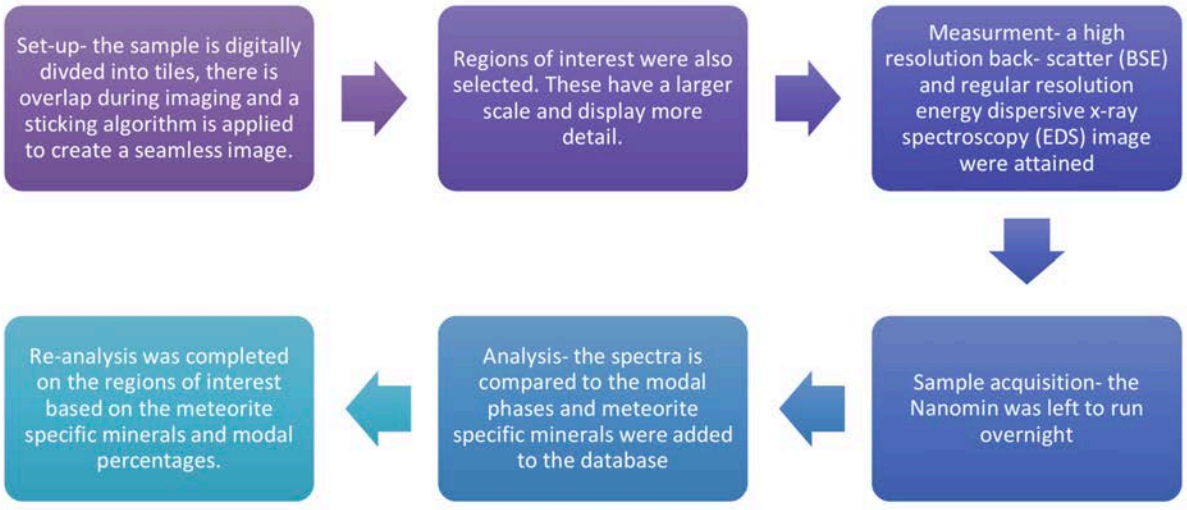

Figure 3.1- *Flow diagram of the steps undertaken during NanoMin analysis.*

The ‘Meteorite Recipe’ that was applied to the samples was developed through comparing and noting the discovered mineralogy of the samples in previous research on these meteorite falls, such as those stated in the sample description. In addition to previous research undertaken on the same samples by Gazi (2016). The overall NanoMin analysis process is demonstrated in the flow diagram seen in Figure 3.1.

The NanoMin results provided in Chapter 4 are to a degree, the initial analysis of the samples. Post processing that was undertaken was completed on the Maps software and included noting the modal percentages, examining unclassified minerals and attempting to assign a spectrum based on their chemistry and texture. From this, minerals where either added or eliminated to the ‘Meteorite Recipe’ and then the sample was re-analysed. The Maps software also provided an interface to navigate, highlight specific features in the sample and export the NanoMin analysis.

3.6 Concluding remarks

The methods applied in this project enabled analysis to be undertaken on the carbonaceous chondrites; NWA 3118, Murchison and Sutter’s Mill. The micro-XRF results were used to gain an idea of the elements present and localities of the chondrules and interesting features. Where applicable, NanoMin and EBSD analysis was undertaken in the same areas, to demonstrate the different types of results these methods produce.

Chapter 4 - Results

4.1 Introduction

This chapter presents the results from the various analytical techniques applied to NWA 3118, Murchison and Sutter's Mill carbonaceous chondrites. It is organised so the results for each meteorite is presented separately and its overall characteristics are outlines in a table based on the BSE, mirco-XRF and NanoMin analysis. More specific features are examined with further NanoMin and EBSD analysis. A larger NanoMin key and additional EBSD for NWA 3118 are provided in the Supplementary Material Chapter. These observed results will be discussed and interpreted in the Chapter 5, with the aim to gain an insight in alteration affecting carbonaceous and ultimately, early Solar System processes.

4.2 NWA 3118 - *CV3*

4.2.1 General features

NWA 3118 is roughly composed of 65% matrix, 30% chondrules and 5% other components - mainly 'agglomerations' (Figure 4.1 & 4.2). The chondrules range in size, the observed smaller chondrules have a diameter of ~ 100 μm, the larger chondrules diameter is ~ 2 mm and on average their diameter is ~ 1 mm. The micro-XRF data indicates it is Fe, Ni rich with some Si and S rich areas (Figure 4.1), where the matrix is relatively homogenous; however, the chondrules are very heterogenous. From the NanoMin and EBSD analysis, the following chondrule types were observed; porphyritic with a fine–grained rim (Chondrules 1 and 2), poikilitic - porphyritic (Chondrules 3 and 4) and granular (Chondrules 5, 6 and 7). Table 1 displays the major component characteristics and then examines in detail the features observed in the individual chondrules or their chondrule group.

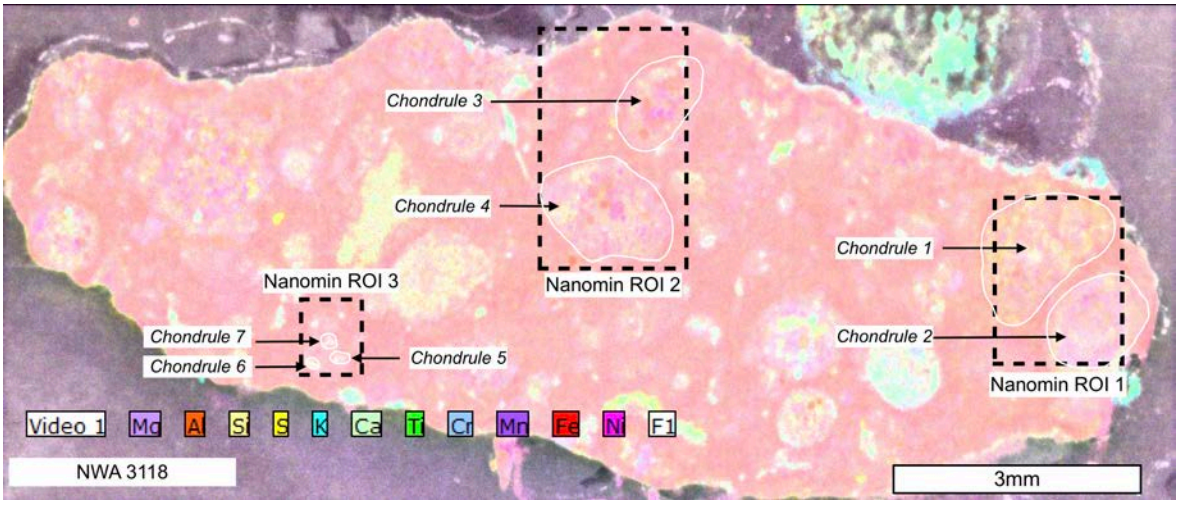

Figure 4.1 *- Annotated, false coloured micro-XRF map of NWA 3118 with the element colours and scale indicated. The NanoMin ROIs and chondrule locations are also shown.*

Table 1- *NWA 3118*

Components and overall modal %	Phase %	Grain Size	Phase Specifics					Minor Phases	Reaction Rim Characteristics
			Texture	Interstitial Material	Zoning	Sub-grain Boundaries	Preferred Orientation		
Matrix 65%	49% enstatite 49% goethite 2% clinochlore	Ranging from < 1 µm to 5 µm. Moderate to high porosity.	~ 49% matrix- ~ 10 µm long, ~ 1 µm wide elongate, platy, tabular and lath-shaped euhedral crystals. ~ 49% matrix- fine-grained (< 1 µm – 3 µm), irregularly shaped, and occur in the interstices of the elongate matrix grains.	~2% clinochlore-anhedral, very fine-grained (< 1 µm) occurs in the interstices of the goethite and enstatite matrix.	No matrix zoning observed in NanoMin data or in BSE analysis.	No EBSD analysis undertaken on matrix.	Weak and mostly defined by the agglomerations and compositional changes in the matrix (presence of clinochlore). Flow banding.	Apatite, fluorite, pyrite, hematite, spinel grains (from ~1 µm to 5 µm) distributed in various places in the matrix.	None observed in the matrix.
Chondrules (general) 30%	Olivine - 70% Enstatite - 20% Interstitial material 10% clinochlore. Fluid inclusions observed too.	Actual chondrules ~ 1 mm on average, smaller ones ~ 100 µm, largest one ~ 2 mm.	Olivine - some isometric (~ 25 – 50 µm), some sub-rounded (rosette) (~ 50 µm), some elongate with rounded edges (~ 150 µm long, ~ 50 µm wide). Enstatite - platy, elongate laths, subhedreal, smaller ones 20 µm long, 5 µm wide, larger ones 20 µm long, 10 µm wide.	Generally, forsterite, clinochlore and chamosite (more detail in individual chondrules, see below).	Fayalite rich rim (1 – 15 µm) on the perimeter of the olivine grains with a forsterite core. Olivine grains are generally more rounded in core and tabular on edge.	Higher frequency of low angle (< 5°) sub-grain boundaries in finer grained material (Chondrules 3, 4). In chondrule 2, there are low angle (< 5°) sub-grain boundaries in association with larger olivine grains.	Chondrules randomly distributed through the sample.	Spherical inclusions. Minor phases discussed below in detail for each chondrule.	Distinct fine-grained observed in ROI 1 - Extremely fine-grained (<1 µm) heterogeneous, olivine rich (~70%), goethite 10%, enstatite 10%, augite 5%, apatite 5%. Petrofabric alignment defined by elongate olivine grains (~ 10 µm long).
Other- 5% Agglomerations	Two compositions 1. Quartz SiO_2 40%, fluorite- 35%, goethite - 25% 2. Diopside - 80% goethite- 20%	From < 1µm rounded grains to ~ 200 µm long and ~ 10 µm wide elongate laths.	Mostly amoeboid shaped, mostly extremely fine-grained (< 1 µm), with some 1 µm rounded grains within the agglomerations.	Not relevant.	Larger agglomerations (> 40 µm) quartz, fluorite, goethite core, and diopside- goethite rims from < 1 µm scale to ~ 10 µm. Smaller grains composed of diopside and goethite.	No EBSD analysis undertaken.	The matrix and the agglomerations 'wrap' themselves around the chondrules.	Hematite, apatite and calcite.	Gradual transition from the rim to core. Distinct boundary between rim composition and euhedral core (quartz, fluorite and goethite).

Chondrule 1 *ROI 1* Unusual porphyritic olivine pyroxene chondrule with FGR **See ssupplementary material for more EBSD data*	Forsterite 15% Enstatite 40% Anorthite 5% Mesostasis 40%	Forsterite small ones ~ 10 µm, larger ones ~ 80 µm. Enstatite average ~ 30 µm. Anorthite average ~ 50 µm	Forsterite - some are sub-rounded, others are rosette shaped. Enstatite - anhedral laths, ~ 30 µm long, 1 – 2 µm wide. Anorthite - amoeboid habit ~ 75 µm long, ~ 10 µm wide.	Two interstitial compositions (50% each). 1. Same as overall FGR (see last column) 2. Same as matrix discussed for ROI 2 & 3.	Forsterite - Fayalite rim and forsterite core. Enstatite - homogenous grains, the fractures have been infilled with fayalite rich. Anorthite - homogenous.	High frequency of sub-grain boundaries in olivine grains.	Enstatite- most dominant CPO. There are 3 distinct clusters and each cluster has the same CPO.	Pixels of spinel and fluorite. Some hematite too.	Not well defined rim surrounding this chondrule. Slightly higher concentration of enstatite and goethite compared to the over FGR. Roughly same grain size.
Chondrule 2 *ROI 1* Porphyritic olivine pyroxene chondrule with FGR **See ssupplementary material for more EBSD data*	Forsterite 80% Enstatite 10% Clinochlore, chamosite and mesostasis 10%	Forsterite - small ones ~ 50 µm, larger ones ~ 200 µm. Enstatite - range from ~ 70 µm to ~ 300 µm	Forsterite - centre of chondrule-rounded. Outer edge- angular, more elongate, rosette shaped. Enstatite - tabular- 100 µm long, 20 µm wide. Clinochlore- very fine grained, < 1 µm scale.	Clinochlore and chamosite - ~95% of interstitial material, porous, higher amount in chondrule core. Jadeite (similar texture to 'agglomerations'). Goethite- 1µm sub-rounded grains.	Forsterite have a fayalitic rim (< 1 µm). Enstatite had a thin (< 1 µm) clinochore rim.	High frequency of sub-grain boundaries close to and same orientation of fractures (also more clinochlore rich area).	Larger forsterite on edge of chondrule have the same Euler angles. Roughly same Euler angles along either side of fractures. Elongate olivine grains are aligned in the same orientation as the fractures.	Some spherical inclusions (~ 10 – 100 µm) that occur on top of the fractures, composed of goethite, hematite, and unclassified material. Some pixels of spinel and anorthite.	Much of the elongate enstatite occurs on the edges. Gradual compositional change surrounding this chondrule (increase in goethite and enstatite) compared to overall FGR.
Chondrule 3 *ROI 2* Poikilitic - porphyritic olivine pyroxene chondrule	Forsterite - 60% Enstatite - 15% Pyroxene - 5% Clinochlore and mesostasis - 5% Minor phases - 5%	Forsterite - 5 – 200 µm Enstatite - 10 – 100 µm Pyroxene - 10 – 200 µm Clinochlore - sub µm Minor phases - 2 - 10 µm	Forsterite - fracturing >90% of grains, sub-rounded, rosette habit- smaller 30µm long, 10 µm wide, larger, 250 µm long, 100 µm wide. Pyroxene - irregularly shaped, small grains ~ 5 µm, larger - 50 µm long, 10 µm wide. Enstatite – tabular - 10 µm long, 20 µm wide, intergrowths with coarse grained rim. Clinochlore - very fine grained, < 1 µm, highly porous.	Clinochlore and chamosite - porous, ~ 80% of interstitial material, < 1 µm scale, fine-grained. Mottled with goethite, enstatite and unclassified material. Some anorthite homogenous grains, irregularly shaped.	Larger, less fractured forsterite grains (~ 40%) have fayalitic rim (< 1 µm). Heavily fractured forsterite grains have gradual compositional zoning from forsterite to fayalite. Enstatite had a thin (< 1 µm) clinochore rim. Pyroxene is homogenous.	High frequency of sub-grain boundaries in smaller and heavily fractured forsterite grains. Very few (< 10%) larger forsterite grains have sub-grain boundaries. No sub-grain boundaries in enstatite. Pyroxene ~ 50% grains have sub-grain boundaries.	Fractured forsterite grains have approximately the same orientation according to all Euler and Euler 1. No pattern observed in larger forsterite grains.	Spherical grains (~ 10 µm diameter) of spinel located in forsterite spherical apertures Spherical inclusions, composed of goethite, hematite and unclassified material, 30% are spherical, 70% are sub-rounded.	Poikilitic relationship with matrix, same composition as matrix; however, olivine and hematite rich. Variable habit in poikilitic grain – near enstatite is tabular and sometimes occurs as intergrowths. Near other grains, more rounded. Poikilitic grain has the same habit as the adjacent chondrule grain.

Chondrule 4 *ROI 2* Poikilitic - porphyritic olivine pyroxene chondrule	Forsterite 70% Mesostasis 15% Minor phases 15%	Forsterite - 100 µm Mesostasis - < 1 µm Minor phases - up to 5 µm.	Forsterite- variable habit- sub-rounded (10 µm diameter), tabular (100 µm long 75 µm wide), cubic (100 µm by 100 µm). Rounded in centre of chondrule, more tabular on edge. Enstatite - tabular - 100 µm long, 20 µm wide, a large one is 400 µm by 100 µm, occurs as intergrowths with mesostasis.	Centre of chondrule (20% of interstitial material) - anorthite 45%, augite 30% and albite 25%, very fine-grained (< 1 µm), acicular crystals Other 80%, clinochlore and chamosite, heterogeneous, porous and fine-grained (< 1 µm). EBSD- anorthite mesostasis.	All forsterite grains have a fayalitic rim (< 1 µm). Heavily fractured forsterite grains have gradual compositional zoning from forsterite to fayalite. Enstatite has abrupt compositional zoning to olivine.	Higher frequency of sub-grain boundaries in forsterite grains on edge of chondrule.	Forsterite in centre has no alignment. Forsterite on edge of chondrule has weak petrofabric alignment, defined by the orientation of the elongate grains. Forsterite adjacent to inclusions is tabular and facing radially outwards. In all Euler analysis, fractured, smaller forsterite grains have the same orientation as adjacent larger grains.	Spherical inclusions, composed of goethite, hematite and unclassified material, ranging in size- larger one 200 µm diameter, smaller ones 20 µm diameter. Hematite (sub-rounded, 100 µm) and spinel grains (5 µm) within forsterite grains. On the edge of the acicular, quench crystals there is a highly porous altered mesostasis that is fine-grained and unclassified with the NanoMin.	Poikilitic relationship with matrix, same composition as matrix; however, olivine and hematite rich. The poikilitic grain generally stops at the fractures encompassing this chondrule, and has a variable alignment.
Chondrules 5, 6 & 7 *ROI 3* Poikilitic – granular olivine chondrules	Forsterite 70% Enstatite 10% Mesostasis 20%	Forsterite - larger 100 µm diameter, smaller 10 µm diameter. Enstatite - 20 µm by 10 µm. Mesostasis - 150 µm diameter.	Forsterite - sub-rounded, heavily fractured. Enstatite - angular, fine grained, heavily fractured.	Mesostasis - heterogeneous, same composition as matrix (goethite and enstatite), olivine rich. Some clinochore and chamosite rich areas found in extremely fractured areas in the mesostasis.	All forsterite grains have a thick fayalitic rim on edges (up to 30 µm), in some cases fayalite composes 90% of the whole grain.	High frequency of sub-grain boundaries on edges of forsterite grains and adjacent to fractures.	These chondrule grains are composed of various forsterite aggregates and these have similar crystal orientations according to all Euler analysis.	Irregularly shaped inclusions (average 10 µm), composition- hematite, goethite and enstatite rich plus unclassified material.	There is a heavily fractured, poikilitic, grain which has the same composition as the matrix and the chondrule is on top of this grain, so it looks like a coarse-grained rim. Especially since the matrix is fine-grained

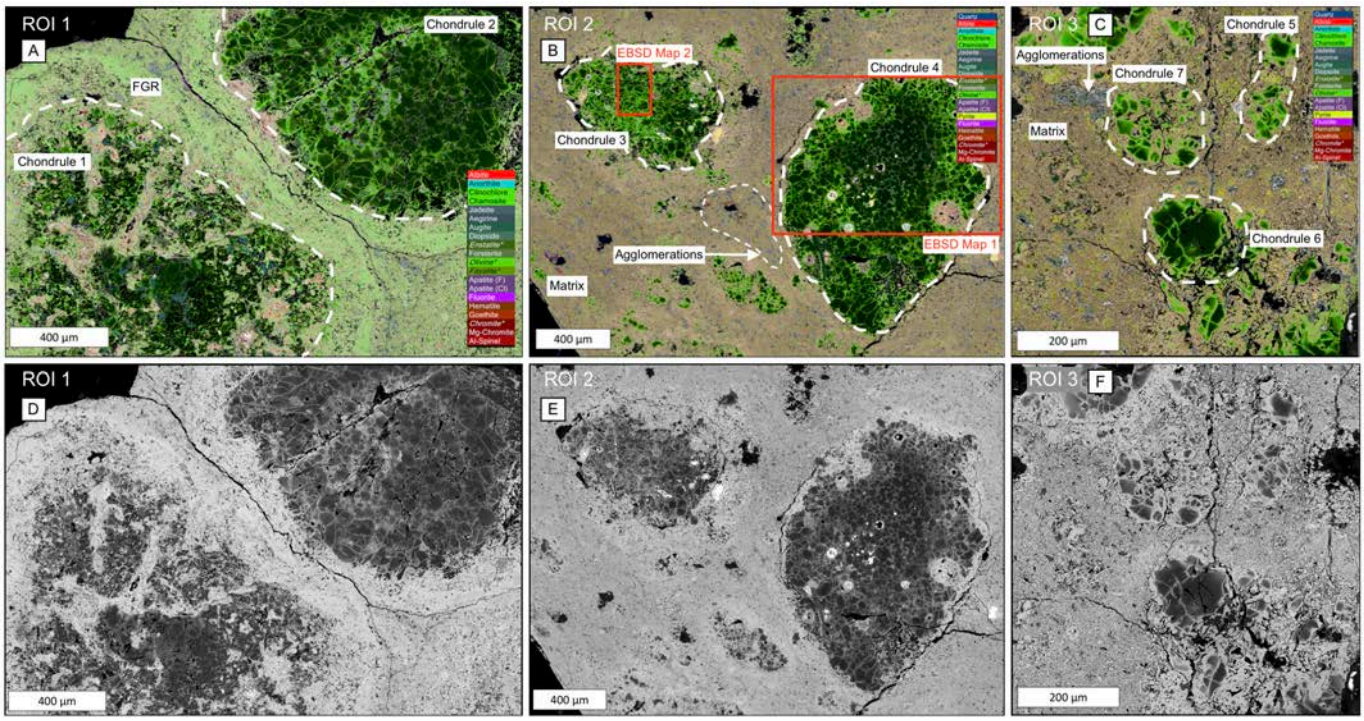

Figure 4.2 *- Results from NWA 3118 NanoMin analysis. Upper maps - annotated, false coloured maps with meteorite recipe applied and BSE underlain. Lower maps - BSE analysis. A) & D) ROI 1. B) & E) ROI 2. C) & D) ROI 3. The scale and locations of EBSD analysis are also shown.*

4.2.2 Matrix and 'agglomeration' characteristics

The matrix forms ~ 65% of the sample, it is composed of ~ 49% goethite and enstatite with minor clinochlore. The grain size ranges from < 1 µm to 5 µm, with a moderate to high porosity (Figure 4.2 & 4.4). Approximately half of the matrix is comprised of ~1 µm wide, elongate, platy crystals. The other half is fine-grained (< 1 µm to 3 µm), irregularly shaped and occurs in the interstices of the elongate matrix grains. The interstitial material of the matrix is comprised of clinochlore, which is very fine grained (< 1 µm). There are also some other phenocrysts randomly (~ 100 µm) distributed through the matrix. The matrix does not have a pervasive petrofabric; rather, there are these 'agglomerations' which wrap themselves around chondrules create a weak petrofabric (Figure 4.2, 4.3 & 4.4). These agglomerations range in size from < 1 µm rounded grains to ~ 200 µm long and ~ 10 µm wide amoeboid shaped grains. The larger agglomerations have two different compositions, where the rim is composed of 80% diopside and 20% goethite and the core contains 40% SiO_2, 35% fluorite and 25% goethite. While the smaller grains only contain diopside and goethite.

Characteristics of chondrules and reaction rims

4.2.3 Porphyritic olivine pyroxene chondrules - with a fine-grained rim and poikilitic

Chondrules 1, 2, 3 and 4 have been identified as porphyritic olivine chondrules, due to their pyroxene and olivine content and general microstructures (Brearley & Jones, 1998). Chondrules 1 and 2 have a fine-grained rim, while Chondrules 3 and 4 are poikilitic with no clear rim. Both

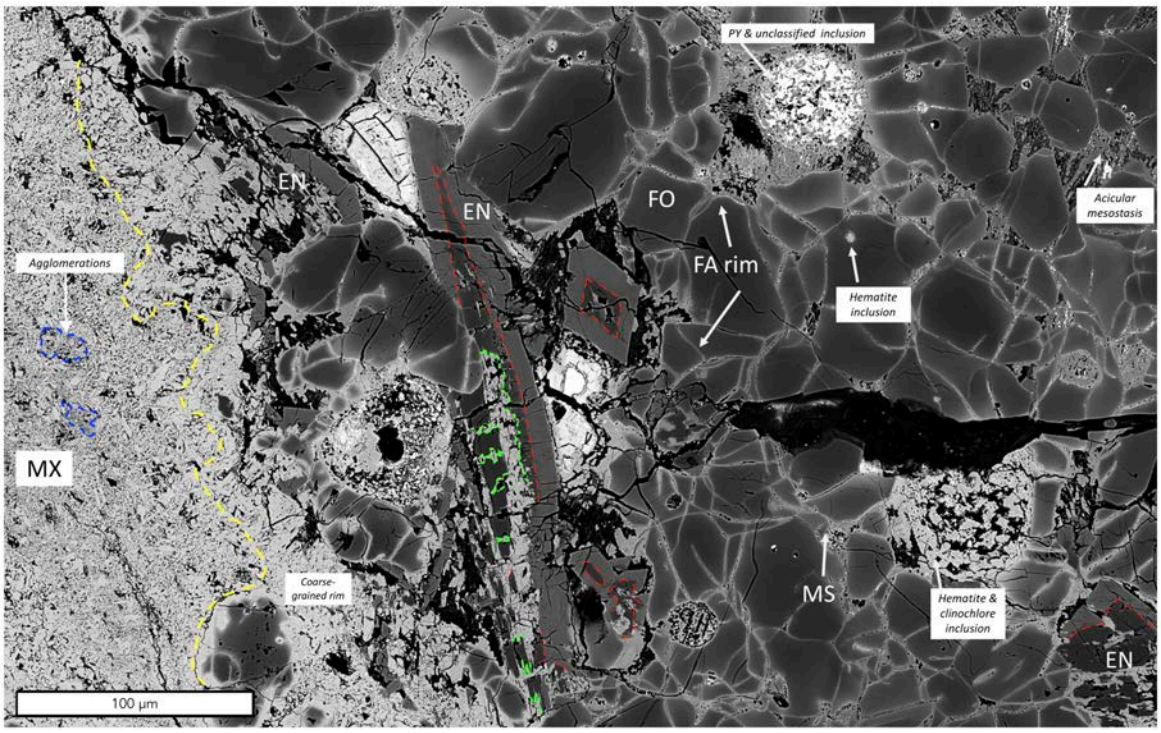

Figure 4.3 *- Site 1 - Annotated smaller scale NanoMin BSE analysis of a section of Chondrule 4 and the matrix. Red - enstatite zoning. Green - enstatite intergrowths. Blue - outline of agglomerations. Yellow - outline of coarse grained rim. MX - matrix, EN - enstatite, FA - fayalite, FO - forsterite, PY - pyrite, MS - mesostasis.*

chondrule groups have the same general patterns. They are dominated by coarse grained forsterite (70%) and enstatite (10%) with a fine grained mesostasis (20%) (Figure 4.2, 4.3 & 4.4). Typically, the chondrules have a relatively homogenous composition of olivine and enstatite and in some, there are spherules composed of mostly hematite and some pyrite and this is particularly seen in ROI 2 (Figure 4.4). Generally, the olivine occurring on the edge of the chondrule displays higher amounts of intragrain orientations compared to the centre olivine grains (Figure 4.5.B). The coarse grains of olivine are forsteritic in composition in the core and fayalitic at the rim. These fayalite rims are generally symmetric around individual grains; but, may vary in thickness from < 1 µm to 3 µm in the rim (Figure 4.2, 4.3 & 4.4).

Olivine grains are generally euhedral and rosette shaped, the larger grains are 200 µm in diameter and the smaller ones are 50 µm in diameter. There are also some areas of the chondrule which contain xenomorphic, fine-grained olivine < 5 µm long. There is a high frequency of low angle sub-grain boundaries in the xenomorphic forsterite, compared to the euhedral forsterite (Figure 4.5.A). In contrast, enstatite is generally finer grained 10 - 100 µm, exhibits a general elongate and xenomorphic morphology occurring interstitially between the olivine grains (Figure 4.5.A). The mesostasis in these chondrules is comprised of 80% clinochlore and chamosite and the remaining 20% is a mottled combination of anorthite, jadeite and unclassified material. This mesostasis is

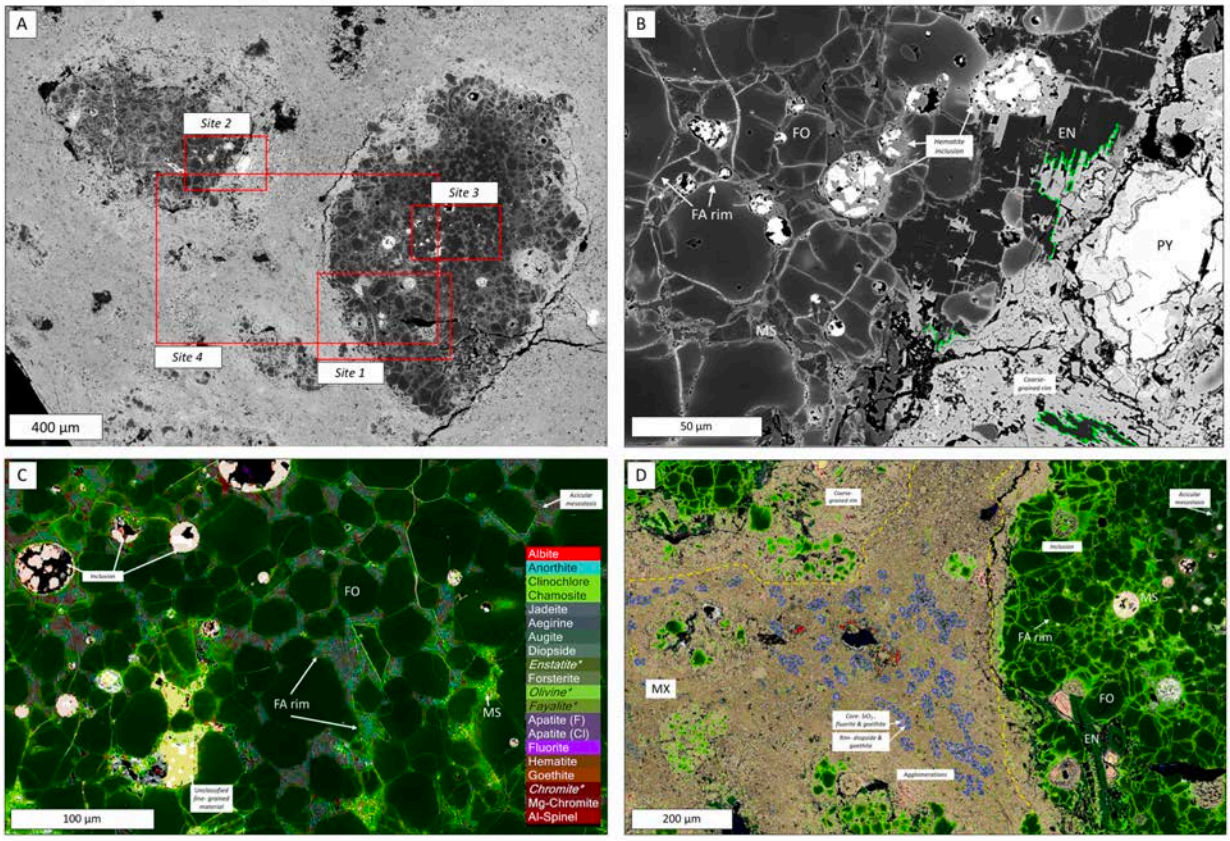

Figure 4.4 *- Annotated analysis from NanoMin ROI 2. A - BSE analysis of the smaller scale map locations. B - Site 2 - BSE analysis of Chondrule 3 and the coarse-grained matrix. C) Site 3 - Small scale analysis with false coloured meteorite recipe applied on the BSE map in Chondrule 4. D) Site 4 - Small scale analysis of matrix between Chondrules 3 & 4. Green - enstatite zoning. Yellow - outline of coarse grained rim. Blue - outline of agglomerations. MX - matrix, EN - enstatite, FA - fayalite, FO - forsterite, PY - pyrite, MS - mesostasis.*

porous and fine grained (< 1 µm). In the centre of chondrule 4 in ROI 2 (Figure 4.3 & 4.4.C) the mesostasis is acicular and composed of anorthite (45%), augite (30%) and albite (25%). There is also an amoeboid shaped (~ 100 µm) grain of unclassified material on the periphery of the acicular mesostasis and clinochlore rich mesostasis. Chondrule 2 (ROI 1) exhibits a series of fractures with a dominance of one orientation and in areas of fracturing, the olivine and enstatite grains are generally finer grained (Figure 4.2.A & 4.2.D). While Chondrules 3 and 4 do not contain any fractures. ROI 1 exhibits a heterogeneous fine-grained rim (< 1 µm) of goethite and enstatite, with some augite and apatite. In comparison Chondrules 3 and 4, in ROI 2, have a poikilitic relationship with the matrix, where the surrounding material has the same composition as the matrix; however, is olivine and hematite rich. It has a variable morphology; but, is generally rounded. In Chondrule 3, the coarse-grained rim is tabular and occurs as an intergrowth with the enstatite (Figure 4.4.A & 4.4.D).

Chondrule 1 is also a porphyritic olivine pyroxene chondrule, with a fine-grained rim; however, it has a different composition to Chondrules 2, 3 and 4. It is composed of forsterite 15%, enstatite 40%, anorthite 5% and mesostasis 40%. The forsterite varies between 10- 80 µm, some grains are

sub-rounded and others are rosette shaped and exhibits a fayalite rim (1 µm) (Figure 4.2.A & 4.2.D). Enstatite grains are ~ 30 µm long and 2 µm wide, homogenous and occur as laths. While anorthite grains are amoeboid shaped, homogenous and typically 50 µm wide. This chondrule shares the same fine-grained rim as Chondrule 2, which is heterogeneous, < 1 µm grain size of goethite and enstatite, with some augite and apatite (Figure 4.2.A & 4.2.D). 50% of the mesostasis is composed of the same composition as the overall fine-grained rim (goethite, enstatite) and the other 50% has the same composition as the matrix (enstatite and goethite with some clinochlore) seen in ROI 2 and 3 (Figure 4.3 & 4.4).

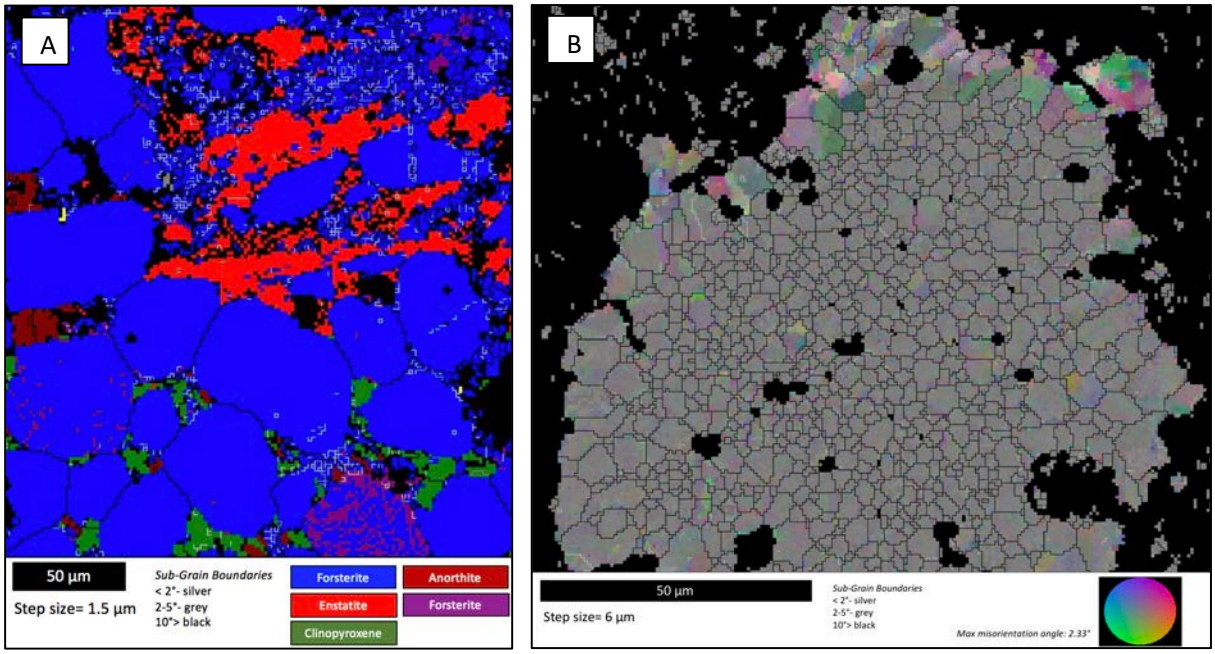

Figure 4.5 *- EBSD analysis from NWA 3118. A) Phase and sub-grain analysis from site from Chondrule 3. Note the high frequency of sub-grain boundaries in the xenomorphic olivine, and the low frequency of subgrain boundaries in euhedral olivine and enstatite. B) Disorientation colour map of Chondrule 4. There is more disorientation colouring on the upper edge.*

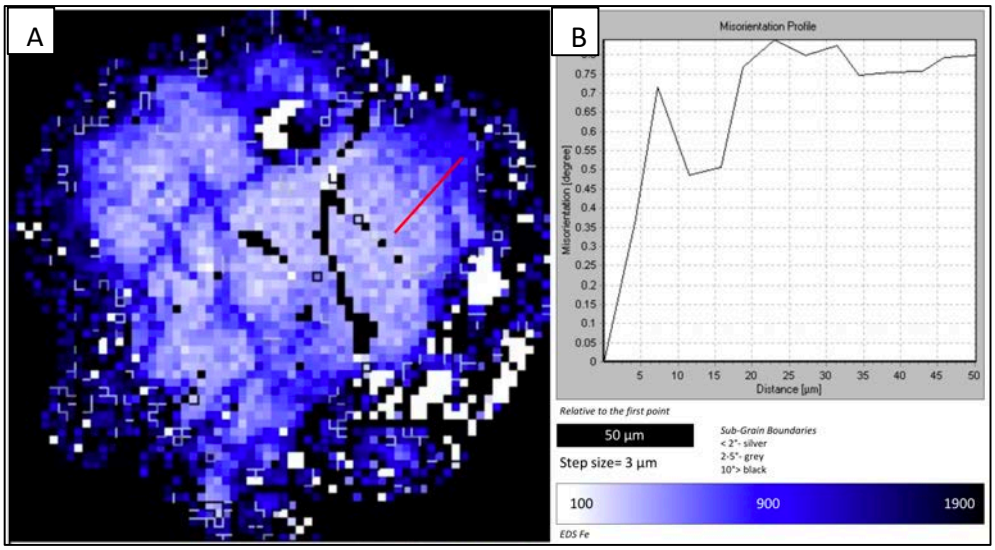

Figure 4.6 *- EBSD analysis of Chondrule 6. A) EDS with the Fe counts applied, the red line is the location of the misorientation profile, shown in B).*

4.2.4 Poikilitic granular olivine chondrule

Chondrules 5, 6 and 7 in ROI 3 (Figure 4.2.C & 4.2.D) have many similarities with porphyritic olivine type IA chondrules described in Section 4.2.3; however, are generally xenomorphic and have a poikilitic morphology. These chondrules are mainly comprised of forsterite (60%) with some enstatite (5%) and a large amount of mesostasis (35%). Forsterite is typically between 10- 100 µm, sub-rounded and heavily fractured and there is a decrease in Fe content towards the centre of the forsterite grains (Figure 4.6). While enstatite occurs as angular, ~10 µm grains. The mesostasis is fine-grained and heterogeneous, with generally the same composition as the matrix; however, in between some forsterite grains there is an increased abundance of clinochlore and chamosite (Figure 4.2.C & 4.2.D). Like the chondrules in Section 4.2.3, these forsterite grains also have a fayalite rim; however, these rims are comparatively thick and asymmetrical. The spherical inclusions (~ 1 µm diameter) are composed of hematite and goethite. Chondrules 5, 6 & 7 are surrounded by a coarse-grained, heavily fractures grain with the same composition as the matrix, therefore forming a poikilitic texture.

4.3 Murchison- *CM2*

4.3.1 General features

Murchison is approximately composed of 75% matrix, 20% chondrules and 5% minor phenocrysts (Figure 4.7 & 4.8). The micro-XRF data (Figure 4.7) shows it has an Fe and Ni rich matrix, with some Mg and S rich areas. The matrix is heterogeneous in composition. The chondrule sites indicate they were approximately 300 µm diameter and the analysed amoeboid olivine aggregates (AOAs) range in size, on average they are 300 µm long and 150 µm wide. Table 2 provides detailed observations on the Murchison matrix, AOAs and SiO_2 phenocrysts based on NanoMin and EBSD analysis.

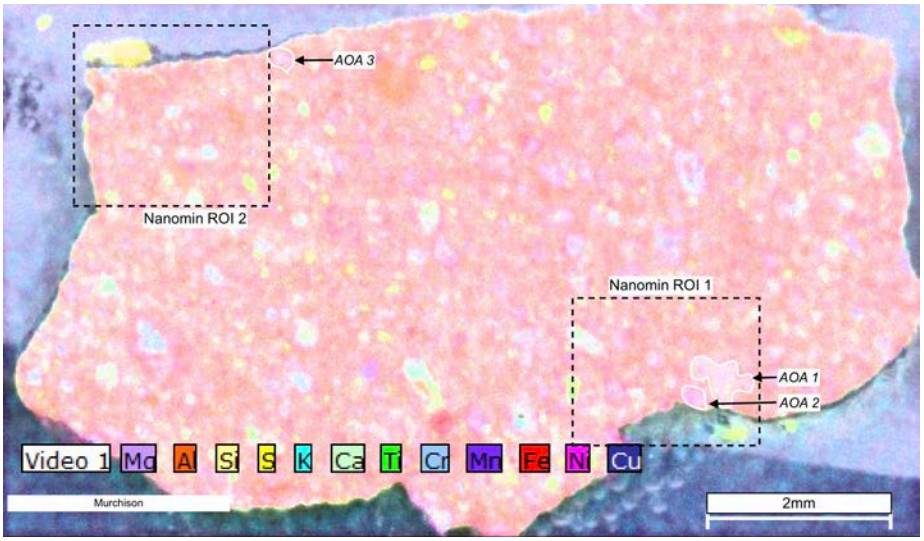

***Figure 4.7** - Annotated, false colour micro-XRF map of Murchison with the element colours and scale indicated. The NanoMin ROI and AOA locations are shown.*

Table 2- *Murchison*

Components Overall Modal %	Phase %	Grain Size	Phase Specifics					Minor Phases	Reaction Rim Characteristics
			Texture	Interstitial	Zoning	Sub-grain boundaries	Preferred Orientation		
Matrix ~75%	Most of matrix - enstatite 50%, goethite 35%, troilite 15%. Olivine rich areas- fayalite 90% and troilite 10%.	<1 µm on average.	~80% of the matrix is mottled, composed of very fine (< 1 µm) grains that have variable compositions. There are also angular phenocrysts (20%) composed of minor phases in the matrix, generally larger ones are 5 µm long, 2 µm wide. Smaller ones, 1 µm diameter.	No EBSD analysis undertaken on matrix	No zoning observed (except for reaction rims)	No EBSD analysis undertaken on matrix	Overall, there is a weak petrofabric alignment seen in the matrix, defined by parallel alignment of grains. Matrix aligns itself surrounding larger meteorite components, this is especially seen around the chondrules. Less so, for the AOAs.	Typically, 2µm long and 1µm wide. SiO_2 5% Apatite 0.5% Hematite 0.5% Cr-spinel: 0.5% Al-spinel: 0.5%	Surrounding many of the chondrule sites, olivine content in the matrix increases and the grain size decreases- forming a FGR. The matrix has a 'flow' like appearance surrounding the chondrules. Tiny fractures (~ 200 µm) occur around the edge of the sample, often associated with unclassified/ phyllosilicate material (Figure 4.10).
Chondrules/ AOAs ~20% *Chondrules were plucked out, this is based on AOA EBSD analysis*	Forsterite 50% Clinoenstatite 40% Diopside 10% Interstitial material 10%	AOA 1 - 400 µm long, 200 µm wide. AOA 2 – 300 µm long, 200 µm wide. AOA 3 – 200 µm long, 150 µm wide. Forsterite - ~ 150 µm long, ~ 100 µm wide. Clinoenstatite - ~ 3µm. Diopside - ~ 5 µm.	Generally, the AOAs contain a few large forsterite grains, which have irregular shapes with sub-rounded edges, these forsterite grains have some fracturing. The finer grained material (enstatite plus minor phases) appears to be heavily fractured, there are little clumps which have the same orientation, as defined by the elongate lath-like enstatite. Clinoenstatite and diopside occur as sub-micrometre grains.	The interstitial material is extremely fine-grained (< 1 µm) and has the same mottled, appearance as some parts of the matrix. It is composed of troilite - 50%, goethite - 35% and augite 15%.	There is no distinct zoning in the studies AOAs, the different minerals are homogenous.	The forsterite has a medium frequency of sub-grain boundaries, typically running in association with fractures. The other phases only contain grain boundaries > 10°.	Forsterite IPF data of sites 1 and 2 indicate that the large forsterite grains have the same range of orientations and site 2 only has this orientation. In site 1 the smaller forsterite grains also have the same orientation relative to each other.	Spherical hematite inclusions, diameter ranging from 1 – 2 µm, occur in forsterite grains.	Surrounding the AOAs, the matrix becomes finer grained-sub-micrometre scale. The olivine content also increases to forsterite 50%, aegrine 30% and troilite 20%.
Other ~5% *SiO_2*	SiO_2 100% according to the NanoMin Other phases near the SiO_2 are discussed in Section 4.3.4	Larger SiO_2 is ~ 100 µm long and ~ 75 µm wide, 1 - 2µm.	Angular, sharp corners and mottled.	Aegrine, forsterite and troilite grains, < 1 µm. Mottled with the SiO_2.	Towards the edges, the olivine and other phases (aegrine and troilite) increases.	Not relevant	Elongate grains aligned in the same orientation as the overall Murchison petrofabric. The reaction rim also follows this alignment, as does the olivine grain surrounded with SiO_2.	Typically, in association with forsterite grains. SiO_2 90%, olivine 5%, aegrine 3% and troilite 2%.	Figure 4.11, there are two clasts and a distinct reaction rim where the SiO_2 content decreases, olivine and troilite (Fe and S content) increase towards the matrix. In Figure 4.12, there is a forsterite clast surrounded by SiO_2 reaction rim, on either side of this site, the matrix is elongate too.

4.3.2 Matrix

The matrix is a mottled composition of enstatite 50%, goethite 35% and troilite 15%, the grain size on average is ~ 1 µm and there is low porosity (Figure 4.8). The minor phase grains are typically 2 µm long and 1 µm wide and either composed of SiO_2 5% (Section 4.3.4), apatite 0.5%, hematite 0.5%, Cr-spinel 0.5% and Al-spinel 0.5%. The matrix has a pervasive petrofabric alignment defined by the parallel alignment of matrix and minor phase grains. The matrix also aligns itself around most of the chondrules sites and there is a fine-grained rim around the chondrule sites. The fine-grained rim is olivine rich, composed of fayalite 90% and troilite 10%, has variable thickness (10 - 50 µm) and is often thicker on the upper and lower regions, where it follows the pervasive matrix alignment.

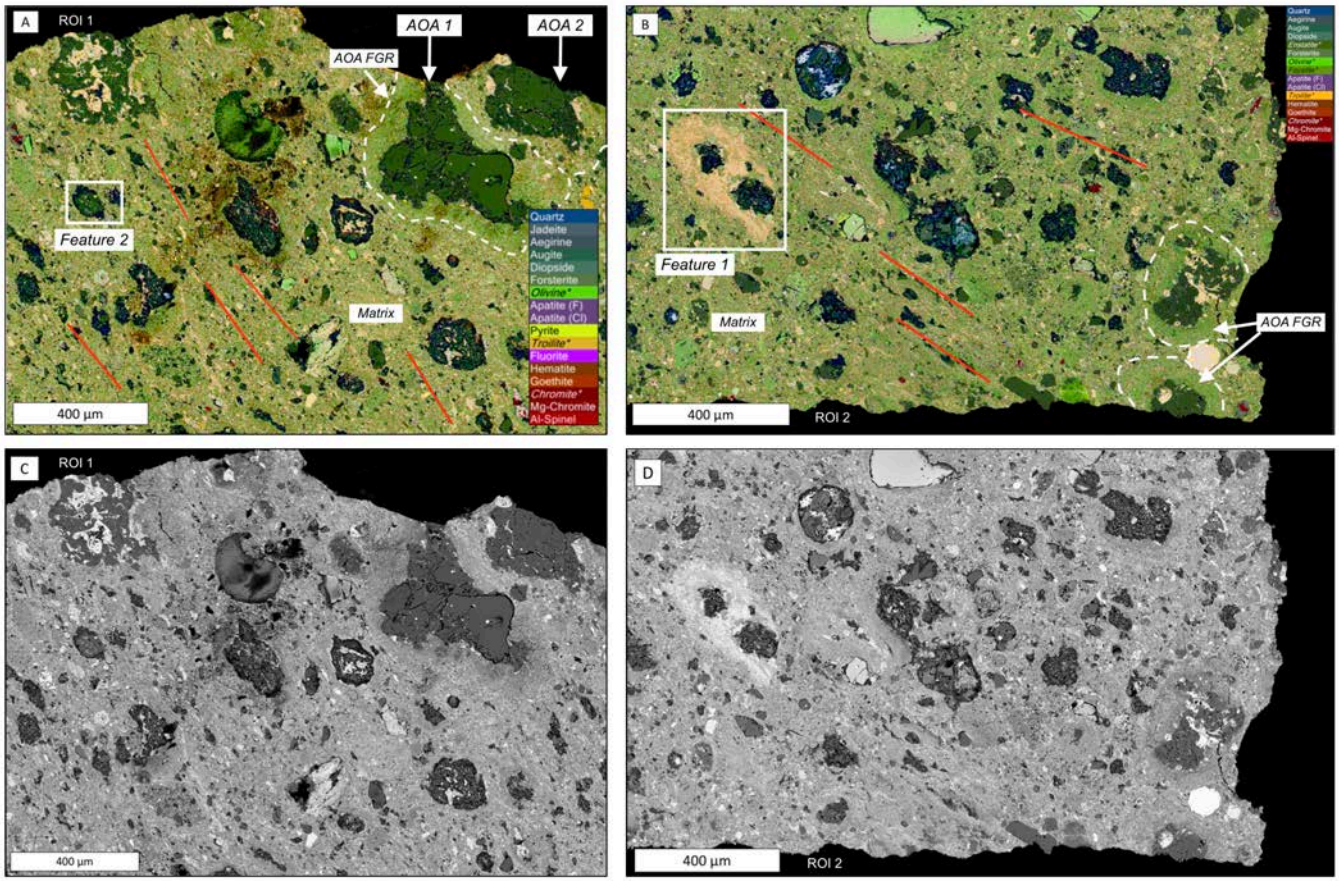

Figure 4.8 *- Results from Murchison NanoMin analysis. Upper maps- annotated, false coloured maps with meteorite recipe applied and BSE underlain. Lower maps - BSE analysis. ROI 1 - left maps- A) and C). ROI 2 - right maps - B) and D). The scale, AOA and Features 1 & 2 locations are also shown. The red lines display the petrofabric alignment.*

4.3.3 Amoeboid Olivine Aggregates (AOAs)

AOAs 1 and 2, contain large forsterite grains (~ 300 µm long) which are irregularly shaped with sub-rounded edges and have some fracturing (Figure 4.9). Within the forsterite grains there are spherical hematite inclusions, 1 - 2 µm diameter. Based on IPF analysis, the larger forsterite grains have the same orientation, compared to the smaller forsterite grains and there is a low frequency of

low-angle sub-grain boundaries within the larger forsterite grains (Figure 4.9.D & 4.9.E). The interstitial material is fine-grained, heavily fractured and dominated by clinoenstatite (85%), diopside (10%) and minor orthopyroxene (5%). AOA 3 is dominated by finer grained, heavily fractured clinoenstatite (50%) and forsterite (30%), with diopside (10%) and orthopyroxene (10%) forming the interstitial material (Figure 4.9.C). In the clinoenstatite and forsterite, there is a low frequency of low-angle sub-grain boundaries and there is also a high amount of intragrain disorientation seen in these larger grains (Figure 4.9.C & 4.9.F). Surrounding these AOAs, the matrix becomes finer grained (< 1 µm) and is olivine rich- forsterite (50%), aegrine (30%) and troilite (20%). The fine-grained rim is ~ 100 µm thick around the AOAs and does not follow the pervasive matrix and chondrule alignment (Figure 4.8 & 4.10). Near the fractures of AOAs, there are unclassified fine-grained clusters, which are identified as phyllosilicates (Figure 4.10). They do not follow any alignment present in Murchison.

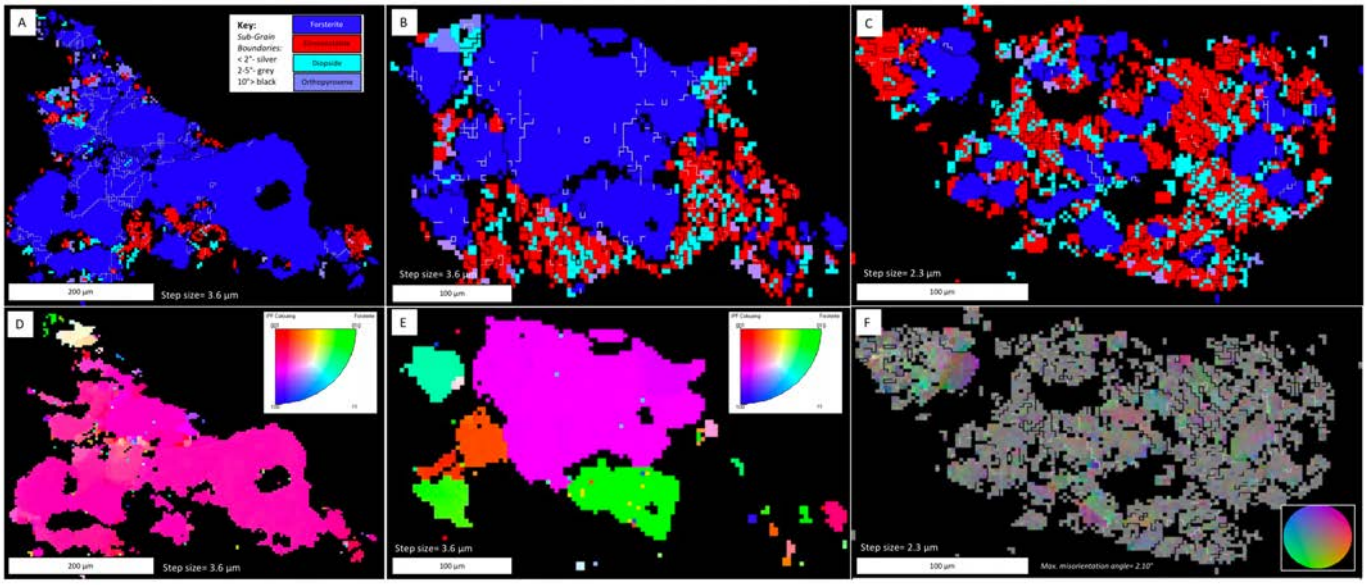

Figure 4.9 *- EBSD analysis of AOAs in Murchison. A), B) & C) Phase and subgrain map of AOA 1, 2 & 3 (respectively), the key is shown in A). D) & E) IPF forsterite analysis of AOA 1 & 2. F) Disorientation colour map of AOA3. The scale and step size is given for each AOA.*

4.3.4 SiO_2 in Murchison

Approximately 5% of this Murchison sample is composed of SiO_2, the grains are ~ 100 µm long and ~ 75 µm wide, angular with sharp corners and mottled (Figure 4.8). Feature 1 shows two clasts where the interstitial material is mottled aegrine, olivine and troilite and towards the edge of clast, the interstitial material increases. The grains are elongate and aligned with the same orientation as the overall Murchison fabric and the surrounding reaction rim also follows this alignment. The reaction rim is symmetric and ~ 40 µm thick and the profile in Figure 4.11 shows how the SiO_2 content decreases, while the forsterite and troilite (Fe and S) content increase towards the matrix (Figure 4.11). Feature 2 displays a fractured, euhedral forsterite clast with 1 - 5 µm spherules of goethite, augite and troilite (Figure 4.12). Surrounding this forsterite clast is a reaction rim of SiO_2,

it is 1 - 2 µm thick on the sides and 10 - 20 µm thick on the upper and lower edge. This clast and SiO_2 grain are aligned with the pervasive matrix and chondrule foliation.

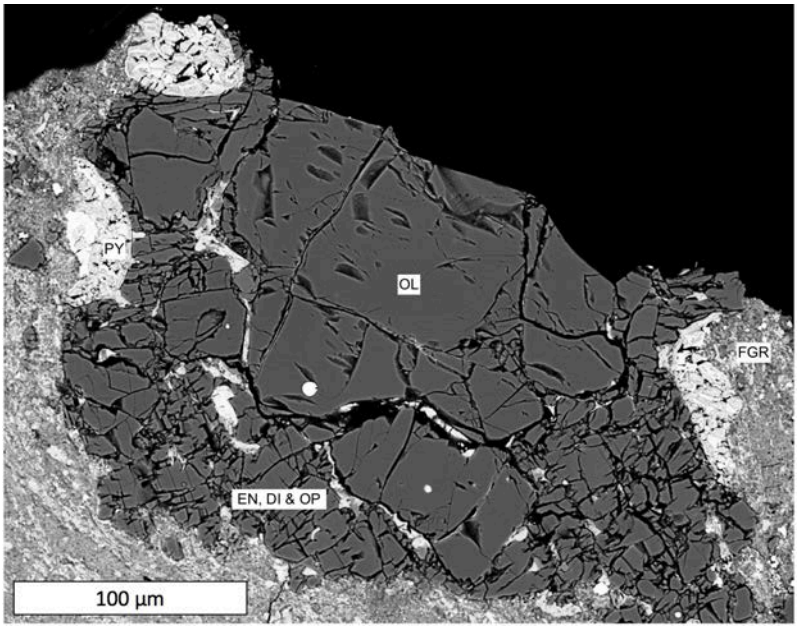

Figure 4.10 – *AOA 2 from ROI 1 NanoMin BSE analysis. The unclassified material occurs on the edges of the AOA and is identified as phyllosilicates. FGR – fine-grained rim, PY – phyllosilicate, OL – olivine, EN – clinoenstatite, DI – diopside, OP – orthopyroxene.*

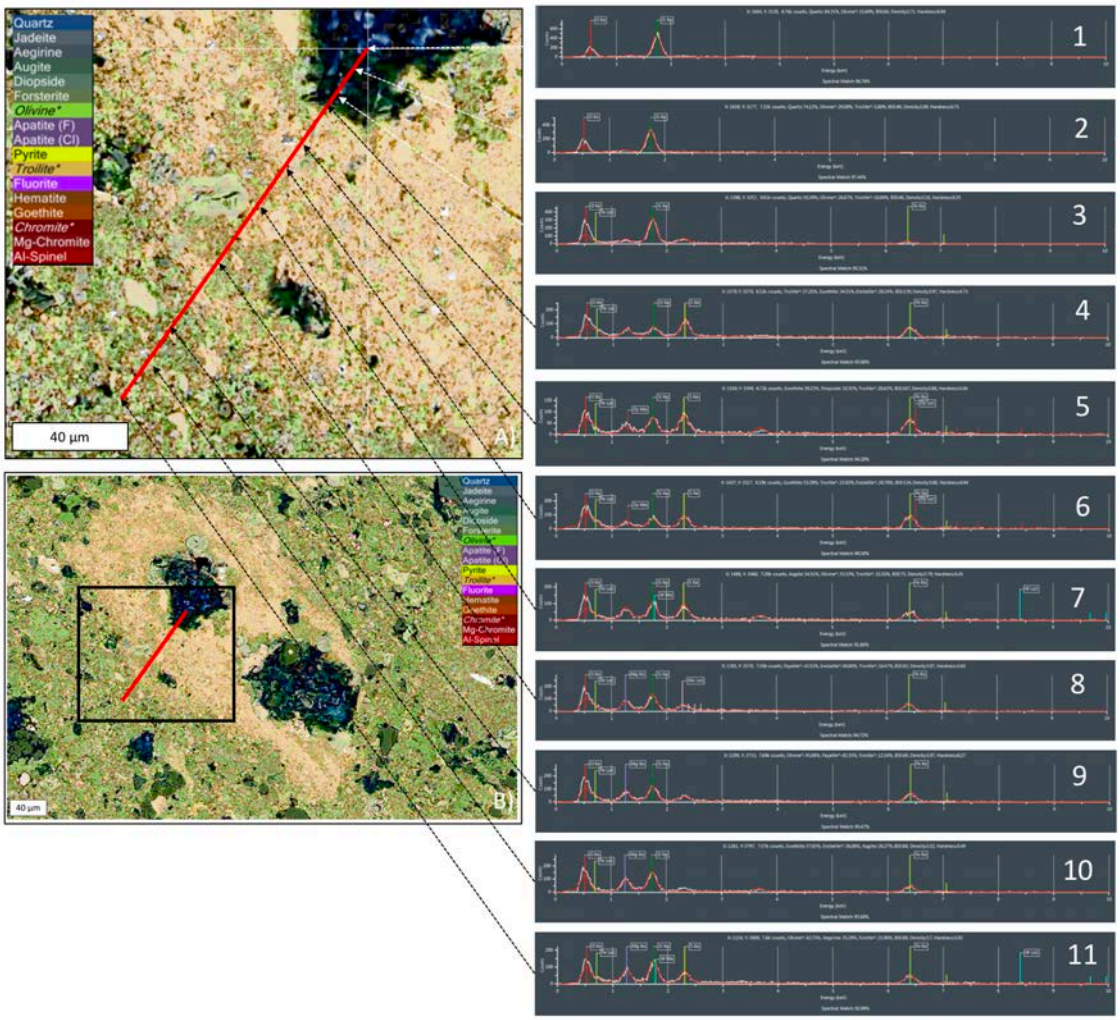

Figure 4.11 - *Feature 1 - reaction rim around two SIO_2 grains, seen in Murchison ROI 2. The transect is indicated with the red line and at each point, shown with the arrows a spectrum was taken (right). The scale and key are provided for each NanoMin map.*

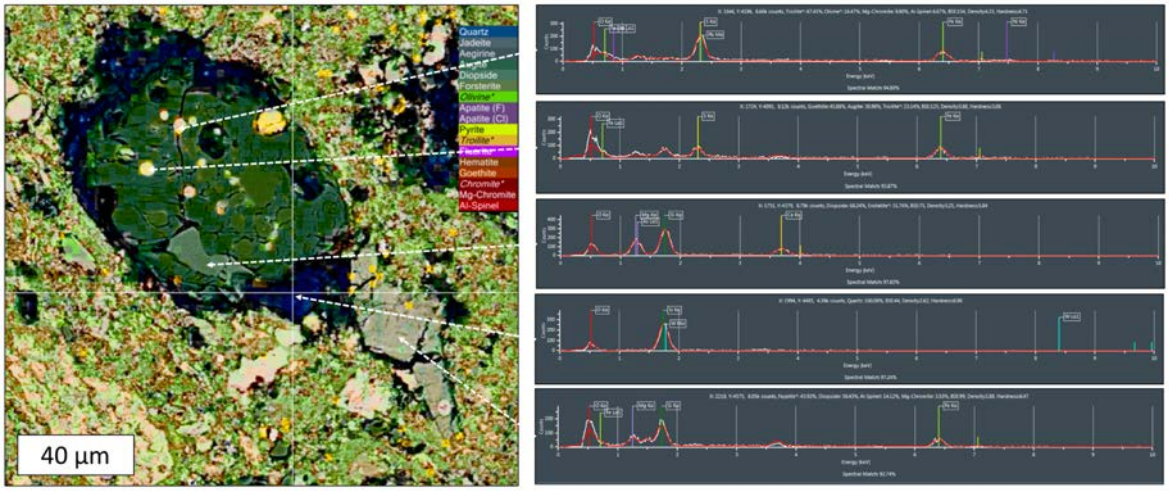

Figure 4.12 *- Feature 2 - olivine phenocryst with SiO_2 reaction rim, seen in Murchison ROI 1. The arrows indicate the spectrum at each analysis point. The scale and key are provided for the NanoMin map.*

4.4 Sutter's Mill - *CM2*

4.4.1 General features

Approximately 80% of Sutter's Mill is composed of matrix, the other 20% is composed of replacement chondrules, phenocrysts and other minor minerals (Figure 4.13.B & 4.13.D). It is very Fe and Ni rich with some minor Si areas (Figure 4.13.D). Table 3 provides detailed observations on Sutter's Mill components, in addition to two interesting features, based on NanoMin analysis.

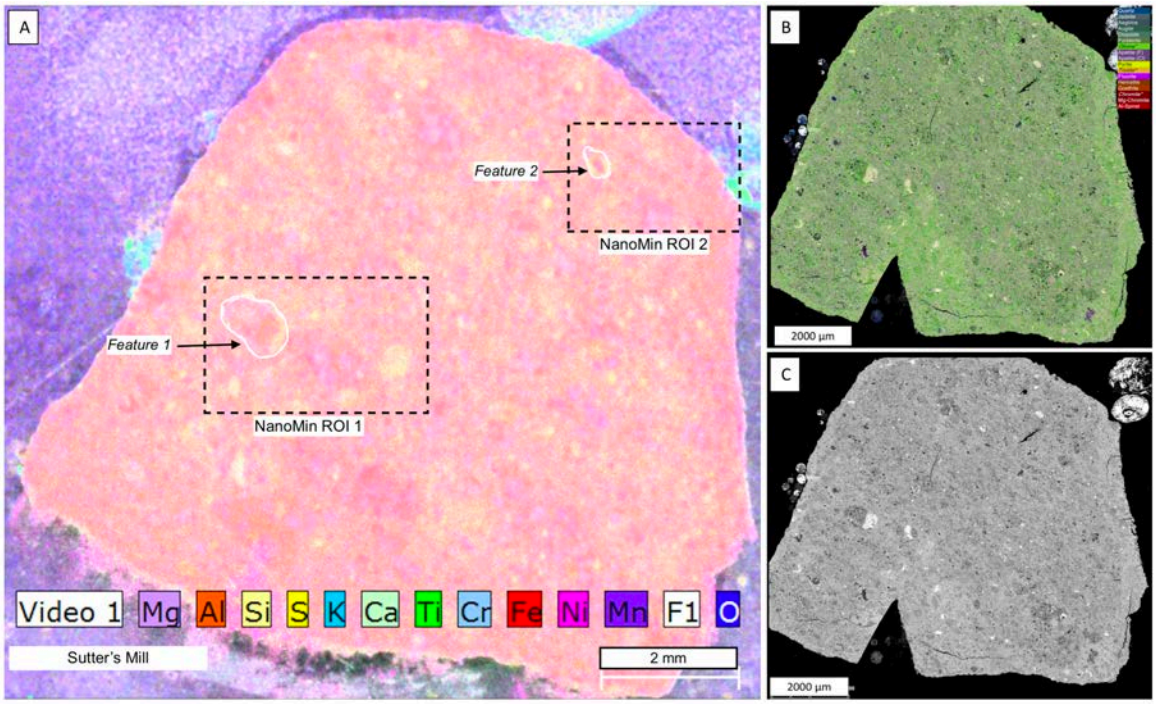

Figure 4.13 *- A) Annotated, false coloured micro-XRF map of Sutter's Mill with the element colours and scale indicated. The NanoMin ROIs and location of Features 1 & 2 are also shown. B) NanoMin analysis of Sutter's Mill, false coloured map with the BSE analysis underlain. The key is shown on the right. C) NanoMin BSE analysis of Sutter's Mill.*

Table 3- *Sutter's Mill*					
Components	**Phase %**	**Grain Size**	**Texture**	**Minor Phases**	**Reaction Rim Characteristics**
Matrix (~80% of whole sample)	Olivine 50% Goethite 10% Aegrine 10% Forsterite 5% Troilite 5% Minor phases 10% Unclassified phases 10%	Larger grains ~ 2 µm diameter. Smaller grains < 1 µm. Overall, fine-grained.	Predominately olivine with other minerals mottled. Most of the matrix is composed of (< 1 µm) olivine grains. Mottled with goethite, troilite and apatite sub-micron grains. The goethite and troilite grains are elongate, lath shaped with no distinct boundaries, ~ 5 µm long, ~ 2 µm wide. The apatite grains are ~10µm long and ~ 3 µm wide, with more distinct grain edges.	SiO_2 2% ~ 50 µm diameter grains. Augite 2% mottled, circular grains ~ 5 µm diameter. Diopside 2% elongate laths, ~20µm long, ~ 5 µm wide. Apatite 2% irregularly shaped grains, 20 µm long. Other 2% - jadeite, pyrite, hematite, chromite and spinel.	Change in porosity around edge of chondrite. This rim varies in thickness, ~ 100 – 200 µm and is more 'dense' and less fractured, compared to the rest of the sample. It has the same composition as the matrix.
Other components (~20% of whole sample)	Olivine 80% Troilite 20%	Olivine ~ 500 µm diameter. Troilite ~ 500 µm long, ~ 100 µm wide.	Olivine- is homogenous, most of the phenocrysts are rounded and have distinct edges. Troilite- more like an interstitial material for the matrix, higher BSE response, very fine grained (< 1 µm) irregularly shaped and no distinct boundaries.	Not relevant	Not relevant
Feature 1 - ROI 1	Olivine ~ 70% Cronstedtite 15% Tochilinite 5% Minor phases 10%	Tabular olivine 100 µm long, 10 µm wide. Sub-rounded olivine, 30 – 70 µm diameter. Cronstedtite anhedral; but, biggest area is 300 µm long, 100 µm wide. Troilite grains 2 µm diameter.	Tabular olivine has a flaky texture and has parallel, ~ 1 µm scale faint veinlets of cronstedtite, it has defined long axis boundaries; but, on the short axis it usually morphs into the other, sub-rounded olivine. Sub-rounded olivine is homogenous and fractured. There are intergrowths with this olivine and the tabular olivine. More intergrowths are seen between the sub-rounded olivine and the cronstedtite. Cronstedtite is extremely fine grained and mottled with olivine. There is a large amount of it on the right side of the feature and a few cronstedtite rich areas on the edges between the tabular and sub-rounded olivine. There is a faint and irregular boundary between the cronstedtite and olivine phases.	2% SiO_2 homogenous, sub-rounded ~ 5 µm diameter grains. Typically occur in the transition between tabular and sub-rounded olivine. 8% hematite heterogeneous, predominately spherical shaped grains, radial patterns. Occurs in association with cronstedtite. A few grains also occur in the transition between the olivines; but, most are associated with the large cronstedtite area.	Surrounding the grain are tochilinite pellets embedded in the matrix, they are more common directly next to the olivine edge and then the amount decreases.
Feature 2 - ROI 2	Troilite ~ 75% Olivine ~ 20% Tochilinite ~ 5%	Whole grain 200 µm long, 100 µm wide. Troilite grains 2 µm diameter. Olivine 20 µm long, 5 µm wide.	The overall grain is ovoid shaped. Troilite is typically pellet shaped and there is a high density in the centre of the grain. In the core of the grain, there are some olivine grains present forming an elongate lath shape (~ 100 µm long, ~ 20 µm wide). There are larger and sub-rounded olivine grains on the edges of the troilite. Surrounding the grain are troilite pellets embedded in the matrix, they are more common directly next to the olivine edge and then the amount decreases.	Not relevant	Aside from the tochilinite pellets (same as Feature 1), the matrix does not demonstrate any reaction rims around this feature.

4.4.2 Matrix

The NanoMin classifies the matrix as being composed of olivine 55%, goethite 10%, aegrine 10%, troilite 5%, minor phases 10% and unclassified material 10%. Overall, the matrix is fine- grained, the larger grains are ~ 2 μm in diameter and the smaller grains are < 1 μm. Most of the matrix is fine-grained olivine, mottled with goethite, troilite and apatite. Goethite and troilite are generally elongate (~ 5 μm, long, ~ 2 μm wide), lath shaped with no distinct boundaries. While the apatite grains have more distinct grain boundaries and are ~ 10 μm long and ~ 3 μm wide. The minor phases include SiO_2, augite, diopside, apatite (Table 3). Surrounding the edge of Sutter's Mill, there is a change in porosity forming a rim around the chondrite, it varies in thickness between ~ 100 – 200 μm and is relatively symmetrical. The composition remains the same and is less fractured compared to the 'core' of the chondrite (Figure 4.13).

4.4.3 Other components

The other component is identified as olivine phenocrysts (80%) and troilite in the matrix (20%). The olivine phenocrysts are homogenous, ~ 500 μm in diameter and have distinct, rounded edges. Troilite grains appear to be an interstitial material within the matrix, they are very fine-grained, irregularly shaped and have no distinct boundaries. Two major grains were also identified as the other components in Sutter's Mill, their locations are seen in Figure 4.13. The mineralogy is discussed in Sections 4.4.4 and 4.4.5 for both features and there are small unclassified pellets, which are very fine grained (< 1 μm). They occur in the interstices of the matrix, have a high BSE response and based on research have been identified as tochilinite.

4.4.4 Feature 1

Feature 1 is dominantly composed of olivine (70%), cronstedtite (15%), troilite (5%) and minor phases (10%) (Figure 4.14). In Feature 1, olivine has two main morphologies. The tabular olivine is 100 μm long and 10 μm wide, it has a flaky texture and has parallel, 1 μm thick veinlets of cronstedtite. The long axis boundaries are well-defined, while the short axis boundaries occur as intergrowths with the olivine type. This other olivine type occurs as sub-rounded grains, 30 – 70 μm in diameter, it is homogenous, fractured and is more common on the edge of the feature, where it also occurs as intergrowths with cronstedtite, where there is a mottled, irregular boundary between the two minerals. Generally, the cronstedtite is anhedral, fine-grained and mottled with olivine, there is a large grain of cronstedtite on the right side of Feature 1 and it also occurs in a few locations between the tabular and sub-rounded olivine. Surrounding Feature 1, there are small tochilinite pellets (2 μm) diameter embedded in the matrix, they are more common directly next to the olivine edge.

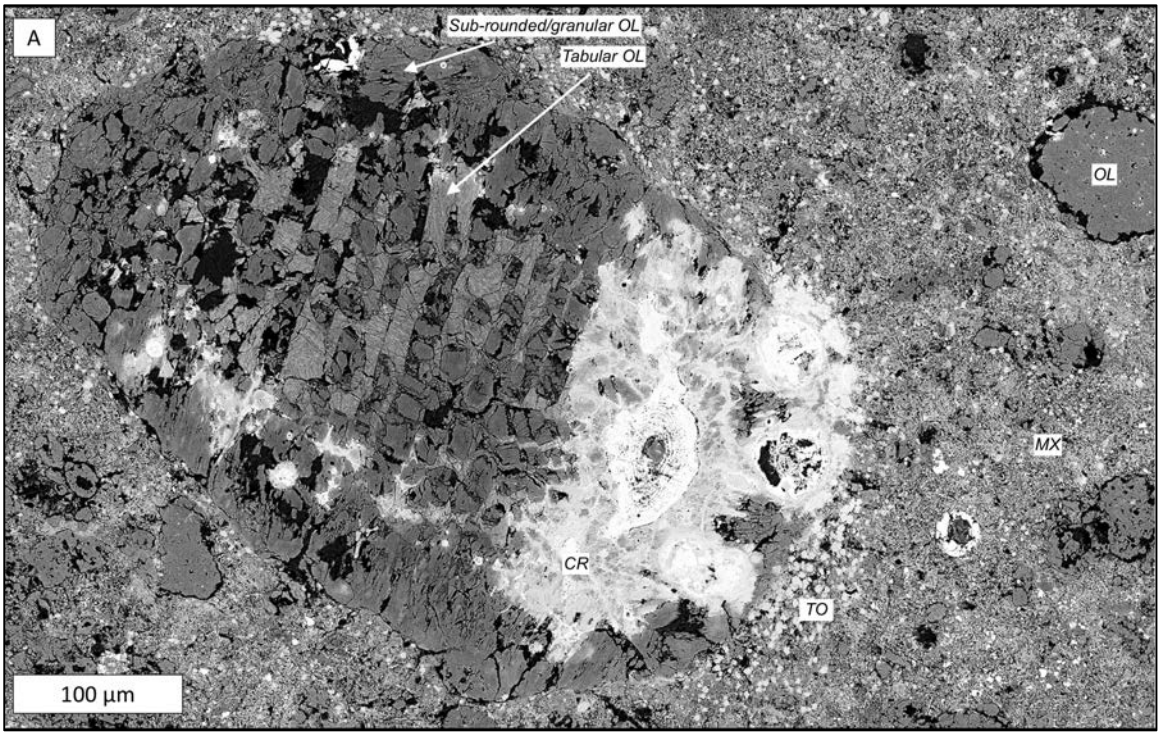

Figure 4.14 *- NanoMin BSE analysis of Feature 1 from ROI 1. The sub-rounded and tabular olivine, troilite are indicated and the hematite is outlined in red. MX - matrix, OL - olivine, TO - tochilinite, CR - cronstedtite.*

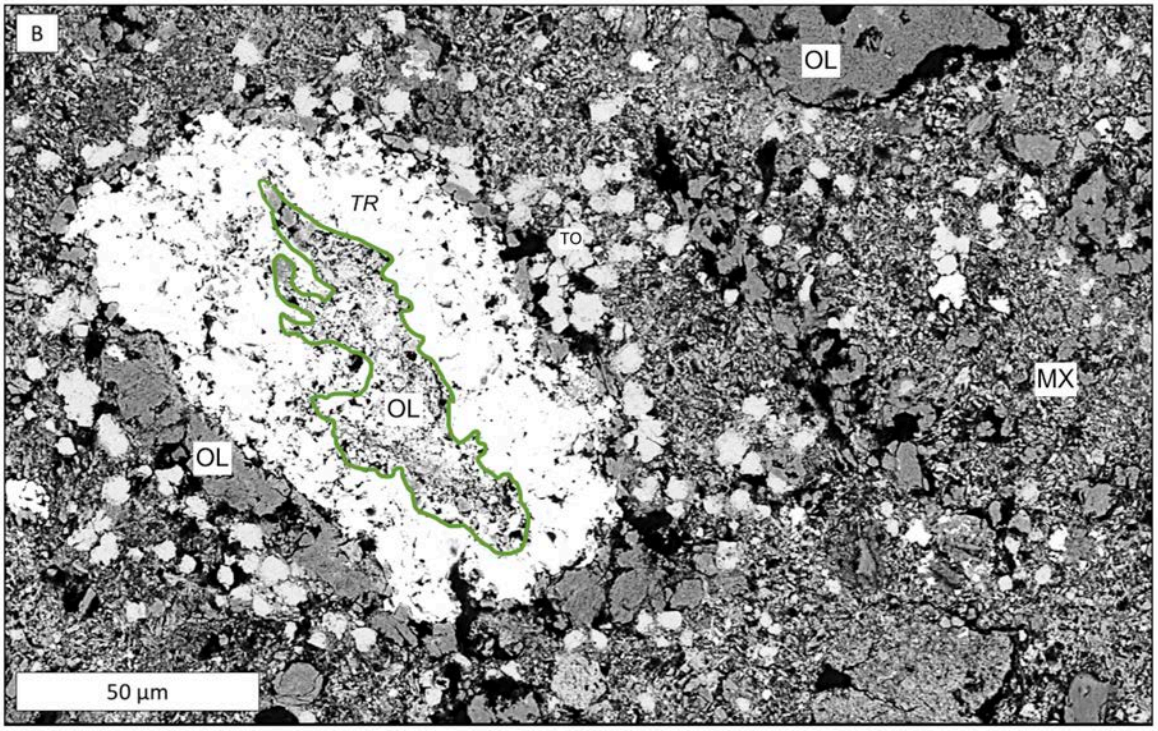

Figure 4.15 *- NanoMin BSE analysis of Feature 2 from ROI 2. The olivine in the centre of the troilite is outlined in green. MX - matrix, OL - olivine, TR – troilite, TO – tochilinite.*

4.4.5 Feature 2

Feature 2 is found in ROI 2, it has an ovoid shape, ~ 200 μm long and ~ 100 μm wide (Figure 4.15). Troilite forms 80% and occurs as ~ 2 μm diameter pellet- shaped grains. There is a high density of troilite pellets in the centre of the grain; however, in the core there are some olivine grains present. This olivine occurs as an elongate, lath shape (~ 100 μm long, ~ 20 μm wide). In addition, olivine surrounds the troilite and forms 20% of Feature 2, the olivine is typically 20 μm long and 5 μm wide and sub- rounded. On the edge of Feature 2, there are tochilinite grains embedded in the matrix and dissipate further away from Feature 2.

4.5 Concluding remarks

Shown within this chapter are the results obtained using NanoMin, EBSD and to a lesser extent, micro-XRF which were used to analyse carbonaceous chondrites. These analysis techniques offer different types of results, which aid in gaining an insight into Solar System processes.

Chapter 5 - Discussion

5.1 Introduction

Presented within this chapter is the discussion of the findings for each carbonaceous chondrite sample examined in this thesis. A geological history for each sample is developed by synthesising the results with reference to previously undertaken research. These are then brought together in two final sections, discussing a) the character and significance of volatiles during planetary formation and b) the advantages and disadvantages of each analytical method used.

5.2 NWA 3118

5.2.1 General features observed in NWA 3118 and their implications for formation processes

Despite the differences seen amongst the three different chondrule types identified in NWA 3118 (Table 1), there are some overarching similarities seen. These include, fayalite rims on olivine grains, a decrease in Fe content towards the centre of the chondrule and a higher frequency of disorientations on the outer chondrule grains.

Each of the olivine grains observed in NWA 3118 contain fayalite rims that vary in thicknesses amongst the different chondrule types (Figure 4.2). Given they occur on all observed olivine grains, it is inferred that thin fayalite rims formed during the chondrule formation process in the solar nebula (Hua et al., 1988, and Weinburtch et al., 1990). The thicker fayalite rims (Figure 4.2.C & 4.2.F) generally occur on the granular chondrules and on the outer edges of the chondrules. It can be inferred that after the chondrite formed and was on its parent body, aqueous alteration then affected the smaller, fractured granular chondrule types and the outer edges of the porphyritic type chondrules (Jogo et al., 2017). Thus, resulting in the disparity between fayalite rim thickness among and within chondrule types.

Further evidence for alteration during chondrite formation is seen with a high frequency of intragrain disorientations on the outer olivine grains compared the centre of the chondrule in porphyritic olivine chondrules (Figure 4.5.B). Additionally, in the granular type chondrules, the Fe content decreases towards the centre of the chondrule (Figure 4.6). The distinctions between the centre of the chondrules and the outer grains, exemplified with the mesostasis, intragrain disorientation and Fe zoning, demonstrates at the time of amalgamation or agglomeration of chondrules and matrix to form a meteoritic parent material, there was some sort of alteration present. A study by Akos et al., (2016) attributed similar phenomena also observed on NWA 3118 to metasomatism by a Fe-rich fluid. The local internal orientation changes of Fe-rich rim olivine can be explained by a replacement mechanism similar to fluid meditated replacement reactions

(Putnis, 2009), where the phase that is in disequilibrium with its surrounding fluid is dissolved and the thermodynamically stable phase is precipitated. Commonly, the new phase is growing epitaxially (i.e. same orientation as its host); but, may show significant orientation changes due to growth defects (Spruzeniece et al., 2016).

5.2.2 Matrix and 'agglomeration' implications

From the NanoMin analysis, matrix grains generally do not have a pervasive petrofabric alignment; however, in-between the chondrules there is a very weak alignment present, which is further amplified with the 'agglomerations' (Figure 4.2). These 'agglomerations' have a flow-like appearance and coalesce in-between the chondrules. The chondrules do not display any shock metamorphism features. It is interpreted from this work and results from Bland et al., (2014) that during chondrite formation, the chondrules acted as 'heat sinks', while the matrix absorbed any formation related stress. The matrix remained relatively unaffected; however, the 'agglomerations' coalesced around chondrules, demonstrating they were still ductile and probably cooling during this process (Akos et al., 2014). It should also be noted that the presence of goethite has been attributed to being a product of terrestrial weathering (Bland et al., 2006). This is possible when considering NWA 3118 is a desert find.

5.2.3 Porphyritic olivine pyroxene chondrules with a fine-grained rim

Chondrules 1 and 2 have a distinct fine-grained rim and exhibit the highest frequency of fracturing compared to the other analysed chondrules (Figure 4.2.A & D). Therefore, these chondrules and their fine-grained rim were potentially the first material to amalgamate in the solar nebula, from a precursor material of nebular condensates. The fine-grained rim has an olivine rich composition and potentially indicates the same origin as the olivine chondrules (see also Metzler et al., 1992).

5.2.4 Poikilitic Chondrules- porphyritic and granular

The poikilitic type chondrules have an intrinsic relationship with the matrix and implies these chondrules formed while interacting with the matrix. The EBSD analysis of Chondrule 3 (Figure 4.5.A) shows how there is a high frequency of low angle sub-grain boundaries in xenomorphic olivine compared to euhedral olivine and no sub-grain boundaries in enstatite. A higher frequency of sub-grain boundaries indicates the phase has higher internal misorientation and therefore more dislocations (Passchier & Trouw, 2005). Based on this and the euhedral nature of olivine, it is inferred that enstatite was partially replaced by olivine, resulting in less dislocations in enstatite (Spruzeniece et al., 2016). This interaction between the chondrule and matrix is further illustrated with enstatite intergrowths with the matrix (Figure 4.3 & 4.4B) and demonstrates grain-boundary reduction when the matrix was amalgamating with the enstatite in the chondrule. This process of

poikilitic chondrule formation was also addressed in Rambaldi et al., (1983) and supports the interpretation of the poikilitic chondrules analysed in NWA 3118.

Generally, the mesostasis in the porphyritic type chondrules is clinochlore and chamosite rich (Figure 4.2, 4.3, 4.4) and because these minerals also occur in the matrix, it suggests that during poikilitic chondrule formation the original chondrule mesostasis underwent alteration. Thus, resulting in an increase of Fe content and higher frequencies of intragrain disorientations on the outer grains of the chondrules. To further this idea, Chondrule 4 is highly porphyritic, not fractured and the mesostasis in the centre has an acicular habit (Figure 4.3 & 4.4). This acicular mesostasis is interpreted as a quench texture (Brearley & Krot, 2013), therefore potentially the relict mesostasis of the porphyritic type chondrules. In the transition zone between the acicular mesostasis and clinochlore, chamosite mesostasis, there are a few pockets of fine-grained unclassified material (Figure 4.4.C). This transition potentially indicates that during chondrite formation, there may have been alteration that initially affected the outer edges of the chondrule and progressed towards the centre. In Chondrule 4, the centre acicular mesostasis was unaffected by this alteration.

5.2.5 NWA 3118 geological time-line

The following section provides an interpreted sequence of events and schematic diagram (Figure 5.1) that produced the NWA 3118 sample used in this thesis.

Step 1: Based on the quench texture in chondrule 4, it is inferred that olivine grains in the solar nebular developed fayalite rims in the solar nebula during chondrule formation. In all the chondrules, olivine is euhedral, therefore it was the first mineral to crystallise. This was also the time when inclusions formed. As this melt cooled, further amalgamation processes caused enstatite to form around the edges of the forming chondrules.

Step 2: From evidence provided by Chondrules 1 and 2, these type of chondrules formed with a fine-grained rim, in the nebula. Then during the formation process, a portion of chondrules (Chondrule 2) are fractured and in-filled with fine-grained rim material and matrix ‘fluid’. During this stage, the poikilitic chondrules were reacting with the matrix dust. The olivine was already cool and did not react with the matrix. However, enstatite was still cooling and subsequently developed intergrowths with the matrix. This interaction also produced some enstatite zoning.

Step 3: Chondrite formation. The granular chondrules were still cooling when they interacted with the matrix to form the poikilitic chondrules. Simultaneously, the porphyritic chondrules were completely cool during this chondrite formation event. During this step, there was some metasomatism that led to the production of the chamosite and clinochlore rich mesostasis, this alteration started from the outer chondrule grains and progressed towards the center. This

metasomatism also potentially facilitated the 'agglomeration' formation, which coalesced in the matrix, in-between the chondrules described above.

Step 4: After the chondrite formed and was on its parent body, there was some aqueous alteration that resulted in thicker fayalite rims.

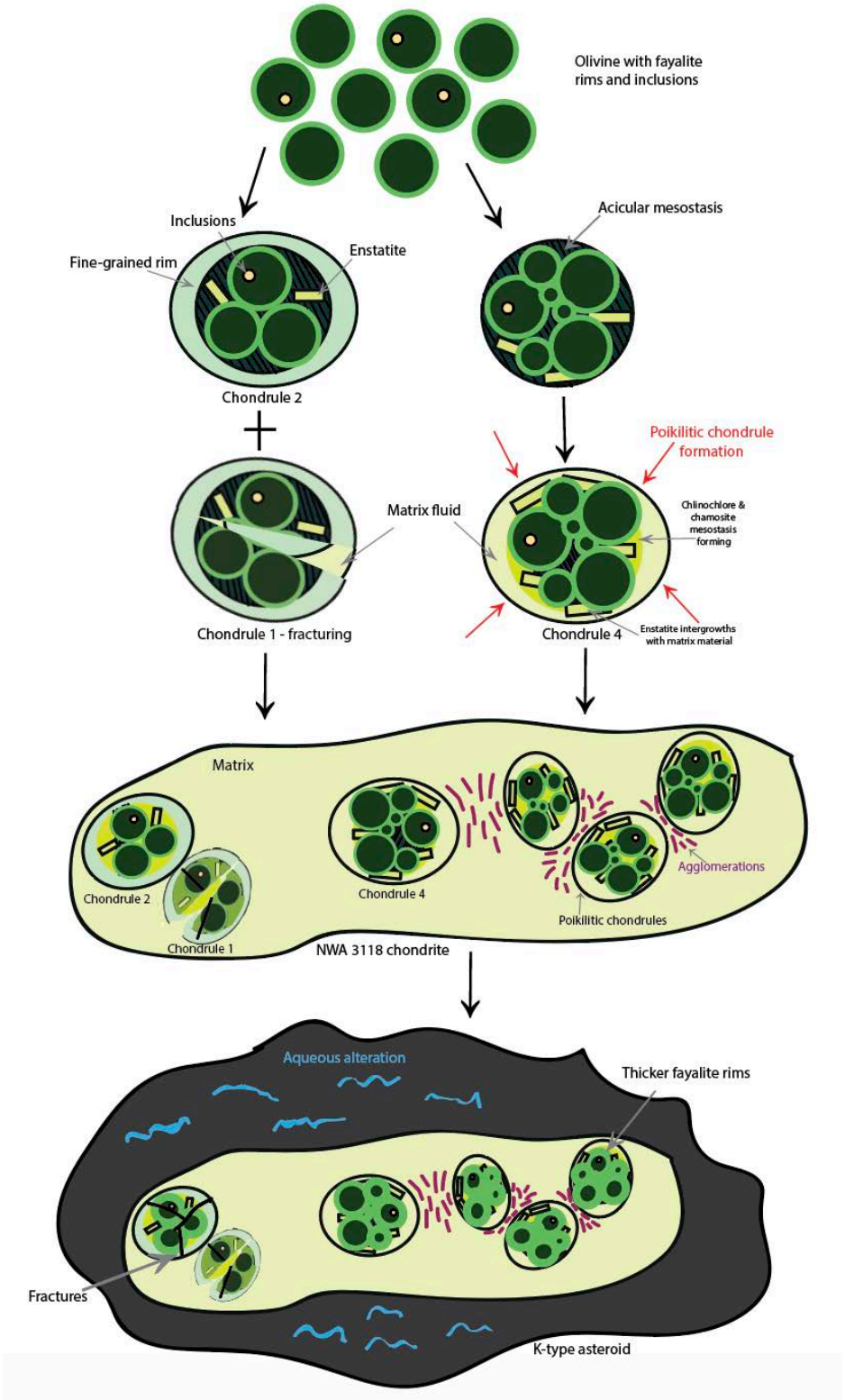

Figure 5.1 *- Schematic diagram of the interpreted sequence of events that led to NWA 3118 formation. Not to scale.*

5.3 Murchison

5.3.1 Matrix implications

This Murchison sample is quite porous and has an overall weak petrofabric alignment defined by the matrix and some chondrules plus their associated fine-grained rims (Figure 4.8). It is also observed that some chondrules, AOAs and their fine-grained rims do not adhere to this alignment and appear independent. The porous nature of the matrix perhaps indicates that some chondrules, their fine-grained rims (Metzler et al., 1992) and the matrix amalgamated in the nebula along with phyllosilicate precursors (Ciesla et al., 2003). Subsequently, impact related differential stresses resulted in a pronounced porosity reduction (Table 2). In addition, the amalgamated matrix, chondrules and fine-grained rims experienced flattening, which is consistent with a shock-related compaction (Scott et al., 1992; Bland et al., 2014 and Hanna et al., 2015).

The matrix interacts with the angular clasts to produce the strain shadows. This phenomenon is exemplified in Feature 2 (Figure 5.2), whereby the olivine porphyroclast began rotation probably during a high directional shock pressure and which created localised low pressure areas in certain areas around the chondrule. These low-pressure areas are observed in the reaction rim, where SiO_2 rich fluids flows towards the low-pressure areas and in-fill the strain shadows during a differential stress regime, aided probably by the rotational movement of the grains and a failure between rim and matrix. This brittle behaviour results in a difference between the flow movement of the matrix on either side of the olivine porphyroclast, this is termed the separatrix (imaginary surface in inhomogeneous flow, separating flow patterns, Passchier & Trouw, 2005). In a similar way, Passchier & Trouw (2005) explain the strain shadow formation process, which agrees with the microstructures observed in this Murchison sample. It has been inferred that dynamic compression and static compaction on the Murchison parent body (a C-type asteroid) was caused by impacts (Fujimara et al., 1983). Hannah et al., (2015) also suggest that impacts on the parent body potentially resulted in pore collapse which resulted in the flattening of the matrix, chondrules and their fine-grained rims.

Murchison would have originated from a C-type asteroid (Young et al., 2003 and King et al., 2017). There is clear evidence of fluid activity from the sample examined and this could have been active on the parent body. Lee & Lindgren (2016) suggest that the fluid was approximately neutral to alkaline and slightly reducing in composition that led to the formation of phyllosilicates. This fluid activity may have been induced from impacts, resulting in cataclasis. A process like this would also explain the reaction rim around two phenocrysts seen in Feature 1 (Figure 4.11). In this reaction rim, the olivine and troilite increase towards the matrix, thereby demonstrating an increase in their Fe and S content (Table 2). A study by Velbel et al., (2015) found that during aqueous alteration, Fe

was leached from the chondrules to form sulphide rims, much like the observed reaction rim, in Feature 1.

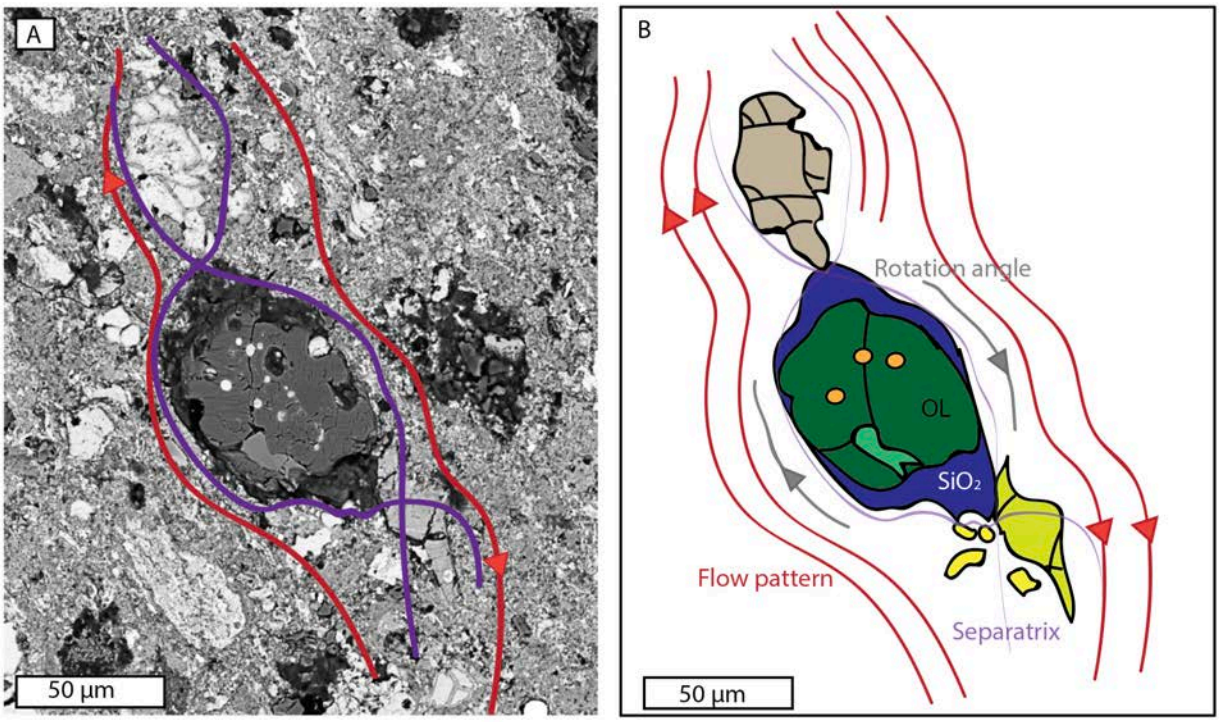

Figure 5.2- *Feature 2 from ROI 2. A) Is the NanoMin BSE analysis. B) An interpreted schematic of the flow pattern, rotation angle and separatrix. Adopted from Passchier & Trouw (2005).*

5.3.2 Amoeboid Olivine Aggregates (AOA) implications

AOA 1, 2 and 3 and their fine-grained rims are shown in Figure 4.8, 4.9 & 4.10. They do not follow the same preferred orientation textured observed in other areas of this Murchison sample and they contain inclusions. It is challenging to precisely explain how these AOAs formed and how they were incorporated into Murchison. However, given they are independent from the pervasive preferred orientation, it is suggested that the AOAs were incorporated into Murchison post cataclasis. The AOA fine-grained rims are not affected by porosity reduction and do not follow the pervasive whole rock alignment. These fine-grained rims were therefore potentially accreted onto the olivine grains in the solar nebula (Metlzer et al., 1992). The AOAs contain metal inclusions which are relicts of the precursor assemblage and escaped melting during amalgamation in the solar nebula (Jones et al., 2000). Ringwood (1961) states that metal in chondrites would have formed through reducing reactions, in the solar nebula where the most abundant reducing agents are hydrogen and carbon. In addition, iron and nickel were probably also lost as volatile components. This idea is further explored by Mahan et al., (2017) where experimental studies of Murchison indicate volatile element depletion is a function of temperature. This would have occurred in a low pressure H_2 environment, such as in the solar nebula.

Given the possibility that AOAs and their fine-grained rims formed in the solar nebula, the next question is, how did they become incorporated into this Murchison sample and have features independent of previous cataclastic processes? A similar problem is presented in Metzler et al., (1992), where this phenomenon is explained through a sort of 'snowfall' process on the parent body. In which case, the amalgamated AOAs and their fine-grained rims fell gently onto the Murchison parent body after cataclasis and were then incorporated into this Murchison sample. The AOAs were probably incorporated around the same time-frame due to the same overall forsterite orientation seen in EBSD analysis (Figure 4.9).

On the edges of the sample, there are clusters of fine-grained unclassified material. These are typically found on the outer edges of the overall sample. A higher frequency of intragrain disorientation is seen in the forsterite and enstatite grains next to the unclassified material (Figure 4.9 & 4.10). The textured indicate these grains have more dislocations and were affected by post-amalgamation processes. This unclassified material does not occur as intergrowths with the AOA or the fine-grained material, nor does it adhere to the overall alignment, which indicates it was introduced after AOA incorporation on the Murchison parent body. The unclassified material has similar textural properties to phyllosilicates in other Murchison studies (Krot et al., 2004 and Lee & Lindgren, 2016). Considering this, plus the phyllosilicate associated AOAs occurring near small fractures, may imply that this Murchison sample spent some time in the internal part of the parent body. In this scenario, melting of accreted ices created interstitial aqueous fluids (Fu et al., 2017) that produced the small fractures (200 μm) and consequently, phyllosilicates near these fractures.

5.3.3 SiO_2 implications

The SiO_2 observed in Features 1 and 2, has previously been explored in Section 5.3.1. In Feature 1 and 2, the presence of SiO_2 is thought to be attributed to the introduction of fluids during cataclasistic deformation processes. EBSD analysis was attempted on these SiO_2 grains with the aim to determine whether it was quartz or a high-pressure quartz polymorph; however, it was unsuccessful as no clear EBSD pattern could be detected. After, extensive research, the occurrence of SiO_2 in Murchison is largely unheard of and undocumented. However, an abstract by Benedix et al., (2015) documents a new unequilibrated chondrite lithology in Murchison. This sample does not adhere to previous studies and is thought to be a chondrite xenolith that has affinities to carbonaceous and ordinary chondrites as well as an unknown chondrite group. Unfortunately, based on the methods applied to the samples examined in this thesis and the subsequent results, no definite conclusions pertaining to the origins of SiO_2 in Murchison can be made. This is future work to be followed up on.

5.3.4 Murchison geological time-line: how to make a CM meteorite

The following section provides an interpreted sequence of events and schematic diagram (Figure 5.3) that produced the alteration and microstructures seen in this Murchison sample used for this research.

Step 1: Amalgamation of chondrules, their fine-grained rims and phyllosilicate precursors in the solar nebula. This explains the porosity and the whole rock petrofabric alignment.

Step 2: This amalgamated chondrite arrived on the parent body. Impacts on the parent body led to pore collapse, cataclasis and fluid activity. This resulted in the formation of phyllosilicates and SiO_2 strain shadows.

Step 3: In the solar nebula, AOAs were amalgamating with their fine-grained rim and then fell onto the Murchison parent body where they were incorporated into the chondrite.

Step 4: On the Murchison parent body, after AOA addition, there were impacts which caused the accreted ices to melt, mobilised fluid and led to aqueous alteration, resulting in the unclassified/phyllosilicate material being near fractures in sample, with no textural relationship to the previous microstructures. This may have occurred when this Murchison sample was in the interior of its parent body.

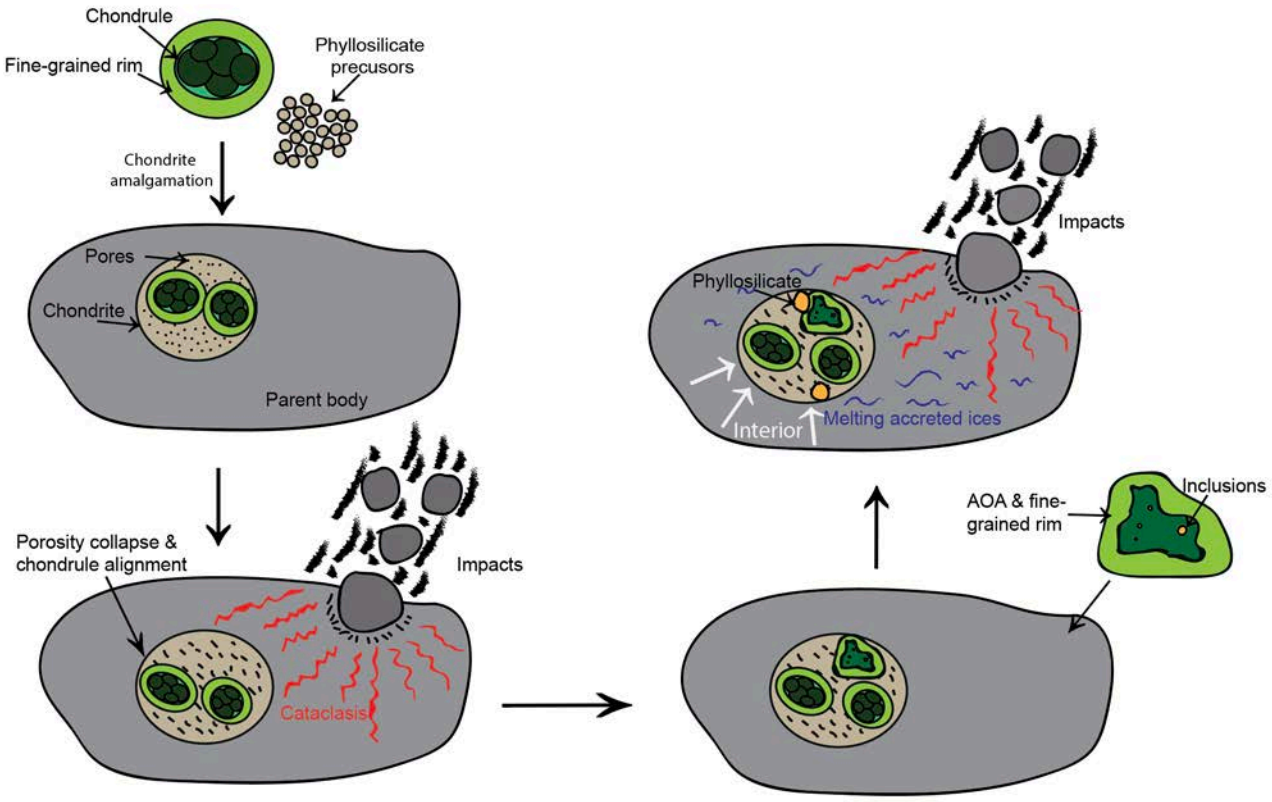

Figure 5.3 - *Schematic diagram of the interpreted sequence of events that led to formation and alteration of Murchison. Not to scale.*

5.4 Sutter's Mill

5.4.1 General features implications

Sutter's Mill does not contain any evidence of 'conventional' chondrules (Figure 4.13), this potentially indicates extreme alteration, or multiple alteration events either completely altered or destroyed the original composition and microstructures.

5.4.2 Matrix character and implications

There are some similar features when comparing the Sutter's Mill and Murchison matrices. Both have similar olivine rich compositions and the BSE maps indicate they have a very similar mottled-fibrous-spinach-like appearance. However, Sutter's Mill has a more homogenous matrix grain size and texture when (Figure 4.13) compared with Murchison, which is heterogeneous. Based on this matrix complementarity between the two samples, it is inferred that during early stages of Sutter's Mill, Murchison and Sutter's Mill potentially shared the same parent body and/or experienced the same alteration processes. In addition, based on this assumption, it is possible that initially Sutter's Mill underwent the same formative processes as Murchison, (Section 5.3). Whereby phyllosilicate matrix precursors, chondrules and their fine-grained rims amalgamated in the solar nebula. Chondrite amalgamation continued on the parent body followed with further alteration.

Comparatively, Sutter's Mill is more homogenous than Murchison (compare Figure 4.8 and 4.13), which indicates Sutter's Mill underwent further re-crystallisation from potential thermal metamorphism at higher temperatures. Zolensky et al., (2014) suggested that the current observed mineralogy of Sutter's Mill is attributed to thermal metamorphism that transformed phyllosilicates to fine-grained olivine, tochilinite to troilite, during which carbonates were destroyed. In this study, NanoMin analysis did not detect any carbonates and this supports this interpretation. Furthermore, during this process Zolensky et al., (2014) also suggest that Sutter's Mill became homogenous and the silicate re-equilibrated at higher temperatures during thermal metamorphism (McSween et al., 1999 & McAdam et al., 2015).

Around the edge of this Sutter's Mill sample, there is a rim with varying thickness (Figure 4.3). There is a reasonably defined boundary between this edge features and the rest of the chondrite, which is defined by a decrease in porosity and fracturing. The composition of the edge is much the same as the overall sample, therefore suggesting the process was isocheimal. This edge feature is somewhat reminiscent of fine-grained rims surrounding chondrules and other major components seen in NWA 3118 and Murchison. However, in Sutter's Mill the process affected the whole outer edge of the chondrite. After extensive literature research, no other Sutter's Mill samples exemplify the same feature. This sample was originally acquired for U-series research (Turner et al., 2017), it

was selected because it was not affected by rain, which occurred shortly after the Sutter's Mill fall. U-series results confirm terrestrial alteration by rain did not occur. The isochemical nature demonstrates that alteration occurred after chondrite formation and it started from the edge; but, did not affect the whole sample. From this, it can be inferred that it reflects a sort of shock feature whereby the shock wave compressed the lithology (Sharp & De Carli, 2006). However, it is not clear why this shock effect was not transmitted through the whole sample.

5.4.3 Feature 1: remanent chondrule with later undercooling and cronstedtite formation

Feature 1 is thought to be remanent chondrule (Figure 4.14). It shows two different olivine textures - barred and granular, both have faint flaky textures. To the right of the olivines there are intergrowths between the edges of the granular olivine clasts and cronstedtite. This implies that the granular olivine was still cooling when cronstedtite was introduced. However, given that the granular olivine appears to be replacing the barred olivine, it is inferred that the olivines were there prior to the cronstedtite formation. The flaky textures of both olivines indicates thermal metamorphism (Zolensky et al., 2014). While the barred olivine texture is a replacement process where high temperatures resulted in melting of the precursor assemblage, and this facilitated multiple nucleation sites, resulting in bars of olivine (Wasson, 1996 and Wasson & Rubin 2003). Then undercooling permitted the nucleation of the sub-rounded olivine clasts (Winter, 2009 and Wasson & Rubin, 2003). Cronstedtite is inferred to be amongst the final product of hydrothermal alteration (Müller et al., 1979 and Palmer et al., 2009), therefore aqueous alteration on the parent body resulted in the formation of cronstedtite.

5.4.4 Feature 2: granular olivine troilite impregnation

Feature 2 also has an overall ovoid morphology and a troilite rich assemblage (Figure 4.15). The troilite has a pellet-like habit and there is a relict olivine grain in the centre region. Surrounding the troilite there is some granular olivine encasing some of the troilite, and some unclassified pellets (inferred to be tochilinite based on Zolensky et al., 2014) dissipate in the matrix, forming a feature reminiscent of a reaction rim. The granular olivine does not have any intergrowths with the troilite, this shows that the granular olivine was cooled when the troilite was added. While the unclassified/tochilinite pellets in the matrix indicate matrix alteration related to the introduction of troilite, perhaps some sort of thermal metamorphism is inferred, due to its pellet-like morphology. Troilite is commonly found on aubrites which originate from E-type asteroids and it is generally thought that high temperatures are the product of radiogenic decay and/or magnetic induction (McCoy et al., 1999 and Weissman et al., 2008).

5.4.5 Sutter's Mill geological time-line

Given the general uncertainty regarding Sutter's Mill, delineating a speculative history proves difficult. It is for this reason, that two possible time-lines are provided below using the observations in this Sutter's Mill sample. Both are asteroid mixing models, where the first (Section 5.4.6 – Figure 5.4) has a preference for most of the alteration processes occurring on E-type asteroids and the second (Section 5.4.7 - Figure 5.5), C-type asteroids. The sequence in time-line 2 correlates to the literature; however, does not explain the unique phenomena observed on this Sutter's Mill sample, therefore, time-line 1 is preferred.

5.4.6 Sutter's Mill geological time-line: option 1 (Figure 5.4)

Step 1: On a C-type asteroid, much like Murchison's, there was CM type chondrule amalgamation. Impact induced melting led fluid mobilisation and the production of phyllosilicates. As much of this Sutter's Mill sample original assemblage has been overprinted, specific processes cannot be inferred; but, it may be similar to Murchison's early history.

Step 2: Asteroid mixing (Gatteccea et al., 2017), probably through impacts, led to the introduction of C-type components onto an E-type asteroid (Zolensky et al., 2012). This might have resulted in impact induced thermal metamorphism (McCoy et al., 1999 and Weissman et al., 2008). Subsequently, the precursor CM assemblage underwent thermal metamorphism and transformed phyllosilicates into fine-grained olivine (Zolensky et al., 2014), along with troilite, barred and granular olivine.

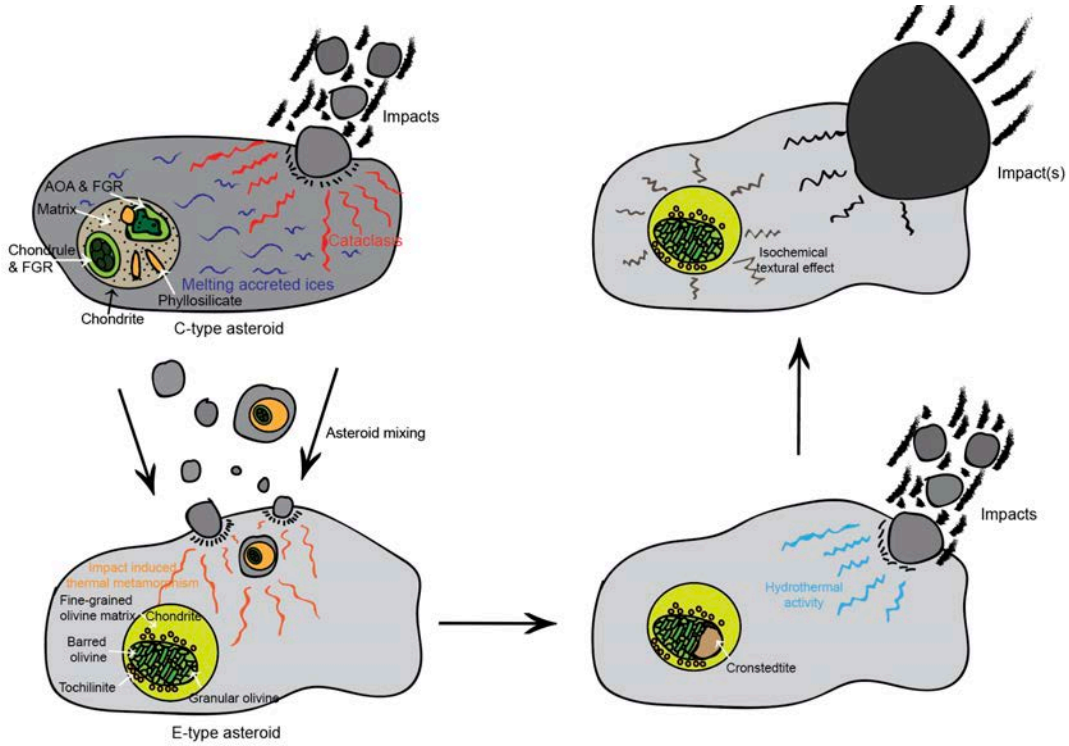

***Figure 5.4** - Timeline 1 - Schematic diagram of the interpreted sequence of events that led to formation and alteration of Sutter's Mill. Not to scale.*

Step 3: Further impact-induced compaction on the E-type asteroid resulted in aqueous alteration, which led to hydrothermal activity producing cronstedtite.

Step 4: During post chondrite-amalgamation, there was another episode of shock activity, perhaps in the nebula (but this is uncertain) which changed the porosity and produced the edge texture.

5.4.6 Sutter's Mill geological time-line: option 2 (Figure 5.5)

Step 1: Same as above - on a C-type asteroid, much like Murchison's, there was CM type chondrule amalgamation. Impact induced melting led fluid mobilisation and the formation of phyllosilicates. As much of this Sutter's Mill sample original assemblage has been overprinted, specific processes cannot be inferred.

Step 2: On an E-type asteroid, there was melting due to radiogenic heating and/or magnetic induction (McCoy et al., 1999 and Weissman et al., 2008). This resulted in troilite being produced, seen in Figure 4.15.

Step 3: Back on the C-type asteroid, potential asteroid mixing (Gatteccea et al., 2017) resulted in some E-type asteroid fragments arriving on this C-type asteroid. This speculation is perhaps not too far-fetched, given there are different olivine morphologies seen on Sutter's Mill (Figure 4.14) which are thought to be due to thermal metamorphism facilitated from impacts and resulted in different olivine morphologies (Wasson 1996; Wasson & Rubin, 2003; Winter, 2009; Nakamura 2005; Tonui et al., 2014; Jenniskens et al., 2012; Zhoa et al., 2014; Bland et al., 2014; Zolensky et al.; 2014 and Zolensky et al., 2012).

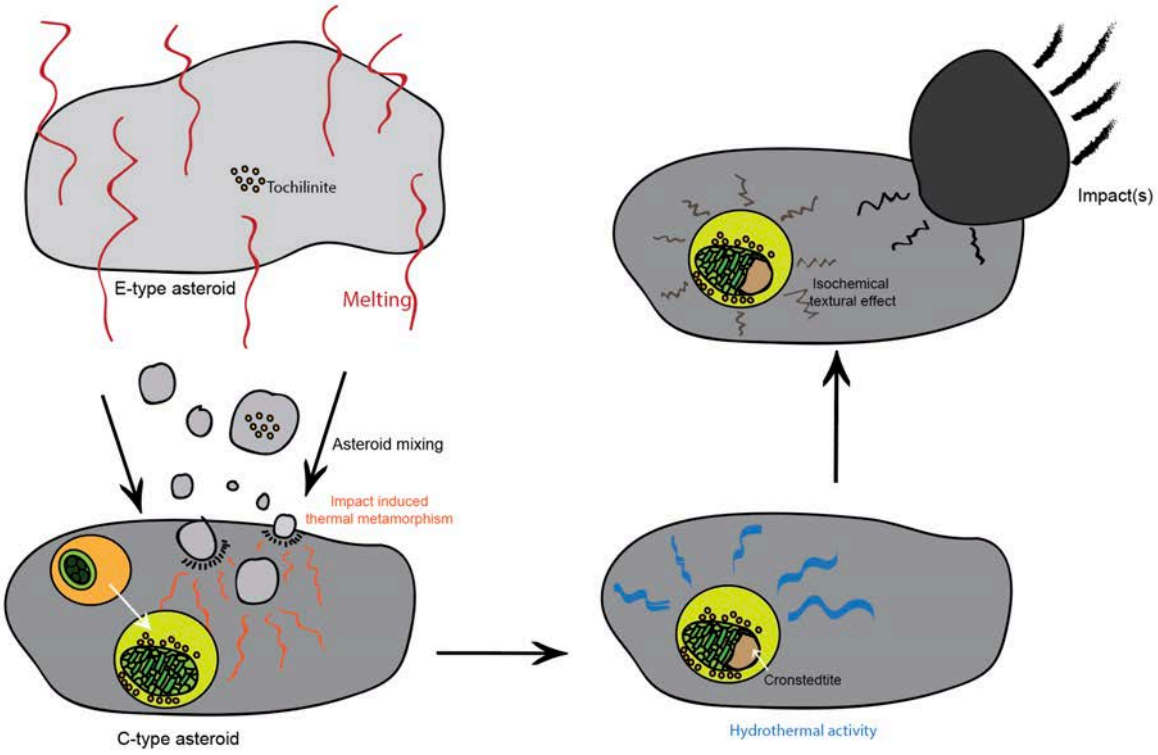

Figure 5.5 – *Timeline 2 - Schematic diagram of the interpreted sequence of events that led to formation and alteration of Sutter's Mill. Not to scale.*

Step 4: On this C-type asteroid, there was aqueous alteration that led to the formation of cronstedtite. It was initiated from the internal heating of accreted ices through the decay of ^{26}Al (Zolensky et al., 1989; Brearely et al., 1999; Brearley & Hutcheon, 2000; Young et al., 2003 and King et al., 2017).
Step 5: Post chondrite-amalgamation, there was another episode of shock activity which changed the porosity and produced the edge texture.

5.5 Planetary processes - a view from alteration history

5.5.1 Timing of alteration - primary formation or secondary process?

The suite of samples used in this thesis provide an insight into complex processes occurring in the Solar System, whether it be from chondrule amalgamation, alteration in the nebula or meteorite parent body, or potentially mixing between asteroids. Many of the chondrule features invoke a two-component model of chondrule formation, and subsequent matrix and chondrules accretion to form the chondrite (Alexander, 2001). Despite deriving from different chondrite types, these samples represent a sequence of events that likely occurred in the early Solar System.

NWA 3118 is the most primitive example. It has experienced the least amount of alteration and establishes a probable sequence of events that occur during chondrule and chondrite amalgamation. It also potentially explains how different chondrule types form through undergoing different processes on the solar nebula and are found in the same chondrite. One chondrule example is interpreted as having undergone fracturing, then being in-filled with fine-grained rim material and a ‘matrix’ fluid. This is a primary process that occurred during chondrule amalgamation. The poikilitic chondrules formed in the solar nebula before they were amalgamated into the NWA 3118 chondrite. Then later, on the NWA 3118 parent body, K-type asteroids experienced further aqueous alteration.

Compared to the other two samples in this study, Murchison lies in the middle of the sequence in terms of the amount of alteration it has undergone. Murchison’s chondrules, their fine-grained rims and matrix have the same petrofabric alignment. This possibly suggests that the chondrite amalgamated in the solar nebula (much like NWA 3118), then experienced secondary alteration on the parent body. Potentially cataclasis through impacts, which resulted in the whole rock alignment and microstructures. Chondrite amalgamation continued and possibly AOAs and their fine-grained rims were added to the Murchison chondrite. Then, further secondary alteration through the form of additional impacts, melted the accreted ices in the parent body and produced further phyllosilicates.

Sutter's Mill is the most perplexing sample. No primary amalgamation features were observed; therefore, it is deduced the features presently observed are due to secondary alteration. It is challenging to relate the observed microstructures to the exact modes of alteration and how they explain the microstructures. However, given the observed features show evidence of processes from two different parent bodies, it is implied that Sutter's Mill experienced secondary alteration on its parent body/bodies. One of these parent bodies is inferred to be the same as Murchison's and therefore establishes a link between Murchison and Sutter's Mill. Furthermore, when compared to this sample collection it represents the most extreme alteration on a carbonaceous chondrite.

5.5.2 Volatiles during planetary formation- their character and significance

The primary and secondary alteration processes, whether they are in the solar nebula or in an asteroidal setting, provide information on the role of volatiles in the early Solar System. The three different carbonaceous chondrite samples in this study each display different microstructural and mineralogical features that permits delineation of different volatile processes. In addition, it has been presented that accretion of hydrated chondrites, such as CMs potentially provided Earth with water and other volatiles (Alexander et al., 2012 and Drake & Righter, 2002), therefore underpinning many processes seen on Earth.

NWA 3118 is a CV3 and the most pristine and primitive compared to the other two samples in this study. The fayalite rims are thought to be indicative of both primary and secondary processes. The thin rims that are seen on each of the olivine grains are interpreted to represent primary amalgamation processes, during which there was condensation and diffusion in the nebula (Hua et al., 1988 and Weinburtch et al., 1990). This would imply an open system, where volatiles were lost and chemical reactions occurred between the chondrule components and the ambient gas (Sears et al., 1996). Cassen et al., (2001) proposed a simple disk model where a hot solar nebula has large amounts of evaporation out to 3 AU, a high accretion rate and where the final chondrite volatile fractionation patterns are achieved in roughly their final formation location. The NWA 3118 timeline provided in this study also interpreted an aqueous alteration event on the parent body resulted in a thicker fayalite rim. This would have occurred on the CV3 parent body, when it had a radius between 110 – 150 km and accreted 3.2 - 3.3 My after chondrule formation (Jogo et al., 2017).

Here, it is inferred that during one stage of the porphyritic chondrule amalgamation, Chondrule 1 was fractured and in-filled with fine-grained rim material and matrix 'fluid'. While Chondrule 2, one of the porphyritic chondrules, contains evidence of glassy mesostasis. In addition, these two chondrules have fine-grained rims, while the other chondrules studied in NWA 3118 are poikilitic

chondrules. Perhaps this difference in chondrule type demonstrates a compositional difference between the matrix and chondrule rims (Bland et al., 2005). This also invokes an ‘open-system’ model (Sears et al., 1996).

Another feature observed in NWA 3118 that provides information on volatiles is typified in Chondrule 4. The inner region preserves a glassy mesostasis, while the clinochlore/chamosite mesostasis occurs on the edge of the chondrule. Sears et al., (1996) attributed this to recondensation of volatiles before they were incorporated into the meteorite, or aqueous alteration-induced element mobility, which resulted in chondrule-matrix complementarity (Bland et al., 2005). This indicates that chondrules formed from a heterogeneous material reservoir and thermal processing produced chondrites that were depleted in volatile elements (Bland et al., 2005).

Murchison is a CM2 which displays additional evidence of alteration when compared with NWA 3118. Feature 1 contains a reaction rim, where towards the matrix the SiO_2 content decreases, while fayalite increases. According to Alexander et al., (1996) this may represent a point in time where during the crystallisation of chondrules, the initial melt is Mg-rich and composed of olivine and pyroxene. Then the residual melt is enriched in FeO and SiO_2 and increased their volatility. This study supports this possible model.

The AOAs appear to have originated from slightly different processes, compared to the other identified features in Murchison. One of these features are the inclusions in AOAs (and NWA 3118 chondrules) are thought to be due to reducing conditions in the solar nebula and are indicative of volatile depletion trends in meteorites. In this case, Mahan et al., (2017) states that depletion is a function of temperature and the liberation of elements (such as SiO_2) occurred in an open-system, at temperatures > 700 °C.

The pervasive alignment seen in the matrix and some chondrules and their fine-grained rims may be attributed to early planetesimal differentiation. Fu et al., (2017) states that when accreted ice is melted, interstitial aqueous fluids are formed. This creates a difference in density between the aqueous fluids and the surrounding rocky matrix, inducing fluid migration. This can lead to a compaction of pore space during fluid ascent. This is an effective process to devolatise the interior of parent bodies. In this case, paired with the unusual mineralogical and compositional trends identified in this Murchison sample, it can be suggested that this sample spent some time in the interior of its parent body. Then fractures allowed the production of phyllosilicates on the edge of the chondrite. The phyllosilicate content seen in Murchison samples demonstrates the parent body formed 3.5 My after Solar System formation (Alexander, 2017a). Alexander (2017b) links CM

parent body volatile trends to the Moon forming impact and postulates this is due to the growth of Jupiter to ~ 20 M_{Earth} approximately 1 Ma after the formation of CAIs. This separated the inner and outer Solar System and scattered carbonaceous chondrites into the inner Solar System after 4 My (Kruijer et al., 2017). While modelling on impact induced compaction by Bland et al., (2014) agreed with the findings that parent bodies of carbonaceous chondrites formed between the giant planets, from 8.0 to 13.0 AU (Walsh et al., 2012). Then when Jupiter migrated, the asteroid belt underwent depletion and excitation, which may explain the impacts depicted in the provided time-lines for Murchison and Sutter's Mill.

Sutter's Mill has been termed a regolith breccia and the interpreted time-line provided in Sections 5.4.6 and 5.4.7, discusses the possibility of mixing between C- and E-type asteroids, as initially discussed by Zolensky et al., (2012).

Fu et al., (2017) states that based on water-rock interaction, Sutter's Mill is representative of a closed-system model which can be attributed to multiple parent body reactions. A closed system means that volatiles were not lost during chondrule formation, nor did the chondrules chemically interact with the surrounding gases (Sears et al., 1996). This is potentially seen in the barred olivine (Feature 1). This has been found to demonstrate high chondrule forming temperatures. Sears et al., (1996) suggest this may be due to multi-stage cooling and from the loss of volatiles and reduction of FeO. Sutter's Mill is also found to have a high abundance of volatile elements (such as S, Zn, Se, Cd, in, Ti, Pb and Bi) and this suggests that it did not undergo extensive thermal heating above 400 °C (Yamakawa & Yin, 2014 and Jenniskens et al., 2012). This can be considered to be consistent with Nakamura (2005) and Tonui et al., (2014) who that propose thermal metamorphism resulting in different olivine textures was between 500 – 750 °C. The multiple thermal metamorphism events led to different nucleation sites and produced various olivine textures.

Troilite is commonly found in enstatite chondrites and this links them to E-type asteroids. One hypothesis might be that the presence of troilite is the coupling factor between C and E-type asteroidal influences on Sutter's Mill. On E-type asteroids, radiogenic decay and/or magnetic induction result in high temperatures (~ 1000 °C) which causes melting and subsequently, the production of troilite (McCoy et al., 1999 and Weissman et al., 2008). Further research by McCoy et al., (1997) discussed the link between volcanism on E-type asteroids and volatiles. It was found that the parent body must have contained several hundred ppm of volatiles until partial melting, then volcanism was driven through the release of these volatile elements.

Davison et al., (2013) found that impacts onto a porous asteroid will compact that material and lead to heating around the crater, which will take between 10 - 100 My to cool and equilibrate. This potentially shows that Sutter's Mill (and potentially Murchison) was still cooling from an initial impact when further impacts heated the chondrite up to sufficient temperatures to yet again change the microstructures. This idea is further explored in Bland et al., (2014) where modelling of impact-induced compaction resulted in transient heating and lithification of the chondrule. Another process that leads to lithification of chondrules is hydrothermal activity, which might offer an explanation to the isocheimal textural change seen around the edge of the Sutter's Mill chondrite.

An additional alteration found feature in Sutter's Mill was cronstedtite occurring on the edge of Feature 1, it is thought to be amongst the final products of hydrothermal activity (Müller et al., 1979). In which case the olivine would have been exposed to Si-rich hydrothermal fluid, and reactions between the olivine and this fluid produced cronstedtite (Palmer, 2009). Zolensky et al., (1989) proposes the fluid temperature was 1 – 25 ℃ and episodic, involving precipitation and re-precipitation (Brearley et al., 1999), this is seen through the different olivine textures. This aqueous alteration would have occurred ~ 7.5 ± 2 My after CAI formation (Brearley & Hutcheon, 2000) on a C-type asteroid, much like Murchison. The aqueous alteration may have been initiated by the internal heating generated thought the decay of ^{26}Al that resulted in melting of accreted ices and subsequent aqueous alteration on the parent body. (Young et al., 2003 and King et al., 2017).

5.6 Characterisation of planetary processes - the use of NanoMin and EBSD

The effectiveness and difficulties of the NanoMin and EBSD have been previously alluded to; however, they will be examined in more detail here.

To begin, meteorites are somewhat challenging to prepare and analyse, this was especially seen during the preparation of Murchison, when the chondrules were plucked out during mechanical polishing. This fact restricts the possible research.

EBSD analysis supplies information on crystalline and structural relationships and can provide information on polymorphs and unlike other analytical techniques, it also provides complete quantitative data on crystallographic orientations and phases. The NanoMin provides high-resolution, high-quality qualitative and quantitative analysis and little processing is needed. The main benefits of the NanoMin, is that it creates phase assemblage maps and at each point, the elemental composition is provided. However, the sample acquisition can be lengthy so it is a compromise between cost, time and resolution.

The NanoMin technology is relatively new and there are a variety of 'teething' problems, one of which is seen in the sample matrices. In NWA 3118, on one point of the matrix, the NanoMin assigns a spectrum of approximately 50% goethite and enstatite with spectral match of ~96%. Although this value is good, ideally one phase should be assigned to this one point and not much research has been undertaken on CV3 matrices, so it is difficult to determine the accuracy of this analysis without other methods. With regards to Murchison and Sutter's Mill analysis, other research on these carbonaceous chondrites, states that for example, phyllosilicates and carbonates should be present. However, the NanoMin did not detect either in the samples. Some unclassified minerals were examined and interpreted to be a certain mineral based on research. For example, tochilinite blebs, cronstedtite and phyllosilicate grains were identified by a combination of literature and analysis. The presence of SiO_2 could also be an artefact of the NanoMin analysis and with more time and different methods applied, it would be beneficial to determine the accuracy of the SiO_2 results. Furthermore, it is also possible that these samples underwent slightly different processes that resulted changes to the 'expected' mineralogy. Such as, extreme alteration in Sutter's Mill that led to phyllosilicates being changed to olivine. This thesis was limited by budget and time, so additional methods could not be applied to these samples. However, with time, mineral standards will be acquired and added to the NanoMin database, which will greatly aid in more valid data acquisition.

Both the NanoMin and EBSD (EDS) are spectra specific and defined by chemical variations. They are both user specific, in that the user determines the minerals that the raw data will be compared with during analysis and this results in some disadvantages. The EBSD is limited to crystalline phases, while the NanoMin (theoretically) provides better analysis on clays and carbonates. Research was undertaken to ensure correct mineral input; however, initially identifying the exact composition would be ideal.

When used together EBSD and NanoMin are a strong combination that can be used to analyse microstructural features in extra-terrestrial samples. Each have their unique benefits and disadvantages; however, together they form a good union of analyses methods. In theory, this combination should have provided seamless analysis; however, complications were encountered, which had to be resolved. As always, with less budget and time limitations, ideally more analysis methods should be applied, such as TEM, XRD and even isotope analysis would provide an even further and more in-depth view into alteration processes in carbonaceous chondrites and therefore early Solar System processes.

5.7 Concluding remarks

It has been displayed within Chapter 5 that the microstructures in NWA 3118, Murchison and Sutter's Mill provide an insight into processes occurring in the early Solar System. NWA 3118 is the most primitive sample where primary chondrule and chondrite amalgamation processes are demonstrated in EBSD and NanoMin analysis. Murchison contains evidence of having undergone more alteration and therefore secondary processes. Sample preparation issues resulted in less EBSD analysis and satisfactory NanoMin analysis; however, a speculative time-line is provided. While Sutter's Mill analysis did not indicate any of its original mineralogy, whether it is due to its mineralogy or NanoMin issues; but, here is interpreted as having undergone extreme secondary alteration, perhaps on two parent bodies.

Chapter 6 – Conclusions and Future Work

The conclusions presented within this thesis demonstrate the importance and wealth of information that meteorites provide to help us understand early Solar System processes. This study focused on results from SEM-EBSD and NanoMin analysis to understand the implications of the currently observed microstructures in three carbonaceous chondrites and the role of volatiles. NWA 3118, a CV3 is thought to illustrate chondrule and chondrite formation processes, with later aqueous alteration on its parent body. Murchison and Sutter's Mill are both CM2s and when compared to NWA 3118, have very different microstructural features that are a result of different alteration processes; including impact induced compaction, thermal metamorphism and hydrothermal activity. The microstructures in Murchison provide information on the chondrule, AOA and subsequent chondrite formation. Then various alteration episodes, induced from impacts on the parent body, resulted in cataclasis and melting of accreted ices and offer an explanation to other identified features. Sutter's Mill microstructures display even more unique features and are thought to be due to parent body mixing. It is that Sutter's Mill and Murchison experienced some of the same early alteration processes, where aqueous alteration occurred on the parent body and impacts induced thermal metamorphism and hydrothermal activity. Despite originating from different parent bodies, these three samples display some common features that indicate they originated from the same carbonaceous chondrite-like bodies in the inner Solar System.

The time-lines provided in this study are based on the observed mineralogy and composition and often do not adhere to prevalent ideas presented in other studies. Many disciplines of geoscience are shrouded with a plethora of unanswered questions and interpretations that only offer an explanation to some phenomenon and not others. This thesis is not exempt from this trend and does not offer an explanation of the processes that lead to chondrules and/or chondrites amalgamating onto their parent bodies. This aspect would be addressed in future work. Another area that needs further research is the occurrence of SiO_2 in Murchison. Aside from a study by Benedix et al., (2015) that examined an unequilibrated chondrite lithology in Murchison, SiO_2 has not been explored in previous findings. Perhaps in the future, other Murchison samples should be re-analysed.

Other further research in this field would be to apply more methods to these meteorites to develop the time-lines and determine the timing of these events through isotope research. This is currently being undertaken by Tuner et al., (2017), with the aim to establish how recently fluid flow occurred on CV and CM chondrites though conducting experimental leaching on chondrites and examining the U-series disequilibria. This study would also attempt to answer many of the unanswered questions regarding volatile behaviour in the early Solar System. There are currently many studies

exploring carbonaceous chondrites; however, through pairing SEM-EBSD and NanoMin analysis a broader insight can be gained. This allows the development of time-lines and processes resulting in the currently observed the NWA 3118, Murchison and Sutter's Mill carbonaceous chondrite microstructures, to answer questions pertaining to the role of volatiles and early Solar System processes.

References

Akos, K., Szivia, O., Sandor, J., Mate, S. & Maria, T. (2014) Analysis of ripple or flow-like features in NWA 3118 CV3 meteorite. *Planetary and Space Science.* **2014:** 200-210

Alexander, C.M. O'D. (1996) Recycling and volatile loss in chondrules formation. In Hewins, R.H., Jones, R.H., Scott, E.R. (eds) *Chondrules and the protoplanetary disk.* Cambridge University Press, New York, pp 233-253

Alexander, C.M. O'D., Boss, A.P. & Carlson, R.W. (2001) The early evolution of the inner Solar System: a meteoritic perspective. *Science.* **293:** 64-68

Alexander, C.M. O'D., Bowden, R., Fogel, M.L., Howard, K.T., Herd, C.D.K. & Nittler, L.R. (2012) The provenances of asteroids, and their contributions to the volatile inventories of the terrestrial planets. *Science.* **337:** 721-723

Alexander, C.M. O'D. (2017a) Asteroidal sources of the volatiles for the terrestrial planets. In *Accretion and Early Differentiation of the Earth and Terrestrial Planets* (2017)

Alexander, C.M. O'D. (2017b) Sources of terrestrial volatiles: primordial atmospheres and planetesimals from the outer Solar System. In *Accretion: Building New Worlds (2017),* Abstract # 2019

Amelin, Y., Krot, A.N. & Twelker, E. (2004) Duration of chondrule formation interval: a Pb isotope study. In *Geochemica et Cosmochimica Acta*, **68.** Abstract # A759

Anders, E. (1964) Origin, age, and composition of meteorites. *Space Science Reviews.* **3:** 583-714

Ashaug, E., Jutzi, M. & Movshovitz, N. (2011) Chondrule formation during planetesimal accretion. *Earth and Planetary Science Letters.* **308:** 369-379

Beck, P., Quirico, E., Montes-Hernandez, G., Bonal, L., Bollard, J., Orthous-Daunay, F.R., Howard, K.T., Schmitt, B., Brissaud, O., Deschamps, F., Wunder, B. & Guillot, S. (2010) Hydrous mineralogy of CM and CI chondrites from infrared spectroscopy and their relationship with low albedo asteroids. *Geochemica et Cosmochimica Acta.* **74:** 4881-4892

Benedix, G.K., Russell, S.S., Forman, L.V., Bevan, A.W.R. & Bland, P.A. (2015) A new unequilibrates chondrite lithology discovered in the Murchison CM2 meteorite. In *46th Lunar and Planetary Science Conference (2015),* Abstract # 1143

Bizzarro, M., Baker, J.A. & Haack, H. (2004) Mg isotope evidence for contemporaneous formation of chondrules and refractory inclusions. *Nature.* **431:** 153-278

Bizzarro, M., Baker, J.A. & Haack, H. (2005) Timing of crust formation on differentiated asteroids inferred from Al-Mg chronometry. In *36th Lunar and Planetary Science Conference (2005),* Abstract # 1312

Bland, P.A., Alard, O., Benedix, G.R., Kearsley, A.T., Menzies, O.N., Watt, L.E., Rogers, N.W. (2005) Volatile fractionation in the early solar system and chondrule/matrix complementarity. *Proceedings of the National Academy of Sciences.* **102** (39): 13755-13760

Bland, P.A., Zolensky, M.E., Benedix, G.K. & Sephton, M.A. (2006) Weathering of chondritic meteorites. In Lauretta, D.S. & McSween, H.Y. (eds) *Meteorites and the Early Solar System II.* The University of Arizona Press, Tucson, pp 853-867

Bland, P.A., Jackson, M.D., Coker, R.F., Cohen, B.A., Webber, B.W., Lee, M.R., Duffy, C.M., Chater, R.J., Ardakani, M.G., McPhail, D.S., McComb, D.W. & Benedix, G.K. (2009) Why aqueous alteration in asteroid was isocheimal: high porosity ≠ high permeability. *Earth and Planetary Science Letters.* **287:** 559-568

Bland, P.A., Collins, G.S., Davison, T.M., Abreu, N.M., Ciesla, F.J., Muxworthy, A.R. & Moore, J. (2014) Pressure-temperature evolution of primordial solar system solids during impact-induced compaction. *Nature Communications.* **(5)** 5451

Boss, A.P. (1996) A concise guide to chondrule formation models. In Hewins, R.H., Jones, R.H., Scott, E.R. (eds) *Chondrules and the protoplanetary disk.* Cambridge University Press, New York, pp 257-263

Bottke, W. & Morbidelli, A. (2017) Using the main asteroid belt to constrain planetesimal and planet formation. In Elkins-Tanton, L.T. & Weiss, B.P. (eds) *Planetesimals; Early Differentiation and Consequences for Planets*. Cambridge Planetary Science, Cambridge, pp 38-69

Brearley, A.J. & Jones, R.H. (1998) Chondritic Meteorites. In Papike, J.J (eds) *Planetary Materials*. Reviews in Mineralogy, Mineralogical Society of America, Washington, pp 3: 1-398

Brearley, A.J., Saxton, J.M., Lyon, I.C. & Turner, G. (1999) Carbonates in the Murchison CM chondrite: CL characteristics and oxygen isotopic composition. In *29th Lunar and Planetary Science Conference (1999),* Abstract # 1301

Brearley, A.J. & Hutcheon, I.D. (2000) Carbonates in the CM1 chondrite ALH84034: Mineral chemistry, zoning and Mn-Cr systematics. In *31st Lunar and Planetary Science (2000),* Abstract # 1407. Lunar and Planetary Institute, Houston.

Brearley, A.J. & Krot, A.N. (2013) Metasomatism in the early Solar System: the record from chondritic meteorites. In Harlov, D.E. & Austrheim, H. (eds) *Metasomatism and the Chemical Transformation of Rock.* Springer-Verlag, Berlin Hedidelberg, pp 659-789

Brearley, A.J. (2006) The action of water. In Lauretta, D.S. & McSween, H.Y. (eds) *Meteorites and the Early Solar System II.* The University of Arizona Press, Tucson, pp 587-625

Bruker. (2017) Lab report XRF 467: Combining micro-XRF and micro-CT: Mineral measurements of drill cores. Bruker Nano Gmbh. Accessed on 10-8-17, from: <https://www.bruker.com/fileadmin/user_upload/8-PDF-Docs/X-rayDiffraction_ElementalAnalysis/mXRF/LabReports/LR_m4_tornado_xrf_467_mxrf_mct_lores.pdf >

Bunch, T.E. & Chang, S. (1980) Carbonaceous chondrites. II: Carbonaceous chondrite phyllosilicates and light element geo- chemistry as indicators of parent body processes and surface conditions. *Geochemica et Cosmochimica Acta.* **44:** 1543-1577

Bunch, T.E. & Rajan, R.S. (1998) Meteorite regolith breccias. In Kerridge, J.F. & Matthews, M.S. (eds) *Meteorites and the Early Solar System*. The University of Arizona Press, Tucson, pp 144-164

Burbine, T.H., DeMeo, F.E., Rivkin, A.S. & Reddy, V. (2017) Evidence for differentiation among asteroid families. In Elkins-Tanton, L.T. & Weiss, B.P. (eds) *Planetesimals; Early Differentiation and Consequences for Planets*. Cambridge Planetary Science, Cambridge, pp 298-320

Bus, S.J. (2011) IRTF near-IR spectroscopy of asteroids V2.0. EAR-A-10046040IRTFSPEC-V2.0. NASA Planetary Data System.

Canup, R.M. & Agnor, C.B. (2000) Accretion of the terrestrial planets and the Earth-Moon system. In Canup, R.M. & Righter, K. (eds) *Origin of the Earth and Moon*. The University of Arizona Press, Tucson, pp 113-133

Canup, R.M. & Righter, K. (2000) *Origin of the Earth and Moon*. The University of Arizona Press, Tucson.

Cassen, P. (2001) Nebular thermal evolution and the properties of primitive planetary materials. *Meteoritics & Planetary Science.* **36:** 671-700

Chambers, J.E. (2004) Planetary accretion in the inner Solar System. *Earth and Planetary Science Letters.* **223:** 241-252

Ciesla, F.J., Lauretta, D.S., Cohen, B.A. & Hood, L.L. (2003) A nebular origin for chondritic fine-grained phyllosilicates. *Science.* **299:** 549-552

Clark, B.E., Ockert-Bell, M.E., Cloutis, E.A., Nesvorny, D., Mothé-Diniz, T. & Bus, S.J. (2009)

Spectroscopy of K-complex asteroids: parent bodies of carbonaceous meteorites? *Icarus.* **202:** 119-133

Connelly, J.N., Bizzarro, M., Krot, A.N., Nordlund, A., Weiland, D. & Ivanova, M.A. (2012) The absolute chronology and thermal processing of solids in the Solar protoplanetary disk. *Science.* **338:** 651-655

Davis, A.M. (2006) Volatile evolution and loss. In Lauretta, D.S. & McSween, H.Y. (eds) *Meteorites and the Early Solar System II.* The University of Arizona Press, Tucson, pp 295-307

Davison, T.M., O'Brien, D.P., Ciesla, F.J. & Collins, G.S. (2013) The early impact histories of meteorite parent bodies. *Meteoritics & Planetary Science.* **48:** 1894-1918

Doyle, P.M., Jogo, K., Nagashima, K., Krot, A.N., Wakita, S, Ciesla, F.J. & Hutcheon, I.D. (2015) Early aqueous alteration activity on the ordinary and carbonaceous chondrite parent bodies recorded by fayalite. *Nature Communications.* **(6)** 7444

Drake, M.J. & Righter, K. (2002) Determining the composition of the Earth. *Nature.* **416**: 39-44

FEI (2016) Scanning Electron Microscope- Teneo. FEI. Accessed on 7-4-17, from: <https://www.fei.com/products/sem/teneo/>

Fu, R.R., Young, E.D., Greenwood, R.C., Elkins-Tanton, L.T. (2017) Silicate melting and volatile loss during differentiation in planetesimals. Elkins-Tanton, L.T. & Weiss, B.P. (eds) *Planetesimals; Early Differentiation and Consequences for Planets.* Cambridge Planetary Science, Cambridge, pp 115-136

Fuchs, L.H., Olsen, E. & Jensen, K.J. (1973) Mineralogy, mineral-chemistry, and composition of the Murchison (C2) meteorite. *Smithsonian Contribution to the Earth Sciences.* **10,** 1

Fujimuru, A., Katio, M. & Kumazawa, M. (1983) Preferred orientation of phyllosilicate [001] in matrix of Murchison meteorite and possible mechanisms of generating the oriented textures in chondrites. *Earth and Planetary Science Letters.* **66:** 25-32

Gaffey, M.J. (1976) Spectral reflectance characteristics of the meteorite classes. *Journal of Geophysical Research.* **81:** 905-920

Gattacceca, J., Krzesinska, A.M., Marrocchi, Y., Meier, M.M.M., Bourot-Denise, M. & Lenssen, R. (2017) Young asteroid mixing revealed in ordinary chondrites: the case of NWA 5764, a polymict LL breccia with L clasts. *Meteoritics & Planetary Science.* (12942) 1-16

Gazi, J.A. (2016) *Evolution of small planetary bodies: a view from carbonaceous chondrites.* Master of Research. Macquarie University. North Ryde, Sydney.

Grimm, R.E. & McSween, H.Y. (1989) Water and the thermal evolution of carbonaceous chondrite parent bodies. *Icarus.* **82:** 244-280

Hanna, R.D., Ketcham, R.A., Zolensky, M. & Behr, W.M. (2015) Impact-induced brittle deformation, porosity loss, and aqueous alteration in the Murchison CM chondrite. *Geochemica et Cosmochimica Acta.* **171:** 256-282

Hardersen, P.S., Mothe-Diniz, T. & Cloutis, E.A. (2011). Constraining meteorite analogues for the Eos dynamical family via mineralogical band analysis. In *42nd Lunar and Planetary Science Conference (2011),* Abstract # 2184

Hood, L.L. & Horányi, M. (1991) Gas dynamic heating of chondrule pre-cursor grains in the solar nebula. *Icarus.* **93:** 259-269

Hood, L.L. & Horányi, M. (1993) The nebula shock wave model for chondrule formation: once-dimensional calculations. *Icarus.* **106:** 179-189

Hua, X., Palme. A.H. & Goresy, A.E. (1988) Fayalite-rich rims, veins, and halos around and in forsteritic olivines in CAIs and chondrules in carbonaceous chondrites: types, compositional profiles and constraints of their formation. *Geochemica et Cosmochimica Acta.* **52:** 1389-1408

Huss, G.R., Rubin, A.E. & Grossman, J.N. (2006) Thermal metamorphism in chondrites. In Lauretta, D.S. & McSween, H.Y. (eds) *Meteorites and the Early Solar System II.* The University of Arizona Press, Tucson, pp 567-586

Ireland, T.R., Fahey, A.J. & Zinner, E.K. (1988) Trace-element abundances in hibonites from the Murchison carbonaceous chondrite: constrains on high-temperature processes in the solar nebula. *Geochemica et Cosmochimica Acta.* **52:** 2841-2854

Ivanova, M., Lorenz, C., Krot, A. & MacPherson, G.A. (2010a) Zr, Y, Sc, Ti, Hf-bearing phase in a composite CAI from the North West Africa 3118 CV chondrite. In *European Planetary Science Congress (2010),* Abstract # 500

Ivanova, M.A., Lorenz, C.A., Krot, A.N. & MacPherson, G.J. (2010b) Mineralogy and bulk chemistry of CAIs from efremovka and NWA 3118 CV chondrites. In *73rd Annual Meteoritical Society Meeting (2010),* Abstract # 5266.

Ivanova, M.A., Krot, A.N., Nagashima, K., Lorenz, C.A., Logan, M.A.V., Kononkova, N. N. & MacPherson, G.J. (2011a). Compound CAIs Containing Zr-Y-Sc-Rich Inclusions from NWA 3118 and Efremovka CV3 Chondrites. In *42nd Lunar and Planetary Science Conference*, Abstract # 1608

Ivanova, M.A., Lorenz, C.A., Krot, A.N. & MacPherson, G.J. (2011b) Complex refractory CAIs from the NWA 3118 and Efremovka CV3 chondrites. In *42nd Lunar and Planetary Science Conference*, Abstract # 5266

Ivanova, M.A., Krot, A.N., Kononkova, N.N. & MacPherson, G.J. (2013) Heterogeneity in bulk compositions of compound CAIs from NWA 3118 and Efremovka CV3 Chondrites. In *44th Lunar and Planetary Science Conference,* Abstract # 1719

Jenniskens P., Fries M., Yin Q.-Z., Zolensky M., Krot A., Sandford S., Sears D., Beauford R., Ebel D., Friedrich J., Nagashima K., Wimpenny J., Yamakawa A., Kunihiko Nishiizumi K., Hamajima Y., Caffee M., Welten K., Laubenstein M., Davis A., Simon S., Heck P., Young E., Kohl I., Thiemens M., Nunn M., Mikouchi T., Hagiya K., Ohsumi K., Cahill T., Lawton J., Barnes D., Steele A., Rochette P., Verosub K., Gattacceca J., Cooper G., Glavin D., Burton A., Dworkin J., Elsila J., Pizzarello S., Ogliore R., Schmitt-Kopplin P., Harir M., Hertkorn N., Verchovsky A., Grady M., Nagao K., Okazaki R., Takechi H., Hiroi T., Smith K., Silber E., Brown P., Albers J., Klotz D., Hankey M., Matson R., Fries J., Walker R., Puchtel I., Lee C.-T., Erdman M., Eppich G., Roeske S., Gabelica Z., Lerche M., Nuevo M., Girten B. & Worden S. (2012) Radar enabled recovery of Sutter's Mill, a unique carbonaceous chondrite regolith breccia. *Science.* **338:** 1521–1524

Jilly, C.E., Huss, G.R., Krot, A.N., Nagashima, K., Yin, Q-Z & Sugiurra, N. (2014) ^{53}Mn-^{53}Cr dating of aqueously formed carbonates in the CM2 lithology of the Sutter's Mill carbonaceous chondrite. *Meteoritics & Planetary Science.* **49** (11): 2104-2117

Jogo, K., Nakamura, T., Ito, M., Shigeru, W., Zolotov, M.Y. & Messenger, S.R. (2017) Mn-Cr ages and formation conditions of fayalite in CV3 carbonaceous chondrites: constraints on the accretion ages of chondritic asteroids. *Geochemica et Cosmochimica Acta.* **199:** 58-74

Johnson, B.C., Minton, D.A., Melosh, H.J. & Zuber, M.T. (2015) Impact jetting as the origin of chondrules. *Nature.* **517:** 339-341

Johnson, B. C., Bowling, T. J. & Melosh, H. J. (2014) Jetting during vertical impacts of spherical projectiles. *Icarus.* **238:** 13–22

Jones, T.H., Lebofsky, L.A., Lewis, J.S. (1990) The composition and origin of the C, P, and D asteroids: water as a tracer of thermal evolution in the outer belt. *Icarus.* **88:** 172-192

Jones, R.H., Lee, T., Connolly, H.C., Love, S.G. & Shang, H. (2000) Formation of chondrules and CAIs: theory vs. observation. In Krot, A.N., Scott, E.R.D. & Reipurth, B (eds) *Chondrites and the protoplanetary Disk.* **341:** 927-962

Jones, R.H., Grossman, J.N. & Rubin, A.E. (2005) Chemical, mineralogical and isotopic properties of chondrules: clues to their origin. *Chondrites and the Protoplanetary Disk.* In ASP Conference Series. **341:** 251-285

King, A.J., Schofield, P.F. & Russell, S.S. (2017) Type 1 aqueous alteration in CM carbonaceous chondrites: implications for the evolution of water-rich asteroids. *Meteoritics & Planetary Science.* 1-19

Krot, A.N., Petaev, M.I., Russell, S.S., Itoh, S., Fagen, T.J., Yurimoto, H., Chizmadia, L., Weisberg, M.K., Komatsu, M., Ulyanov, A.A. & Keil, K. (2004) Amoeboid olivine aggregates and related objects in carbonaceous chondrites: records of nebular and asteroid processes. *Chemie der edre Geochemictry.* **64:** 185-239

Kruijer, T.S., Touboul, M., Fischer-Gödde, M., Bermingham, K.R., Walker, R.J. & Kleine, T. (2014) Protracted core formation and rapid accretion of protoplanets. *Science.* **344** (6188): 1150-1154

Larimer, J.W. & Anders, E. (1967) Chemical fractionations in meteorites. II. Abundance patterns and their interpretations. *Geochemica et Cosmochimica Acta.* **31:** 1239-1270

Lee, M.R. & Lindgren, P. (2016) Aqueous alteration of chondrules from the Murchison CM carbonaceous chondrite: replacement, pore filling and the genesis of polyhedral serpentine. *Meteoritics & Planetary Science.* **51** (6): 1003-1021

Libourel, G. & Krot, A.N. (2007) Evidence for the presence of planetesimal material among the precursor of magnesian chondrules of nebular origin. *Earth and Planetary Science Letters.* **254:** 1-8

Lichtenberg, T., Parker, R.J. & Meyer, M.R. (2016) Isotopic enrichment of forming planetary systems from supernova pollution. *Monthly Notices of the Royal Astronomical Society.* **000:** 1-15

Lindgren, P., Price, M.C., Lee, M.R. & Burchell, M.J. (2013) Constraining the pressure threshold of impact induced calcite twinning: Implications for the deformation history of aqueously altered carbonaceous chondrite parent bodies. *Earth and Planetary Science Letters.* **384:** 71-80

Mahan, B., Moynier, F.. Beck, P., Pringle, E.A. & Siebert, J. (2017) A history of violence: insights into post-accretionary heating in carbonaceous chondrites from volatile element abundances, Zn isotopes, and water contents. *Geochemica et Cosmochimica Acta.* (In press).

McAdam, M.M., Sunshine, J.M., Howard, K.T. & McCoy, T.M. (2015) Aqueous alteration on asteroids: Linking the mineralogy and spectroscopy of CM and CI chondrites. *Icarus.* **245:** 320-332

McCoy, T.J., Dickinson, T.L. & Lofgren, G.E. (1999) Partial melting of the Indarch (EH4) meteorite: a textural, chemical, and phase relations view of melting and melt migration. *Meteoritics & Planetary Science.* **34:** 735-746

McSween, J.Y. (1999) *Meteorites and their parent planets.* Cambridge University Press, Cambridge.

Metlzer, K., Bischoff, A. & Stöffler, D. (1992) Accretionary dust mantles in CM chondrites: evidence for solar nebula processes. *Geochemica et Cosmochimica Acta.* **56:** 2873-2897

Mothé-Dinz, T., Carvano, J.M., Bus, S.J., Duffard, R. & Burbine, T.H. (2008) Mineralogical analysis of the Eos family from near-infrared spectra. *Icarus.* **195:** 277-294

Müller, W.F., Kurat, G. & Kracher, A. (1979) Chemical and crystallographic study of cronstedtite in the matrix of the Cochabamba (CM2) carbonaceous chondrite. *Tschermaks Mineralogische und Petrographische Mutteilungen.* **26:** 293-304

Nakamura, T. (2005) Post-hydration thermal metamorphism of carbonaceous chondrites. *Journal of Mineralogical and Petrological Sciences.* **100:** 260-272

Naumann, C.F. (1826) Lehrbuch der mineralogie. Engelman, Leipzig

Nesvorný, D., Brož, M. & Carruba, V. (2015) Identification and dynamical properties of asteroid families. In DeMeo, M.F.E & Bottke, W.F. (eds) *Asteroids IV.* University of Arizona Press, Tucson, pp 297-322

Nichizumi, K., Caffee, M.W., Hamajima, Y., Reedy, R.C. & Welton, K.C. (2014) Exposure history of the Sutter's Mill carbonaceous chondrite. *Meteoritics & Planetary Science.* **49** (11): 2056-2063

Palmer, E.E. (2009) Volatiles on Solar System Objects: Carbon dioxide on Iapetus and Aqueous Alteration in CM Chondrites. *Ph.D. Thesis.*

Palmer, E.E. & Lauretta, D.S. (2009) Kamacite grains as aqueous alteration indicators in CM chondrites. In *72nd Annual Meteoritical Society Meeting (2009),* Abstract # 5087

Passchier, C.W. & Touw, R.A.J. (2005) *Microtectonics.* (2nd ed) Springer-Verlag Berlin Heidelberg. New York.

Putnis, A. & Austrheim, H. (2010) Fluid-induced processes: metasomatism and metamorphism. *Geofluids.* **10:** 254-269

Rambaldi, E.R., Rajan, R.S., Wang, D. & Housley, R.M. (1983) Evidence for relict grains in chondrules of Qingzhen, an E3 type enstatite chondrite. *Earth and Planetary Science Letters.* **66:** 11-24

Ringwood, A.R. (1960) Chemical and genetic relationship among meteorites. *Geochemica et Cosmochimica Acta.* **24:** 159-197

Russell, S.S., Zolensky, M., Righter, K., Folco, L., Jones, R., Connolly, H.C., Grady, M.M. & Grossman, J.N. (2005) The Meteoritical Bulletin, No. 89, 2005 September. *Meteoritics & Planetary Science.* **40** (9): A201-A263

Sapah, M.S. (2015) *Characterisation and chronology of refractory inclusions (CAIs) in the CV3 chondrite NWA 4502.* Australian National University, Canberra.

Sarafin, A.R., Nielson, S.G., Marshcell, H.R., McCubbin, F.M. & Monteleone, B.D. (2014) Early accretion of water in the inner Solar System from a carbonaceous chondrite-like sources. *Sciences.* **346** (6209): 623-626

Scott, E.R.D., Keil, K. & Stöffler, D. (1992) Shock metamorphism of carbonaceous chondrites. *Geochemica et Cosmochimica Acta.* **56:** 4281-4293

Scott, E.R.D. (2007) Chondrites and the protoplanetary disk. *Annual Reviews of Earth and Planetary Sciences*. **35**: 577-620

Sears, D.W.G., Shaoxiong, H. & Benoit, P.H. Open-system behaviour during chondrule formation. In Hewins, R.H., Jones, R.H., Scott, E.R. (eds) *Chondrules and the protoplanetary disk.* Cambridge University Press, New York, pp 221-231

Seiler, H. (1983) Secondary electron emission in the scanning electron microscope. *Journal of Applied Physics.* **54** (11): R1- R18

Sharp, T.G. & DeCarli, P.S. (2006) Shock effects in meteorites. In Lauretta, D.S. & McSween, H.Y. (eds) *Meteorites and the Early Solar System II.* The University of Arizona Press, Tucson, pp 653-677

Shearer, C.K., Papike, J.J. & Rietmeijer, F.J.M. (1998) The planetary sample suite and environments of origin. In Papike, J.J (eds) *Planetary Materials.* Reviews in Mineralogy, Mineralogical Society of America, Washington, pp 1: 1-24

Spruzeiece, L., Piazolo, S. & Maynard-Casely, H.E. (2017) Deformation-resembling microstructures created by fluid-mediated dissolution-precipitation reactions. *Nature Communications.* **8** (14032)

Sunshine, J.M., Connolly, H.C., McCoy, T.J., Bus, S.J. & La Croix, L.M (2008) Ancient asteroids enriched in refractory inclusions. *Science.* **320:** 514-517

Tonui, E., Zolensky, M., Hiroi, T., Nakamura, T., Lipschutz, M.E., Wang, M-S. & Okudaira. (2014) Petrographic, chemical and spectroscopic evidence for thermal metamorphism in carbonaceous chondrites I: CI and CM chondrites. *Geochemica et Cosmochimica Acta.* **126:** 284- 306

Turner, S., McGee, L., Humayun, M. & Zanda, B. (2017) *How Recently Did Fluid Flow Occur on CV and CM chondrites?* Accrete Conference, 2017.

Velbel, M.A., Tonui, E.K. & Zolensky, M.E. (2015) Replacement of olivine by serpentine in the Queen Alexandra Range 93005 carbonaceous chondrite (CM2): Reactant–product compositional relations, and isovolumetric constraints on reaction stoichiometry and elemental mobility during aqueous alteration. *Geochemica et Cosmochimica Acta.* **148:** 402-425

Wai, C.M. & Wasson, J.T. (1977) Nebular condensation of moderately volatile elements and their abundances in ordinary chondrites. *Earth and Planetary Science Letters.* **36:** 1-13

Walsh, K.J. Morbidelli, A., Raymond, S.N., O'Brien, D.P.O. & Mandell, A.M.M. (2011) A low mass for Mard from Supiter's early gas-driven migration. *Nature.* **475:** 206-209

Walsh, K.J., Morbidelli, A., Raymond, S.N., O'Brien, D.P. & Mandell, A.M. (2012) Populating the asteroid belt from two parent source regions due to the migration of giant planets - ''The Grand Tack''. *Meteoritics & Planetary Science.* **47** (12): 1941-1947

Wasserburg, G.J., Busso, M., Gallino, R. & Nollett, K.M. (2006) Short-lived nuclei in the early Solar System: possible AGB sources. *Nuclear Physics.* **777:** 5-69

Wasson, J.T. & Chou, C.L. (1974) Fractionation of moderately volatile elements in ordinary chondrites. *Meteoritics.* **9:** 69-84

Wasson, J.T. & Rubin, A.E. (2003) Ubiquitous low-FeO relict grains in type II chondrules and limited overgrowths on phenocrysts following the final melting event. *Geochemica et Cosmochimica Acta.* **67** (12): 2239-2250

Wasson, J.T. (1996) Chondrule formation: energetics and length scales. In Hewins, R.H., Jones, R.H., Scott, E.R. (eds) *Chondrules and the protoplanetary disk.* Cambridge University Press, New York, pp 45-54

Watt, L.E., Bland, P.A., Prior, D.J. & Russell, S.S. (2006) Fabric analysis of Allende matrix using EBSD. *Meteoritics & Planetary Science.* **41** (7) 989-1001

Weinbruch, S., Palme, H., Müller, W.F. & Gorsey, A.E. (1990) Fe-O rims and veins in Allende forsterite: evidence for high temperature condensation at oxidising conditions. *Meteoritics.* **25:** 115-125

Weisberg, M.K., McCoy, T.J. & Krot, A.N. (2006) Systematics and evaluation of meteorite classification. In Lauretta, D.S. & McSween, H.Y. (eds) *Meteorites and the Early Solar System II.* The University of Arizona Press, Tucson, pp 19-52

Weissman, P.R., Hicks, M.D., Abell, P.A.Choi, Y-J. & Lowry, S.C. (2008) Rosetta target asteroid 2867 Steins: An unusual E-type asteroid. *Meteoritics & Planetary Science.* **43** (5): 905-914

Winter, J.D. (2009) *Principles of Igneous and Metamorphic Petrology* (2nd Edition). Pearson.

Wood J. A. & Pellas P. (1991) What heated the parent meteorite planets? In Sonett C. P., Giampapa M. S. & Matthews M. S. *The Sun in Time.* University of Arizona Press, Tucson, pp 740-760

Yamakawa, A. & Yin, Q-Z. (2014) Chromium isotopic systematics of the Sutter's Mill carbonaceous chondrite: Implications for isotopic heterogeneities of the early solar system. *Meteoritics & Planetary Science.* **49** (11): 2118-2127

Yesiltas, M., Kebukawa, Y., Peale, R.E., Mattson, E., Hirschmugl, C.J. & Jenniskens, P. (2014) Infrared imaging spectroscopy with micron resolution of Sutter's Mill meteorite grains. *Meteoritics & Planetary Science.* **49** (11): 2027-2037

Young, E.D., Zhang, K.K. & Schubert, G. (2003) Conditions for pore water convection within carbonaceous chondrite parent bodies - implications for planetesimal size and heat production. *Earth and Planetary Sciences Letters*. **213**: 249-259

Zellner, B., Leake, M. & Morrison, D. (1977) The E asteroids and the origin of the enstatite achondrites. *Geochimica et Cosmochimica Acta.***41:** 1759-1767

Zhoa, X., Lin, Y., Yin, Q-Z., Zhang, J., Hao, J., Zolensky, M. & Jenniskens, P. (2014) Presolar grains in the CM2 chondrite Sutter's Mill. *Meteoritics & Planetary Science.* **49** (11): 2038-2046

Zolensky, M.E., Bourcier, W.L. & Gooding, J.L. (1989) Aqueous alteration on the hydrous asteroids: results of EQ3/6 computer simulations. *Icarus.* **78:** 411-425

Zolensky M. E., Krot A. N. & Benedix G. (2008) Record of low-temperature alteration in asteroids. Rev. Mineral. Geochem. **68:** 429–462.

Zolensky, M., Mikouchi, T., Higiya, K., Ohsumi, K., Komatsu, M., Jenniskens, P., Le, L., Ross, D.K., Yin, Q-Z. (2012) Sutter's Mill: Possible mixing of C and E asteroids. In *75th Annual Meteoritical Society Meeting (2012),* Abstract # 5264

Zolensky, M., Mikouchi, T., Fries M., Bodnar, R., Jenniskens P., Yin, Q-Z., Hagiya K., Ohsumi, K., Komatsu, M., Colbert, M., Hanna, R., Maisano, J., Ketcham, R., Kebukawa, Y., Nakamura, T., Matsuoka, M., Sasaki, S., Tsuchiyama, A., Gounell, M., Le, L., Martinez, J., Ross. K. & Rahman, Z. (2014) Mineralogy and petrography of C asteroid regolith: The Sutter's Mill CM meteorite. *Meteoritics & Planetary Science.* **49** (11): 1997-2016

Supplementary Material

NanoMin Keys

NWA 3118

Murchison

Sutter's Mill

Additional EBSD Data

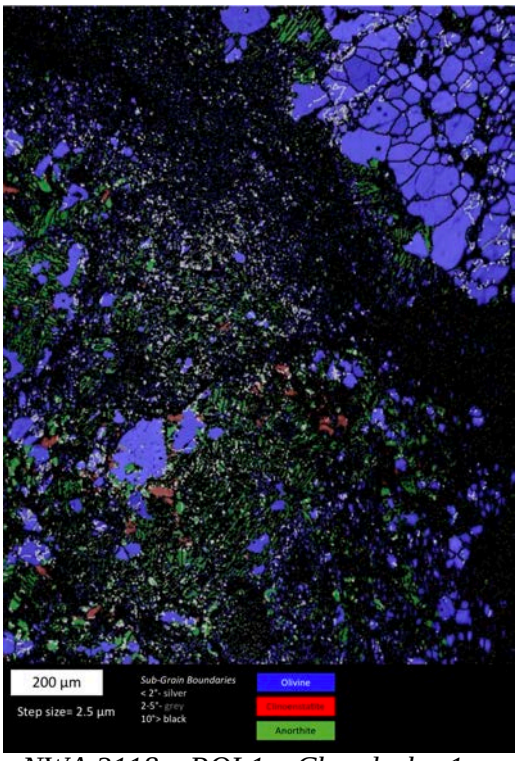

NWA 3118 – ROI 1 – Chondrules 1 & 2 – phase maps and sub-grain maps with BSE analysis underlain.

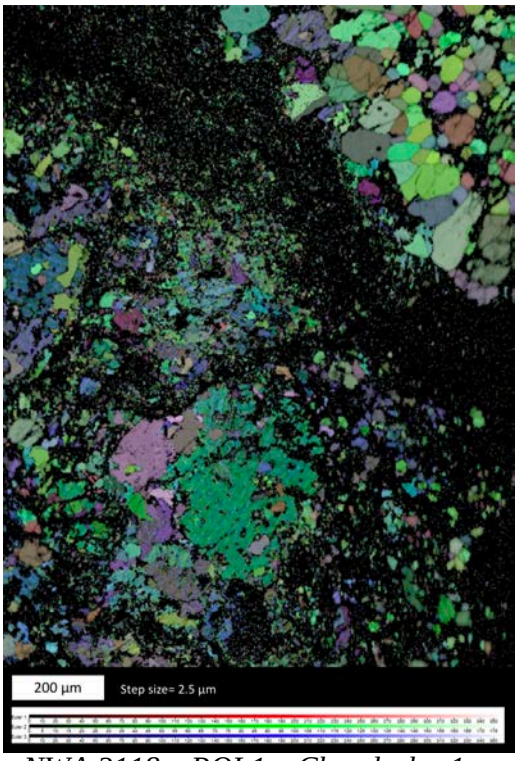

NWA 3118 – ROI 1 – Chondrules 1 & 2 – all Euler analysis with BSE analysis underlain.